

Low-energy level structure of ^{151}Sm by neutron capture reactions and theoretical interpretation

G. Vandenput,* P. H. M. Van Assche, L. Jacobs, and J. M. Van den Cruyce
Department of Physics, University of Leuven, B-3030 Leuven, Belgium
and Nuclear Energy Centre, B-2400 Mol, Belgium

R. K. Smither
Argonne National Laboratory, Argonne, Illinois 60439

K. Schreckenbach and T. von Egidy
Technical University Munich, Munich, Federal Republic of Germany

D. Breitig, H. A. Baader, and H. R. Koch
Technical University Munich, Munich, Federal Republic of Germany
and Research Establishment, Risø, Denmark

(Received 4 April 1985; revised manuscript received 9 December 1985)

A nuclear structure study of ^{151}Sm is presented on the basis of low-energy γ -ray and conversion electron spectroscopy, in connection with thermal neutron capture, and high-energy primary γ -ray measurements following average resonance neutron capture. The level scheme is established up to 1020 keV and incorporates 44 levels. Unique spin and parity assignments are made for 34 levels, and narrow limits are set for the remaining levels. Further possible levels are given between 355 and 1220 keV. Theoretical calculations are presented in the framework of the quasiparticle-rotor model, introducing Coriolis coupling and $\Delta N=2$ interaction. Comparisons between theoretical and experimental results are made for level energies, branching ratios, and multipole mixing ratios.

I. INTRODUCTION

A familiar description of the transition from spherical to deformed nuclei assumes that it arises from the interplay between pairing and quadrupole components in the nuclear interaction. As one moves away from closed shells, the long-range quadrupole force gradually becomes more effective, and a stable deformation ultimately sets in. Over the last 30 years it has been established that the unified model and its many variants provide a satisfactory interpretation of the nuclear structure of deformed nuclei. No such simple model is available for transitional nuclei.

An exhaustive investigation into the characteristics of the spherical to deformed phase transition as applied to the case of ^{150}Sm - ^{152}Sm has been published by Kumar.¹ It may already be surmised from this work that the nuclear structure of the even-odd nucleus ^{151}Sm is likely to be complex and may not lend itself easily to model interpretation. This has subsequently been confirmed by numerous experimental studies²⁻²⁰ and the fact that most low-spin states observed in ^{151}Sm continue to defy straightforward theoretical description.^{8,19-23}

Previous experimental studies can roughly be classified in the following three groups: those involving reactions of the $(\alpha, xn\gamma)$ type,^{14,19,20} those dealing with the β decay of ^{151}Pm (Refs. 2-5, 9-12, 15, and 18), and those based on reactions with one- or two-particle transfer,^{6,8,13} inelastic scattering,⁷ and Coulomb excitation.¹⁷ Reactions of the $(\alpha, xn\gamma)$ type selectively populate high-spin states in rotational bands built on low-lying configurations.

The β -decay studies reveal complex γ spectra with many unresolved multiplet structures. The high-resolution curved-crystal spectrometer measurements presented in this paper are aimed at obtaining the best possible energy precision for γ transitions and levels. These measurements also made it possible to considerably extend the level scheme. Results from average neutron capture experiments, often in combination with results from β decay, from the third group of reactions mentioned above, and from the (n, e^-) measurements presented herein, have allowed the assignment of numerous spin-parity values.

Finally, an interpretation has been sought for the low-energy part of the level scheme in terms of the particle-rotor model, and Coriolis coupling calculations have been introduced in an attempt to obtain an adequate theoretical description of the observed phenomena. The theoretical considerations have taken full account of previously published results.^{8,19,21,23}

II. EXPERIMENTAL PROCEDURES AND RESULTS

A. High-resolution measurements of the low-energy (n_{th}, γ) spectrum

Risø bent-crystal spectrometer measurements

Energies and intensities of γ transitions ranging from 50 keV to about 1100 keV and originating from deexcitation of low-lying states in ^{151}Sm populated by thermal

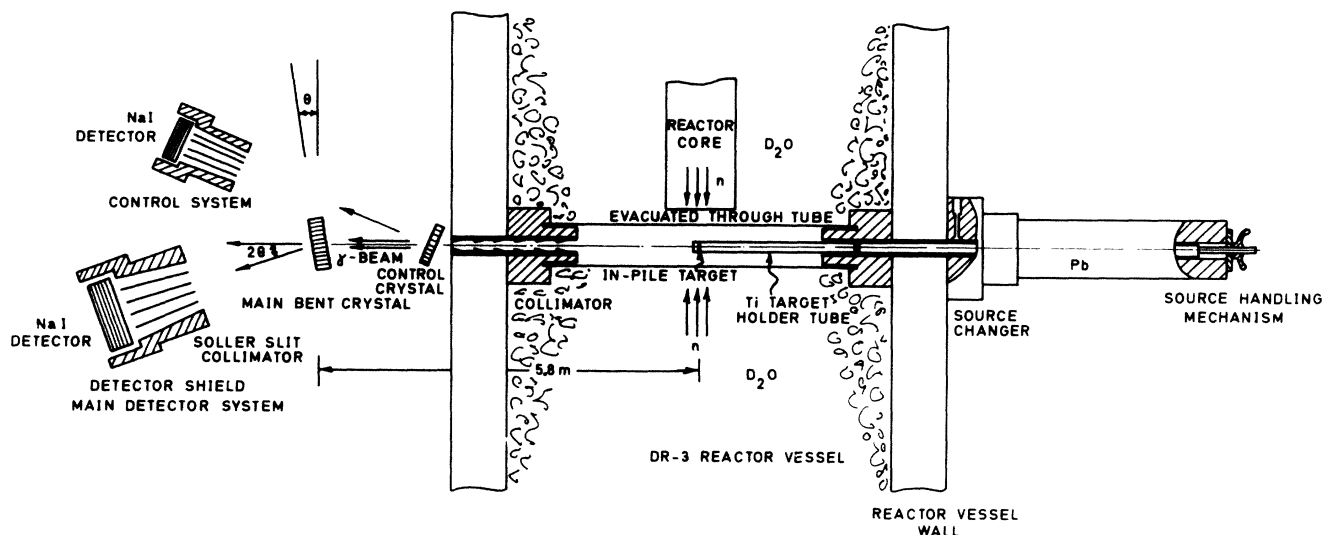


FIG. 1. Schematic drawing of Risø 5.8-m bent-crystal diffraction spectrometer and tangential reactor tube layout.

neutron capture, have been measured with high resolution in two runs of up to five orders of diffraction, using the 5.8 m curved-crystal spectrometer at Risø, Denmark. Targets, consisting of 25 mg of Sm_2O_3 powder enriched to 99.97% in ^{150}Sm , were wrapped in 0.035 mm thick Al foil and pressed between 0.2 mm thick ground aluminum U-shaped profiles to keep the source material plane to 0.01 mm or less. The sources had final dimensions of $25 \times 4.5 \times 0.05 \text{ mm}^3$ after pressing and were freely suspended from thin wires in the center of a tangential beam tube at the Risø DR-3 research reactor, the fine edge facing the diffracting crystal. A schematic drawing of the reactor channel, target manipulation facilities, and the bent-crystal diffraction spectrometer is shown in Fig.

1. Targets were hit by a thermal neutron flux of $(3.9 \pm 0.5) \times 10^{13} \text{ cm}^{-2} \text{ sec}^{-1}$. The isotopic composition of the enriched target material as furnished by the supplier (Isotopes Sales Division, Union Carbide Corporation, Oak Ridge, Tennessee), along with the relative contribution of each component to the thermal neutron capture rate, is given in Table I.

A detailed description of operating characteristics and performance of the Risø curved-crystal spectrometer has been given by Koch *et al.*²⁵ The most conspicuous feature of the Risø spectrometer is its high energy resolution. The crystal is a 4 mm thick slab of quartz ($70 \times 80 \text{ mm}^2$) reflecting at the (110) planes in Laue diffraction, i.e., in transmission, with a grating constant of 2.47 Å. Only

TABLE I. Isotopic composition and relative contribution of each component to the thermal neutron capture rate of targets used in the Risø bent-crystal experiment. Only those elemental impurities that contribute more than 0.01% to the capture rate have been given.

Identification	Composition (%)	Thermal neutron capture cross section (b) ^a	Relative contribution to capture rate (%)
^{144}Sm	<0.01	~0.7	$<5.7 \times 10^{-5}$
^{147}Sm	<0.01	64 ±5	$<5.2 \times 10^{-3}$
^{148}Sm	<0.01	2.7 ±0.6	$<2.2 \times 10^{-4}$
^{149}Sm	0.017	41 000 ±2000	5.7
^{150}Sm	99.973	102 ±5	83.4
^{152}Sm	0.01	206 ±6	1.68×10^{-2}
^{154}Sm	<0.01	5.5 ±1.1	$<4.5 \times 10^{-4}$
Cd	<0.05	2450 ±20	<1.00
Eu	<0.02	4600 ±100	<0.75
Gd	<0.02	49 000 ±1000	<8.0
Dy	<0.1	930 ±20	<0.76
Ta	<0.05	700 ±200	<0.29

^aFrom Mughabghab and Garber (Ref. 24).

one-half of a circular aperture of 42 mm diameter is exposed to the incoming γ beam. The wavelength of diffracted γ rays obeys the usual Bragg law

$$n\lambda = 2d \sin\theta. \quad (1)$$

Of all the possible aberrations from the ideal source and crystal geometry that contribute to line broadening,²⁶ those resulting from the finite source width and defocalized source position are predominant. While the latter contribution can be minimized to $\sim 0.6''$, the former is responsible for at least $1.8''$ using sources of dimensions as given above. The total angular linewidth obtained experimentally amounted to $\sim 2''$ and was virtually independent of energy and reflection order and was unaffected by the counting rate. This leaves at most $0.7''$ for the sum of the intrinsic crystal linewidth and the width resulting from nonideal curvature, similar to the value found during previous experiments.²⁵ Using Bragg's law the connection between angular linewidth and energy resolution can easily be obtained. This leads to the following relation for the FWHM (full width at half maximum)

$$\Delta E = 4.0 \times 10^{-6} E^2 n^{-1} \text{keV}^{-1}. \quad (2)$$

This corresponds to a relative linewidth of $(0.04 - 0.24)n^{-1}\%$ in the energy range of highest sensitivity from about 100 to 600 keV.

Purely statistical errors on peak centroid determination vary from $0.01''$ for strong lines to $0.25''$ for weak lines. The occurrence of γ transitions in multiple diffraction orders provides an internal check on the linearity of the spectrometer. Nonlinearities introduced by the crystal driving mechanism are partly eliminated by applying a polynomial correction function, the coefficients of which are obtained from a least-squares adjustment to a total of 124 strong and well-isolated reflections, covering the whole angular range. Remaining deviations from the ideal peak locations arising from any residual instrumental nonlinearities are of random nature. They are accounted for by introducing an equivalent statistical error situated in the $0.15''$ to $0.35''$ bracket. This results in a combined uncertainty in the energy of a single γ reflection given by

$$\sigma_E = (0.3 - 0.7) \times 10^{-6} E^2 n^{-1} \text{keV}^{-1}. \quad (3)$$

The absolute photon detection efficiency of a curved-crystal spectrometer is naturally limited due to its small solid angle, which is no more than 1.5×10^{-6} at Risø. The relative spectrometer efficiency in different diffraction orders has been taken from Ref. 27. Using sources shaped as thin blades in the beam direction, strong absorption of low-energy γ rays in the source itself is inevitable. However, due to the small but finite solid angle under which the diffracting crystal is viewed, one has to consider that part of the radiation "leaks" from the sides of the target, skimming along its lateral surfaces, and consequently experiences attenuation in the aluminium target holder only. Under a number of simplifying assumptions, one can represent the self-absorption including this edge effect by

$$\alpha(E) = \left[\frac{1 - e^{-\mu x}}{\mu x} \right] \times \left[1 + \frac{2\theta b}{\pi a} \left[\frac{1}{2} \frac{1 + e^{-\mu x}}{1 - e^{-\mu x}} - \frac{1}{\mu x} \right] \left[\frac{1 - e^{-\mu' x'}}{\mu' x'} \right] \right], \quad (4)$$

where μ (μ') is the absorption coefficient of the target (holder), x (x') is the depth of the target (holder) in the beam direction, θ is the angle spanned by the diffracting crystal at the source position, and b/a is the ratio of depth to thickness of the target. The narrow linewidth observed can be regarded as evidence for the major idealizing assumptions regarding target shape and orientation being justified.

Relative intensities of measured γ lines are obtained from fitted peak areas, relative spectrometer efficiency, and self-absorption correction. In regions where the peak height to background ratio is favorable (see Fig. 2 for spectrometer sensitivity), a contribution in the percent error of 1% for strong lines and more than 25% for weak lines should be attributed to peak area fits and 7–15% to the efficiency calibration. The major source for intensity errors of low-energy lines, however, has to be sought in the poor determination of the effective target depth x entering expression (4) for the self-absorption $\alpha(E)$. The relative error in $\alpha(E)$ can be calculated from

$$\delta\alpha/\alpha = (1 - \alpha e^{-\mu x})\delta x/x, \quad (5)$$

where the error in the mass absorption coefficient,

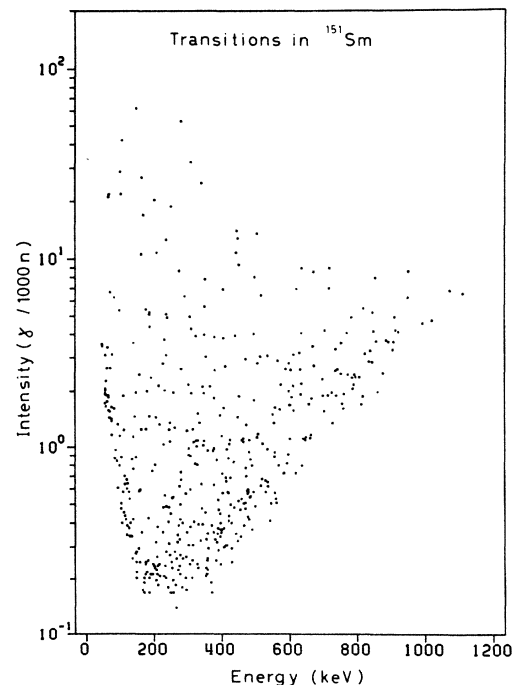


FIG. 2. Plot of relative intensity versus energy of all ^{151}Sm transitions observed with the Risø bent-crystal spectrometer. Lower boundary in this plot represents energy dependence of spectrometer sensitivity.

$\delta\mu/\mu \sim 1\%$, has been neglected. It is clear that at the lowest energies $\delta\alpha/\alpha$ approaches the relative error in the target surface density, which has been estimated to be $\delta x/x \sim 20\%$.

A graphic representation of the spectrometer sensitivity is provided in Fig. 2. The γ intensity of all observed transitions is plotted versus their energy. The salient features of this graph can be understood by noting that at small diffraction angles, in addition to reduced crystal reflectivity, an appreciable amount of undiffracted γ radiation is scattered into the detector collimator. The sharp turn upward at low energies reflects the pronounced effect of absorption. Moreover, the low-energy region increasingly suffers from background which is diffracted by the crystal, composed of Compton scattered reactor γ rays in the target environment. Reactor hall background has been reduced to a minor fraction by adequate detector shielding.²⁸

A total of 20260 angular positions have been scanned, progressing in angular steps of $0.5''$. At low angles, the counting time per angular position was 50 sec. It was set to 40 sec for $\theta > 1.2^\circ$, equivalent to γ energies $E_\gamma < 120$ keV in first order. The entire measurement took about 270 h and was integrally repeated in an independent second run.

Figure 3 shows a representative portion of the $^{150}\text{Sm}(n,\gamma)^{151}\text{Sm}$ spectrum around 340 keV, taken in different diffraction orders. It is intended to illustrate the excellent resolving power of the higher orders, separating lines that appear as unresolved complex structures in first order. Standard data reduction techniques have been utilized for spectral analysis. Table II lists all γ lines detected by bent-crystal spectrometry after thermal n capture in a ^{150}Sm target. Energies and intensities are weighted averages over different runs and diffraction orders.

It is useful to critically examine the compatibility of these independent measurements, because inconsistencies imply either fallacious error estimates or the presence of unknown systematic errors. One method for testing whether N measurements χ_i of an observable χ with "a priori" assigned errors σ_i are compatible, is based on the so-called Birge ratio.²⁹ It consists of assigning an uncertainty to the weighted average $\bar{\chi}$ by the criterion of external consistency

$$(\sigma^{(e)})^2 \equiv \left[\sum_1^N (\chi_i - \bar{\chi})^2 / \sigma_i^2 \right] \left[(N-1) \sum_1^N (1/\sigma_i^2) \right]^{-1}, \quad (6a)$$

apart from the usual internal consistency error

$$(\sigma^{(i)})^2 \equiv \left[\sum_1^N (1/\sigma_i^2) \right]^{-1}, \quad (6b)$$

and defining the Birge ratio as

$$R \equiv \sigma^{(e)} / \sigma^{(i)}. \quad (7)$$

Values of R significantly larger than unity might indicate systematic errors or that some or all of the σ_i have been underestimated.³⁰ As a consistency test, Birge ratios R for all energy and intensity averages have been verified. The errors quoted in Table II are $\sigma^{(e)}$ or $\sigma^{(i)}$, whichever is larger. For the purpose of energy calibration, the Sm K_α

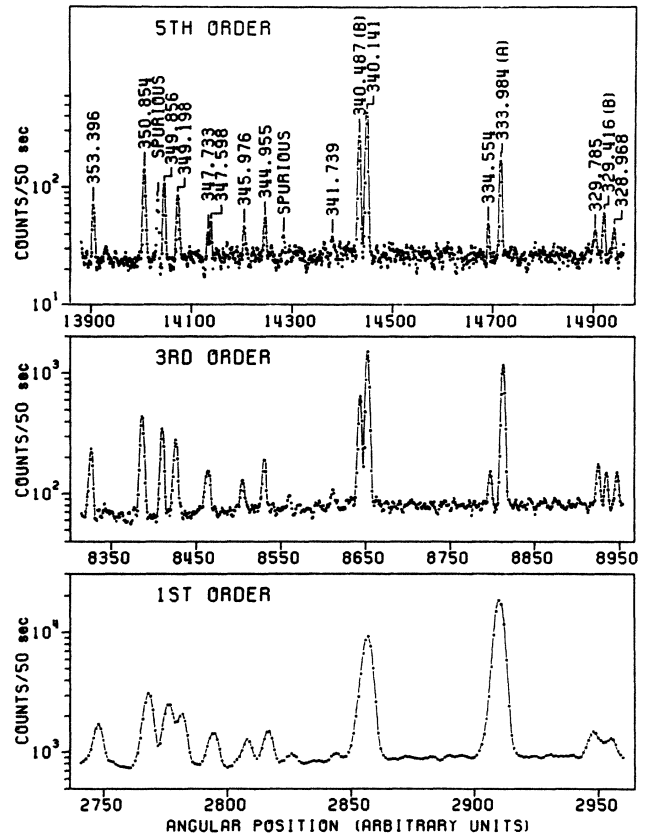


FIG. 3. Portion of $^{150}\text{Sm}(n,\gamma)^{151}\text{Sm}$ spectrum in the region 328–354 keV for first, third, and fifth diffraction order measured at the Risø bent-crystal spectrometer. Two lines in fifth order, labeled as spurious, are due to cross talk from the fourth order. Lines marked by "A" or "B" belong to ^{150}Sm or ^{152}Sm , respectively. The latter results from neutron capture in ^{151}Sm built up during irradiation.

lines have been scanned. Unfortunately, the x rays were not connected in a continuous fashion with the region of lowest γ -ray energies. This very discontinuity may be responsible for a possible systematic deviation of 0.02–0.03% in all energies. Since systematic errors are irrelevant for level scheme development, the errors given in Table II do not include calibration errors.

Also indicated in Table II is the origin of a number of lines that are present in the spectrum but do not belong to ^{151}Sm . From Table I it is clear what kind of interference is to be expected. Although one would initially have an appreciable capture rate contribution of Gd, the very high cross section ensures that this impurity burns out quickly during the first hours of irradiation. Possibly, some ^{114}Cd lines and one ^{152}Eu line are present. Decay of ^{151}Sm only produces a 21.54 keV transition in ^{151}Eu . Lines pertaining to the reaction $^{149}\text{Sm}(n,\gamma)^{150}\text{Sm}$ can easily be identified by comparison with the precise bent-crystal data of Smither.³¹ Those resulting from double neutron capture in ^{150}Sm , and therefore decaying from levels in ^{152}Sm , are recognized by their growing intensity as a function of time, according to

$$I(t) = N[\exp(-\sigma_0\phi t) - \exp(-\sigma_1\phi - \lambda_1)t], \quad (8)$$

TABLE II. Low-energy γ -ray transitions from thermal neutron capture in an enriched ^{150}Sm target, as measured by the Risø bent-crystal diffraction spectrometer.

E_γ (σE_γ) ^a (keV)	R_e ^b	I_γ ^c ($\gamma/1000$ n)	σI_γ ^d (%)	R_t ^b	Assignment $E_i(\text{keV})-E_f(\text{keV})$	N_γ ^e	Comment ^f
1112.58(28)						2	^{152}Sm
1110.9(6)		5.3	42			1	
1085.86(22)						2	^{152}Sm
1073.1(4)		5.5	27			2	
1048.1(5)						(1)	^{150}Sm
1020.8(6)		3.8	45			1	
1005.38(22)	1.4					3	^{152}Sm
995.7(5)						(1)	^{152}Sm
993.6(4)		3.7	35			2	
964.11(11)	0.6					4	^{152}Sm
961.2(5)						(1)	^{152}Sm
951.28(15)	0.9	7.0	14	0.4	951.4-0.0	3	$E1(+M2)$
948.73(22)		5.1	19		953.6-4.8	2	$E1(+M2)$
926.8(3)						1	^{152}Sm
922.14(21)	1.0	3.3	27	0.8		3	
919.52(7)	0.4					6	^{152}Sm
913.3(3)		3.4	34			1	
910.48(21)		4.0	20			2	
907.4(4)		3.0	32			2	
905.4(4)		2.7	43			(1)	
901.53(13)	0.9					3	^{152}Sm
891.76(23)		3.0	24			2	
885.97(23)		3.0	28		951.4-65.8	2	
876.8(4)		2.0	47			(1)	
867.34(12)	0.9					3	^{152}Sm
861.0(5)		1.6	61			1	
856.33(20)	0.5	3.0	31	1.0		3	
855.31(6)	0.8					8	^{152}Sm
853.04(8)	0.7	6.5	14	1.6		6	
848.81(14)	0.4	3.4	17	0.7	953.6-104.8	4	$E1(+M2)$
845.9(6)		4.2	29			(1)	
843.80(29)		2.3	27			2	
841.63(6)	0.8					5	^{152}Sm
838.7(3)	0.4	2.7	25	1.0		3	
834.83(28)		2.3	33			2	
822.0(6)		2.6	36		822.0-0.0	(1)	
818.76(7)	0.8	4.5	11	0.8		6	
817.1(3)		1.5	44		822.0-4.8	1	
812.6(4)		1.4	51			(1)	
810.59(8)	1.2					4	^{152}Sm
807.55(19)		1.9	24			2	
795.82(25)		1.9	33			1	
792.08(13)	0.9	2.0	21	0.7	960.5-168.4	3	
790.30(27)	0.4	1.8	25	0.4		3	
787.4(7)		1.7	46			1	
785.23(14)	0.7	1.9	23	0.6	953.6-168.4	3	$E1(+M2)$
783.57(8)	0.7	4.0	10	1.0	951.4-167.8	5	
772.98(14)		2.0	28			2	
769.65(7)	0.7	3.3	13	0.9		6	
761.51(16)	1.1	1.6	24	1.0		3	
759.35(25)		1.3	33			2	
756.11(25)		1.4	37			1	
752.96(14)	0.5	2.0	18	0.5	822.8-69.7	5	
752.42(12)		2.9	46		822.0-69.7	(2)	
749.23(24)						2	^{150}Sm
741.83(15)		2.1	18			2	
739.02(21)		1.5	27		804.7-65.8	2	
737.38(7)	0.9					3	^{150}Sm

TABLE II. (Continued).

E_γ (σE_γ) ^a (keV)	R_e ^b	I_γ ^c ($\gamma/1000$ n)	σI_γ ^d (%)	R_i ^b	Assignment E_i (keV)- E_f (keV)	N_γ ^e	Comment ^f
736.24(12)	1.3	2.7	12	0.7	741.2-4.8	4	
735.49(11)		2.1	31			2	
728.1(3)		1.1	47			1	
725.23(20)		1.6	31			1	
717.90(4)	1.0	7.3	7	0.5	822.8-104.8	7	
717.11(4)	0.5	5.7	9	0.9	722.0-4.8	7	
					822.0-104.8		
714.39(10)	0.6	1.55	17	0.8		4	
712.19(9)	0.9					3	¹⁵⁰ Sm
704.29(6)	1.1	3.4	9	1.1	774.0-69.7	6	
703.34(17)		1.3	27		703.3-0.0	2	
699.77(10)	0.8	1.55	15	0.5	804.7-104.8	5	
698.51(9)	0.6	1.89	13	0.8	703.3-4.8	5	
688.759(28)	0.6					9	¹⁵² Sm
675.74(13)						2	¹⁵⁰ Sm
674.76(3)	0.7					7	¹⁵² Sm
672.52(12)	1.6	2.22	12	0.28	1017.3-345.0	3	
671.43(4)	1.5	7.0	13	2.6	741.2-69.7	8	¹⁵¹ Sm(+ ¹⁵² Sm)
669.23(5)	0.5	2.81	9	0.8	774.0-104.8	6	
665.38(8)	0.4	1.49	18	1.1		4	
663.64(13)		0.95	23		663.6-0.0	2	
661.75(14)		0.91	26		1017.3-355.7	2	
658.16(9)	0.4	1.39	15	0.16	663.1-4.8	3	
656.579(28)	0.9					8	¹⁵² Sm
648.78(6)	0.8	0.93	20	1.1	951.4-302.6	5	
646.6(4)		0.9	41			1	
640.34(9)	0.7	0.91	21	0.9		4	
637.39(21)		0.65	39		703.3-65.8	(1)	
					951.4-313.9		
636.71(17)		1.8	55		804.7-167.8	1	
636.317(25)	1.0	7.3	4	0.8	741.2-104.8	9	
635.83(10)		3.3	51		920.8-285.0	1	
633.74(8)	0.11	1.57	13	0.5		3	
632.07(5)	1.4	2.13	9	0.9	632.1-0.0	8	
629.44(3)	0.3	2.60	8	1.2		8	
620.562(24)	0.7	5.66	4	1.1	620.6-0.0	9	
619.54(18)		0.59	39			(1)	
612.93(15)		1.3	31		822.0-209.0	1	
612.28(4)	0.7	2.54	7	1.1		7	
611.87(14)		1.7	46			1	
606.56(6)	0.9	1.52	10	0.7	951.4-345.0	5	
603.67(4)	0.9	2.11	13	1.2		5	(¹⁵² Sm)
603.01(6)	1.0	1.38	18	1.3		5	
601.46(15)		0.90	32		1017.3-415.7	2	
599.99(8)	0.7	1.37	13	0.9		4	
598.73(9)		1.6	19		774.0-175.4	2	
598.12(6)	1.5	2.29	9	0.9		7	
597.81(12)		1.7	39		663.6-65.8	1	
595.71(11)	0.15	0.74	21	0.5	804.7-209.0	3	
					951.4-355.7		
593.47(9)	0.5	0.67	21	0.7	663.1-69.7	3	
588.15(5)	1.3	2.13	10	0.8		5	
585.07(16)		0.59	29			2	
584.41(4)	0.5					3	¹⁵⁰ Sm
583.34(9)		0.6	58			2	
575.28(3)	1.1	1.76	7	0.9		8	
571.90(7)	1.0	1.30	15	0.6		3	
568.55(8)	1.0	0.65	20	0.6	1017.3-448.6	5	
565.121(28)	0.7	2.36	6	0.8	920.8-355.7	8	

TABLE II. (Continued).

E_γ (σE_γ) ^a (keV)	R_e ^b	I_γ ^c ($\gamma/1000$ n)	σI_γ ^d (%)	R_i ^b	Assignment E_i (keV)- E_f (keV)	N_γ ^e	Comment ^f
564.104(28)	0.7					7	^{152}Sm
563.068(22)	0.6					8	^{152}Sm
562.30(20)		0.41	46		632.1-69.7	(1)	
559.71(21)		0.43	36			2	
558.15(6)	1.2	1.33	10	0.9	663.1-104.8	5	$^{151}\text{Sm} + (^{114}\text{Cd})$
557.33(11)		0.47	29			2	
556.34(23)		0.8	61			2	
555.84(11)		0.72	27		951.4-395.6	1	
554.76(6)	0.8	1.10	12	0.8	620.6-65.8	4	
550.86(3)	0.7	1.22	9	0.8	620.6-69.7	7	
545.93(11)		0.41	30		754.8-209.0	2	
543.33(17)		0.33	48			(1)	
536.82(12)	0.7	0.50	26	0.5	822.0-285.0	3	
536.26(12)		0.53	32			(1)	(^{114}Cd)
535.513(28)	0.6	2.50	7	1.3	703.3-167.8	7	
534.85(7)		0.79	18		703.3-168.4	2	
531.11(13)		0.47	39			(1)	
530.14(8)	0.6	0.54	19	0.8		4	
523.26(5)	1.7					6	^{152}Sm
521.21(6)	0.8	0.85	12	0.9	521.2-0.0	4	
519.65(5)	0.5	0.55	21	0.9	804.7-285.0	4	
516.92(13)		0.51	35			(1)	
516.364(17)	1.1	5.22	6	1.5	521.2-4.8	10	
514.786(29)	0.8	2.48	10	0.8	960.5-445.7	4	
508.25(25)		1.0	40		822.0-313.9	(1)	
505.70(6)		2.3	47		951.4-445.7	1	
505.55(3)						2	^{150}Sm
505.038(12)	0.6	11.0	4	0.9		10	
504.17(10)		0.9	49			(1)	
499.67(13)		0.39	44			(1)	
497.488(13)	0.8	6.53	4	1.1	502.3-4.8	10	
496.50(8)		1.46	15			2	
495.246(17)	0.7	3.26	5	1.0	663.1-167.8	8	
494.59(14)		0.47	48		663.1-168.4	(1)	
493.64(8)						(2)	^{152}Sm
490.77(19)		0.30	61		804.7-313.9	(1)	
490.36(4)	0.4	0.65	14	1.0	490.4-0.0	6	
486.7(3)		0.45	55			(1)	
485.95(13)						2	^{150}Sm
485.26(11)		0.70	20			2	
483.77(17)		0.44	67			(1)	
482.33(9)						2	^{152}Sm
481.86(13)		0.34	45			(1)	
481.40(7)		0.89	26			2	
481.18(7)	1.3	0.77	15	0.4		3	
479.52(21)		0.47	37		774.0-294.9	(1)	
478.52(7)		0.49	34			2	
477.94(13)		0.35	47		822.8-345.0	1	
477.18(22)		0.46	38		822.0-345.0	1	(^{114}Cd)
475.90(23)		0.47	42			1	
473.30(11)		0.57	31			(1)	
472.963(25)	0.9	1.07	12	1.2		6	
472.29(8)		0.63	26		920.8-448.6	1	
471.33(9)		0.42	26		774.0-302.6	2	
470.83(16)		0.39	49			(1)	
470.471(14)	1.0	2.40	7	1.4	470.4-0.0	9	
466.88(25)		0.32	47		774.0-306.8	(1)	
465.03(27)		0.41	30			2	
464.29(3)	1.1	0.91	18	1.1	632.1-167.8	4	

TABLE II. (*Continued*).

E_γ (σE_γ) ^a (keV)	R_e ^b	I_γ ^c ($\gamma/1000$ n)	σI_γ ^d (%)	R_i ^b	Assignment E_i (keV)- E_f (keV)	N_γ ^e	Comment ^f
464.02(5)	1.4	0.87	20	1.5		4	
459.80(12)		0.89	18		754.8-294.9 804.7-345.0	1	
459.35(8)		0.43	32			1	
456.47(29)		0.28	47			2	
455.76(8)		0.38	39			2	
452.161(18)	0.7	1.53	8	1.1	620.6-168.4	7	
451.467(9)	0.5	7.6	4	1.3	521.2-69.7	10	<i>E</i> 1(+ <i>M</i> 2)
450.23(6)	1.2	0.43	33	1.0		3	
448.613(9)	0.6	10.4	4	1.4	448.6-0.0	10	
448.159(26)	0.4	1.18	16	1.2		4	
447.50(8)		0.26	33			2	
445.758(9)	0.6	11.4	5	1.5	445.7-0.0	10	<i>E</i> 1(+ <i>M</i> 2)
444.031(12)	0.5					5	¹⁵² Sm
443.809(13)	1.4	8.7	6	1.4	448.6-4.8	8	
442.63(11)	0.5	0.29	33	0.5		3	
440.942(11)	0.8	3.2	22	4.6	445.7-4.8	9	<i>E</i> 1(+ <i>M</i> 2)
439.466(12)	0.8				754.8-315.3	7	¹⁵⁰ Sm(+ ¹⁵¹ Sm)
437.60(8)		0.39	36			(1)	
435.95(9)		0.7	53			(1)	
430.89(12)		0.20	50		754.8-324.0	(1)	
430.22(11)		0.24	45		951.4-521.2	(1)	
429.69(8)		0.33	33			(1)	
427.25(4)	0.6	0.41	16	0.9	741.2-313.9	4	
426.63(8)		0.56	51			(1)	(¹¹⁴ Cd)
424.637(29)	1.3	0.89	8	1.1	490.4-65.8	7	
423.038(18)	0.8	0.85	9	1.0	632.1-209.0	6	
421.57(6)		0.35	22			2	
421.25(6)	1.7	0.33	23	1.0		3	
420.73(6)		0.46	26		490.4-69.7	2	
420.22(6)		0.71	39			(1)	
418.48(6)		0.47	22		920.8-502.3	1	
416.06(6)						2	¹⁵² Sm
415.715(29)	1.3	0.80	15	1.8	415.7-0.0	6	
414.93(21)		0.25	47		722.0-306.8	(1)	
414.011(28)	0.6	0.54	11	0.7		5	
413.34(8)		0.6	54			(1)	
411.50(5)	0.8	0.25	23	0.4	620.6-209.0	3	
410.865(12)	1.1	2.20	5	1.1	415.7-4.8	10	
408.07(17)		0.25	39		722.0-313.9	(1)	
407.08(5)		0.30	22		822.8-415.7	2	
406.644(14)	0.8	1.32	6	0.7	722.0-315.3	8	
405.201(10)	1.2	3.10	6	1.5		10	
404.617(9)	1.2	5.62	5	1.3	470.4-65.8	10	
403.10(4)		0.47	19			2	
402.19(12)		0.6	81			(1)	
401.71(6)		0.30	32			(1)	
400.738(15)	0.8	0.93	8	1.1	470.4-69.7	9	
398.87(6)		0.29	31		490.4-91.5	2	
397.45(8)		0.20	39		502.3-104.8	2	
396.75(13)		0.32	30		1017.3-620.6	(1)	
396.47(4)	1.1	0.30	18	1.1	703.3-306.8	4	
396.06(13)		0.36	27		741.2-345.0	(1)	
395.75(7)		0.28	35		395.6-0.0	2	
395.374(13)	1.0	1.21	6	0.9		7	
391.38(4)	1.3	0.38	19	1.1		3	
390.79(4)	0.3	0.23	21	1.2	395.6-4.8	4	
390.34(7)		0.43	49			(1)	
388.85(3)	0.8	0.31	13	0.7		4	

TABLE II. (Continued).

E_γ (σE_γ) ^a (keV)	R_e ^b	I_γ ^c ($\gamma/1000$ n)	σI_γ ^d (%)	R_i ^b	Assignment $E_i(\text{keV})-E_f(\text{keV})$	N_γ ^e	Comment ^f
387.89(3)	0.26	0.29	22	1.3	703.3-315.3	3	
385.59(6)		0.26	27		490.4-104.8	1	
385.407(18)	0.6	0.70	11	0.8		4	
383.75(7)		0.21	25			2	
380.23(3)	1.1	0.27	19	0.8		4	
379.917(8)	0.9	2.10	6	1.4	445.7-65.8	9	$E1(+M2)$
378.912(6)	0.5	3.14	8	2.2	448.6-69.7	10	
378.066(9)	1.1	1.50	7	1.3	663.1-285.0	10	
377.76(4)		0.51	34			(1)	
376.998(10)	0.8	0.79	7	1.3	822.8-445.7	10	
376.27(4)		0.29	37		822.0-445.7	2	
374.42(3)		0.8	62			(2)	
371.05(17)		0.14	44			(1)	
370.60(4)		0.32	21			2	
368.67(6)	0.9	0.15	26	0.14	663.6-294.9	3	
366.275(8)	0.8	1.72	5	1.2	722.0-355.7	10	
360.95(4)		0.24	20		663.6-302.6	2	
359.21(6)		0.18	37		754.8-395.6	(1)	
358.995(23)	1.1	0.21	24	1.4	804.7-445.7	5	
358.56(5)	1.4	0.29	22	1.1		3	
358.317(10)	0.4	0.78	6	1.0	774.0-415.7	10	
357.93(5)		0.21	30			(1)	
356.20(4)	0.8	0.17	21	0.5	663.1-306.8	3	
354.39(5)		0.19	33			(1)	
354.14(5)	1.1	0.27	17	0.21	445.7-91.5	3	
353.396(6)	0.7	2.47	6	2.0	521.2-167.8	10	$M1+E2$
352.74(4)	0.6	0.17	24	0.5	521.2-168.4	3	
352.07(6)		0.37	49			(1)	
350.854(5)	0.7	6.4	6	2.0	355.7-4.8	10	
349.856(6)	1.0	4.6	7	2.2	415.7-65.8	10	$M1+E2$
349.198(6)	0.7	3.23	7	2.1	663.1-313.9	10	
347.734(10)	0.9	0.88	14	0.9	663.1-315.3	6	
347.598(8)	0.9	1.59	5	0.8	703.3-355.7	9	
345.976(10)	1.2	0.83	8	1.5	415.7-69.7	10	
344.955(7)	1.1	1.72	7	1.8	345.0-0.0	10	$E1(+M2)$
343.788(16)	0.7	0.32	12	0.7	448.6-104.8	7	
341.739(13)	1.1	0.39	12	1.0		7	
340.86(4)		0.52	22		445.7-104.8	(1)	
340.487(5)	0.7					9	^{152}Sm
340.141(5)	0.7	20.2	6	1.8	345.0-4.8	10	
337.38(3)		0.26	26			2	
334.554(7)	0.7	1.10	7	1.2	502.3-167.8	9	
333.985(6)	0.6					9	^{150}Sm
331.652(21)	0.6	0.32	15	1.0		4	
330.62(4)		0.19	33			2	
329.785(6)	0.9	1.24	6	0.9	395.6-65.8	9	$E1(+M2)$
329.416(6)	1.0					9	^{152}Sm
328.968(7)	0.7	0.88	8	1.2		8	
328.383(26)		0.7	53		960.5-632.1	(1)	
327.83(4)	1.1	0.20	22	0.9		3	
325.906(8)	0.9	0.82	7	1.2	395.6-69.7	9	
325.242(7)	0.9	0.88	6	0.8	632.1-306.8	8	
323.984(5)	0.9	3.18	6	1.7	324.0-0.0	10	$E1(+M2)$
322.016(10)	0.7	0.66	7	0.7	490.4-168.4	8	
320.237(9)	0.9					8	^{152}Sm
318.03(3)	1.1	0.33	15	1.0		3	
317.147(8)	1.2	0.87	6	1.0		9	
316.108(9)	1.1					8	^{152}Sm
315.343(8)	1.2	1.01	6	0.8	315.3-0.0	8	

TABLE II. (Continued).

E_γ (σE_γ) ^a (keV)	R_e ^b	I_γ ^c ($\gamma/1000$ n)	σI_γ ^d (%)	R_i ^b	Assignment E_i (keV)- E_f (keV)	N_γ ^c	Comment ^f
315.004(17)	0.7	0.25	14	0.8	490.4-175.4	6	
313.93(3)	1.3	0.21	20	0.7	313.9-0.0	4	
312.341(19)	0.6	0.17	28	1.0		4	
310.853(7)	1.3	1.59	12	2.1	415.7-104.8	9	
310.502(6)	1.4	3.48	8	1.9	315.3-4.8	9	
309.038(5)	1.3	26.2	5	1.3	313.9-4.8	9	
308.083(9)	0.7	0.49	10	0.9	632.1-324.0	7	
307.66(4)		0.31	46		703.3-395.6	(1)	
307.378(6)	0.8	0.73	8	1.1	663.1-355.7	9	
306.827(5)	1.3	4.03	7	1.8	306.8-0.0	9	
306.332(25)	0.8	0.20	23	0.9		3	
302.666(6)	1.3	1.76	6	1.3	470.4-167.8	9	
302.609(23)		0.8	56		302.6-0.0	1	
302.48(5)		0.25	56			1	
301.994(8)	1.3	0.74	10	1.5	306.8-4.8	7	
298.07(5)		0.29	40			(1)	(¹⁵⁰ Sm)
297.823(5)	1.0	1.00	7	0.7	302.6-4.8	10	
295.993(18)	1.4	0.22	18	1.0		5	¹⁵¹ Sm(+ ¹⁵² Sm)
295.53(10)		0.14	46		741.2-445.7	(1)	
294.850(7)	1.0	0.46	10	1.1	294.9-0.0	8	
293.45(6)		0.16	32			2	
290.775(4)	1.2	5.2	6	1.6	395.6-104.8	9	<i>E</i> 1(+ <i>M</i> 2)
287.551(6)	0.9					8	¹⁵² Sm
286.456(14)						(1)	¹⁵² Sm
285.832(14)	0.8	0.21	21	0.9		4	
284.972(11)	0.7	0.32	11	0.6	285.0-0.0	6	
283.18(8)		0.14	42			(1)	
280.851(8)	1.0	0.55	10	0.5	448.6-167.8	7	
280.64(5)		0.60	21			(1)	
280.210(11)	1.4	2.1	34	1.4	448.6-168.4	3	
280.151(3)	0.8	43	7	2.2	285.0-4.8	9	
278.259(12)	0.9	0.41	12	0.20		4	
278.133(30)	1.5	0.34	18	1.0		3	
277.99(4)		0.22	36		445.7-167.8	(1)	(<i>E</i> 2)
277.29(5)		0.17	24		445.7-168.4	2	
276.347(24)		0.19	35		632.1-355.7	2	
276.104(17)		0.50	47		1017.3-741.2	(1)	
275.601(21)		0.27	25		620.6-345.0	2	
275.243(5)	1.3	7.0	6	1.5	345.0-69.7	9	<i>E</i> 1(+ <i>M</i> 2)
273.333(8)	0.9	0.31	11	0.9	722.0-448.6	7	
272.403(21)	0.5	0.18	24	0.6		3	
271.269(22)	0.6	0.18	22	0.3		4	
270.748(11)	0.7	0.28	12	0.8	741.2-470.4	7	
269.768(15)	0.9	0.26	18	1.3		5	
267.407(11)	0.8	0.21	17	0.7	663.1-395.6	6	
266.46(8)		0.11	45			(1)	
264.41(4)		0.15	46		754.8-490.4	(1)	
262.330(15)	0.6	0.23	22	0.5		3	
261.416(5)	1.0	1.04	7	1.0	470.4-209.0	9	
258.154(4)	1.2	1.60	8	1.3	324.0-65.8	9	<i>E</i> 1(+ <i>M</i> 2)
257.523(6)	1.0	0.44	11	1.1	703.3-445.7	8	
257.10(4)		0.13	53			(1)	
256.24(4)		0.16	44			(1)	
254.645(14)	0.6	0.19	16	0.9	703.3-448.6	5	
254.270(6)	0.9	0.44	10	0.9	324.0-69.7	8	
252.56(5)		0.20	30			1	
251.650(4)	0.7					9	¹⁵² Sm
250.832(3)	0.5	15.3	8	2.2	355.7-104.8	9	
249.473(6)	0.3	0.36	14	1.5	315.3-65.8	7	

TABLE II. (Continued).

E_γ (σE_γ) ^a (keV)	R_e ^b	I_γ ^c ($\gamma/1000$ n)	σI_γ ^d (%)	R_i ^b	Assignment $E_i(\text{keV})-E_f(\text{keV})$	N_γ ^c	Comment ^f
248.75(7)		0.14	43			(1)	
247.911(4)	0.5	0.87	8	0.8	415.7-167.8	9	
247.365(14)	1.1	0.22	21	0.8	663.1-415.7	5	
247.263(4)	0.8	1.10	11	2.2	415.7-168.4	8	
245.608(4)	0.9	1.01	8	1.0	315.3-69.7	8	
244.725(3)	1.0					9	^{152}Sm
244.229(24)		0.25	35			2	
244.128(8)	0.6	0.39	13	0.5	313.9-69.7	5	
243.588(8)		0.33	29			2	
241.04(7)		0.15	50		306.8-65.8	1	(M2)?
240.111(3)	0.6	3.99	7	1.0	345.0-104.8	9	E1(+M2)
237.105(3)	1.0	10.2	8	2.1	306.8-69.7	10	
236.808(3)	0.9	4.1	9	1.7	302.6-65.8	9	
236.711(9)	0.11	0.40	22	0.5	445.7-209.0	3	(E1)
236.421(17)	0.3	0.23	22	0.6	632.1-395.6	3	
236.197(3)	1.2	2.53	8	1.1	521.2-285.0	10	
235.22(6)		0.16	42			1	
233.767(8)	0.6	0.19	19	1.2		6	
232.943(3)	1.0	1.64	10	2.1	302.6-69.7	10	
232.439(3)	1.2	3.05	9	2.3	324.0-91.5	10	M1+E2
232.352(10)		0.45	42			(1)	
229.761(28)		0.17	41			(1)	(^{114}Cd)
229.019(4)	0.9	0.84	9	1.3	294.9-65.8	9	
227.850(6)	0.4	0.39	12	1.3	395.6-167.8	7	(M1,E2)
227.206(4)	0.4	2.27	9	1.9	395.6-168.4	7	(E1)
227.027(19)		0.29	27			(1)	
217.412(21)		0.17	40			2	
217.309(4)	0.9	1.08	10	1.5	663.1-445.7	7	
216.31(9)		0.20	75		632.1-415.7	(1)	
215.264(3)	1.0	1.74	11	2.2	285.0-69.7	7	
212.541(5)	1.5					7	^{152}Sm
211.801(23)		0.15	53			(1)	
211.111(10)	1.2	0.19	19	0.3	302.6-91.5	5	
210.485(9)	1.7	0.31	12	0.9	315.3-104.8	6	
210.115(15)		0.21	38			1	
209.967(21)		0.17	38			1	
209.031(5)	1.9	8.8	9	2.0	209.0-0.0	7	M1(+E2)
207.342(10)	0.6	0.18	20	1.0	521.2-313.9	4	
206.669(5)	1.6	1.17	10	1.5	415.7-209.0	7	M1+E2
206.020(22)		0.16	42			(1)	
205.868(6)	1.0	0.26	13	0.4	521.2-315.3	7	
204.207(3)	0.8	0.66	10	1.2	209.0-4.8	7	(E2)
203.001(23)		0.19	47			1	
201.972(3)	1.1	16.6	10	2.3	306.8-104.8	7	E1(+M2)
200.776(7)	0.16	0.19	17	0.6	722.0-521.2	6	
197.806(8)	0.4	0.20	18	0.28	302.6-104.8	5	
195.559(17)		0.17	53		490.4-294.9	(1)	
195.500(4)	1.1	0.61	11	1.2	502.3-306.8	7	
192.611(4)	1.5	1.92	10	1.4	663.1-470.4	7	
189.44(4)		0.17	42			(1)	
188.471(2)	0.7	3.6	11	1.6	502.3-313.9	7	
187.904(2)	0.7	4.3	11	1.5	355.7-167.8	7	
187.006(2)	0.5	4.2	11	1.7	502.3-315.3	7	
186.595(2)	0.5	1.20	11	1.1	395.6-209.0	7	(E1)
185.940(11)		0.17	33			2	
185.523(24)		0.14	54			(1)	
183.437(4)	0.8	0.34	13	1.0	632.1-448.6	6	
182.929(13)		0.21	49			(1)	
180.129(3)	0.4	1.63	12	1.7	285.0-104.8	6	

TABLE II. (*Continued*).

E_γ (σE_γ) ^a (keV)	R_e ^b	I_γ ^c ($\gamma/1000$ n)	σI_γ ^d (%)	R_i ^b	Assignment E_i (keV)- E_f (keV)	N_γ ^c	Comment ^f
179.311(14)		0.18	53			(1)	
177.185(2)	0.9	4.4	12	1.9	345.0-167.8	6	<i>M1+E2</i>
176.540(3)	0.5	1.02	12	1.2	345.0-168.4	6	(<i>E1</i>)
176.225(8)	1.3	0.20	21	0.3	521.2-345.0	4	
175.407(15)		0.20	31		175.4-0.0	2	
174.91(3)		0.17	37			1	
170.516(11)		0.16	34			2	
170.476(15)		0.17	33			2	
170.062(20)		0.14	55			(1)	
168.419(3)	0.5	13.8	13	1.6	168.4-0.0	5	<i>M1+E2</i>
167.772(3)	0.5	81	13	2.4	167.8-0.0	5	<i>E1</i>
165.501(11)		0.14	33		521.2-355.7	2	
163.599(3)	0.7	21.7	14	2.4	168.4-4.8	5	<i>M1+E2</i>
163.204(13)		0.29	32			(1)	
163.139(7)		1.02	19			1	
162.950(3)	0.8	8.6	13	1.9	167.8-4.8	5	(<i>E1</i>)
159.300(4)	1.0	0.48	17	1.2		5	
158.065(13)		0.20	45			(1)	
157.371(5)	1.9	1.99	15	2.0	502.3-345.0	5	
156.214(4)	1.2	0.47	15	0.7	324.0-167.8	5	
155.143(10)		0.24	36			(1)	
155.02(3)		0.24	52			(1)	
148.853(13)		0.18	49		953.6-804.7	(1)	
148.586(16)		0.23	35		324.0-175.4	2	
148.068(11)		0.20	44			1	
147.546(2)	0.4	50	16	2.6	315.3-167.8	4	<i>E2(+M1)</i>
147.159(15)		0.16	55			(1)	
146.902(2)	0.7	1.60	15	1.1	315.3-168.4	4	
146.500(9)		0.22	43			2	
146.453(3)	0.4	0.72	16	0.3	470.4-324.0	4	
143.187(3)	1.4	1.19	17	1.7	209.0-65.8	5	<i>M1+E2</i>
139.314(3)	1.5	2.9	17	1.7	209.0-69.7	4	<i>M1+E2</i>
139.042(3)	0.5	0.62	19	0.8	306.8-167.8	4	
138.396(4)	1.2	0.93	18	0.8	306.8-168.4	3	
137.591(19)		0.34	40			(1)	
136.015(12)		0.21	56			(1)	
134.879(7)	0.9	0.28	30	0.6	302.6-167.8	3	
134.222(8)	2.5	0.70	32	2.7	302.6-168.4	4	
130.426(5)	0.5	0.32	28	0.5	445.7-315.3	3	
127.906(8)		0.28	40			(1)	
127.319(6)		0.43	30			2	
125.548(4)	0.8	0.47	24	0.8	521.2-395.6	3	
125.485(8)		0.31	48		470.4-345.0	1	
122.365(6)		0.52	33			1	
121.791(2)	0.7					3	¹⁵² Sm
120.300(8)		0.32	45			(1)	
119.775(7)		0.49	43			1	
119.578(10)		0.28	57			(1)	
119.480(5)		0.55	33		822.8-703.3	1	
116.500(8)		0.34	45			(1)	
113.475(18)		0.35	51			1	
113.373(12)		0.52	41			1	
113.040(3)	1.0	0.57	24	0.4	415.7-302.6	4	
110.921(6)		0.37	37			2	
110.885(3)	0.6	1.01	22	0.9	632.1-521.2	3	
109.572(3)		1.5	21		175.4-65.8	2	
108.065(13)		0.47	43			(1)	
105.492(6)		0.32	47		521.2-415.7	(1)	
104.851(5)	2.2	34	20	0.9	104.8-0.0	3	<i>M1+E2</i>
103.202(4)		0.7	59			2	

TABLE II. (Continued).

E_γ (σE_γ) ^a (keV)	R_e ^b	I_γ ^c ($\gamma/1000$ n)	σI_γ ^d (%)	R_i ^b	Assignment $E_i(\text{keV})-E_f(\text{keV})$	N_γ ^e	Comment ^f
103.019(6)	0.4	0.41	33	0.6		3	
102.572(5)		0.39	42		168.4-65.8	(1)	
101.933(2)	1.2	18	20	0.4	167.8-65.8	3	<i>E1</i> (+ <i>M2</i>)
100.019(2)	0.9	23	20	0.22	104.8-4.8	3	<i>M1</i> (+ <i>E2</i>)
98.705(3)	1.0	0.93	23	0.8	168.4-69.7	3	(<i>M1</i> , <i>E2</i>)
98.059(4)	1.9	4.3	21	0.5	167.8-69.7	3	(<i>E1</i>)
98.008(13)		0.65	46		920.8-822.8	1	
93.383(5)		1.1	29			2	
92.978(5)		0.50	37		395.6-302.6	2	
89.191(9)		0.7	47			(1)	
85.991(9)		0.8	45			(1)	
83.613(12)		0.7	57			(1)	
81.798(5)		1.3	33			1	
81.572(3)		5.1	23			1	
76.222(3)		2.5	25		167.8-91.5	2	(<i>E2</i>)
74.999(8)		0.9	60			(1)	
74.955(7)		1.1	47			(1)	
74.465(7)		1.2	47			(1)	
74.391(6)		1.3	42			1	
70.707(3)		2.1	32		355.7-285.0	2	
69.710(2)		5.4	25		69.7-0.0	2	<i>M1</i> + <i>E2</i>
69.350(9)		1.3	57			(1)	
68.006(6)		1.2	51			(1)	
65.894(6)		1.5	49		1017.3-951.4	1	
65.839(2)		18	22		65.8-0.0	2	<i>M1</i> + <i>E2</i>
65.249(5)		1.3	51			(1)	
65.130(5)		1.5	44			(1)	
64.887(1)		17	22		69.7-4.8	2	<i>M1</i> + <i>E2</i>
62.925(3)		2.8	33		167.8-104.8	1	
61.583(5)		1.4	51			(1)	
61.270(4)		1.5	48			(1)	
60.862(3)		2.1	38			1	
58.469(4)		1.8	46			1	
57.607(5)		1.4	54			1	
56.631(4)		1.6	47			1	
56.333(5)		1.7	54			1	
56.172(3)		2.5	43			1	
56.113(4)		1.6	50			1	
55.657(4)		1.6	57			(1)	
54.814(5)		1.4	58			1	
46.819(1)		2.8	20			1	<i>E2</i> (+ <i>M1</i>)
46.587(2)		2.9	21			1	
46.545(3)		2.9	21			1	

^aA calibration error of 0.03% in the energy has to be added to the errors quoted.

^bBirge ratios R for energy and intensity averages are included as a consistency test.

^cIntensities of transitions of interfering isotopes are not given because these are not constant throughout the measurement.

^dA systematic error of 12% has to be added to obtain absolute intensities.

^eThe multiplicity N_γ designates the total number of independent measurements of a given transition. Birge ratios are not calculated if the multiplicity is less than three.

^fMultipolarities are derived from electron conversion coefficients (Table VI and Ref. 2), and from angular correlation measurements (Refs. 3-5).

$$N = \epsilon \eta N_0 \sigma_0 \sigma_1 \phi^2 / (\sigma_1 \phi - \sigma_0 \phi + \lambda_1), \quad (9)$$

where N_0 stands for the initial number of ^{150}Sm nuclei, λ_1 for the β -decay constant of ^{151}Sm , σ_0 and σ_1 for the thermal neutron capture cross section in ^{150}Sm and ^{151}Sm , respectively, ϕ for the thermal neutron flux, η for the

number of photons emitted per captured neutron, and ϵ for the probability of detection per photon emitted. For γ lines observed in no more than one diffraction order, one has to rely exclusively on comparison with the well-known ^{152}Sm decay properties.³²

The weakest transitions are usually observed in but one

diffraction order. Some of these may not be clearly distinguishable from background fluctuations. Parentheses in the seventh column of Table II indicate that the corresponding transition is, in this sense, somewhat questionable. The multiplicity N_γ in this column is defined as the number of observations of a given γ transition. Some of the multiplicities reported are based on conversion coefficients derived from the complementary (n,e⁻) measurements of Sec. IIC. Some result from a reevaluation of the conversion coefficients of Ref. 2, using the present, more reliable γ intensities and a calibration per level against the e⁻ intensities after β decay of ¹⁵¹Pm. The remaining multiplicities are taken from angular correlation experiments.³⁻⁵

Argonne bent-crystal spectrometer measurements

The low-energy (n, γ) spectrum was measured with the 7.7 m Argonne bent-crystal spectrometer.³³⁻³⁵ The neutron flux at the in-pile sample position was 3×10^{13} cm⁻²sec⁻¹. Three different samples were used to identify γ rays from ¹⁴⁹Sm(n, γ)¹⁵⁰Sm (Ref. 31), ¹⁵²Sm(n, γ)¹⁵³Sm (Ref. 34), and ¹⁵⁰Sm(n, γ)¹⁵¹Sm (the one used primarily in this publication). All samples were Sm₂O₃. The ¹⁵⁰Sm sample was enriched to 95.48 at. % and had the same isotopic abundance as the average resonance neutron capture (ARC) sample (see Sec. IIB). This sample consisted of 112 mg of Sm₂O₃ packed into a cavity in a Mg (85%)—Al (15%) holder which constrained the sample to a volume 7 cm high, 1 cm deep, and 0.014 cm wide forming a narrow line source for the bent-crystal spectrometer. The measurements covered the range from 20 keV to 1.4 MeV. The energies and intensities obtained from the Argonne data are consistent with the Risø data given in Table II for all the strong to medium strength transitions, but the sensitivity of the Argonne data was 3–5 times higher for

TABLE III. New lines found in the special high-sensitivity runs performed with the Argonne bent-crystal spectrometer.

E_γ (keV)	ΔE_γ (keV)	I_γ ($\gamma/1000$ n)	$\Delta I_\gamma/I_\gamma$ (%)	Assignment
25.71	0.01	6.6	10	91.6–65.8
35.13	0.01	0.39	10	104.8–69.7
39.01	0.01	0.036	30	104.8–65.8
61.01	0.005	0.102	25	65.8–4.8
63.58	0.005	0.153	20	168.4–104.8
145.459	0.015	0.30	20	313.9–168.4
376.036 ^a		0.30	30	445.7–69.7
382.780 ^a		0.23	30	448.6–65.8

^aThe position of the line was fixed at this energy during the fitting process. The energy values come from the level energy differences in the final level scheme.

weak lines below 500 keV. This high sensitivity data was used to verify the existence of weak lines in the Risø data, eliminating those that were only statistical fluctuations in the background and improving the accuracy of the intensities of the weak lines that were found to be real. The Argonne spectrometer was also used to search for weak lines of special theoretical importance. The approach used in this search was to automatically cycle the spectrometer so that it alternately passed over the energy region of interest and a nearby calibration line. The calibration line was used to monitor both the energy and intensity stability of the spectrometer as a function of time and correct the individual passes over the region of interest before they were summed. This autocycling was continued until either the line was identified and a value for its intensity was obtained or a sufficiently low upper limit was set on its intensity to give a meaningful interpretation to its absence. Tables III and IV summarize the results of

TABLE IV. Reference lines used to calibrate the energies and intensities of the new γ rays in the special high-sensitivity runs made with the Argonne bent-crystal spectrometer (see Table III).

E_γ (keV)	ΔE_γ (keV)	I_γ ($\gamma/1000$ n)	$\Delta I_\gamma/I_\gamma$ (%)	Assignment
Energy calibration only				
22.7065	0.0005			Sm K-MIII x ray, second order
28.309	0.005			¹⁵² Sm(n, γ) ¹⁵³ Sm line
35.843	0.005			¹⁵² Sm(n, γ) ¹⁵³ Sm line
39.5224	0.0006			Sm K-LII x ray, first order
40.1181	0.0006			Sm K-LIII x ray, first order
40.8920	0.0006			Sm K-LII x ray, first order
41.5421	0.0006			Sm K-LIII x ray, first order
Energy and intensity calibration from ¹⁵⁰ Sm(n, γ) ¹⁵¹ Sm lines				
62.924	0.005	2.1	9	
64.883	0.003	13.4	8	
65.833	0.003	13.0	8	
69.710	0.005	4.7	9	
100.023	0.005	31.9	5	
101.938	0.005	23.0	5	
104.848	0.005	44.7	5	Primary standard
147.546	0.008	63.5	5	Primary standard
309.052	0.015	25.8	5	Primary standard

these special searches. The high sensitivity of the Argonne spectrometer is due to the very large quartz crystal (30 cm \times 30 cm) used in the diffraction process and a special precollimator positioned between the bent crystal and the source in the reactor. This precollimator shielded the spectrometer from the reactor environment and made it possible to remove all material shields between the spectrometer and the source (except for a small amount of ^6Li) without materially increasing the background. This decrease of the in-beam material was particularly important for the observation of the very low energy lines and made it possible to make meaningful measurements down to 20 keV.

B. Average resonance neutron capture measurements

The average resonance neutron capture measurements were performed at the Argonne National Laboratory. The basic approach is to average the neutron capture γ spectrum over many neutron resonances. This averaging reduces the strong Porter-Thomas fluctuations in the intensities of the primary γ rays normally associated with neutron capture in single resonances. When the averaging is done over a sufficient number of resonances the primary γ -ray intensities are grouped corresponding to their multipolarity and to the population systematics of the capture states.³⁶ This group structure can then be used to set limits on the spin and parity of the energy levels to which these transitions decay.

The Argonne in-pile (\bar{n}, γ) facility at the CP-5 research reactor was used to measure the strength of the primary γ rays following average resonance neutron capture (ARC) in the $^{150}\text{Sm}(n, \gamma)^{151}\text{Sm}$ reaction. The capturing sample

consisted of 4 g of Sm_2O_3 that was enriched in ^{150}Sm to 95.48 ± 0.10 at. % The other isotopes of Sm were present with the following abundance (at. %): ^{144}Sm , 0.05 ± 0.02 ; ^{147}Sm , 0.39 ± 0.03 ; ^{148}Sm , 0.47 ± 0.03 ; ^{149}Sm , 1.70 ± 0.05 ; ^{152}Sm , 1.46 ± 0.05 ; and ^{154}Sm , 0.45 ± 0.04 . The sample was surrounded by 3.2 mm of ^{10}B and positioned in the center of a through tube near the core of the reactor where the fast flux was relatively high. The ^{10}B shield absorbed virtually all of the incident neutrons with energies below 100 eV. This limited the effective range of neutron energies contributing to the average resonance capture spectrum to the region from 100 eV to 4 keV, with most of the S -wave capture strength concentrated below 2 keV. Part of the ARC γ -ray spectrum is shown in Fig. 4. The peaks associated with the average resonance capture reaction $^{150}\text{Sm}(\bar{n}, \gamma)^{151}\text{Sm}$ are labeled with the spin, parity, and energy of the level (in keV) to which the γ ray decays. The assignment of gamma transitions to the $^{150}\text{Sm}(\bar{n}, \gamma)^{151}\text{Sm}$ reaction was made by comparing the data with similar ARC data for the $^{144}\text{Sm}(\bar{n}, \gamma)^{145}\text{Sm}$, $^{147}\text{Sm}(\bar{n}, \gamma)^{148}\text{Sm}$, $^{148}\text{Sm}(\bar{n}, \gamma)^{149}\text{Sm}$, $^{149}\text{Sm}(\bar{n}, \gamma)^{150}\text{Sm}$, $^{152}\text{Sm}(\bar{n}, \gamma)^{153}\text{Sm}$, and $^{154}\text{Sm}(\bar{n}, \gamma)^{155}\text{Sm}$ reactions. The strong lines from capture in the other Sm isotopes show up weakly in the ^{151}Sm data. Their relative intensities are down by about the ratio of their relative abundance. The arrows labeled "A" and "B" are examples of ARC lines from other Sm isotopes. The line labeled "B" is one of the strongest of these "other isotope" lines. It is generated by the $^{152}\text{Sm}(\bar{n}, \gamma)^{153}\text{Sm}$ reaction and has an intensity that is similar to that of the weakest group from the $^{150}\text{Sm}(\bar{n}, \gamma)^{151}\text{Sm}$ reaction. The weak lines assigned to $^{150}\text{Sm}(\bar{n}, \gamma)^{151}\text{Sm}$ appear only in the ^{151}Sm data. Most of

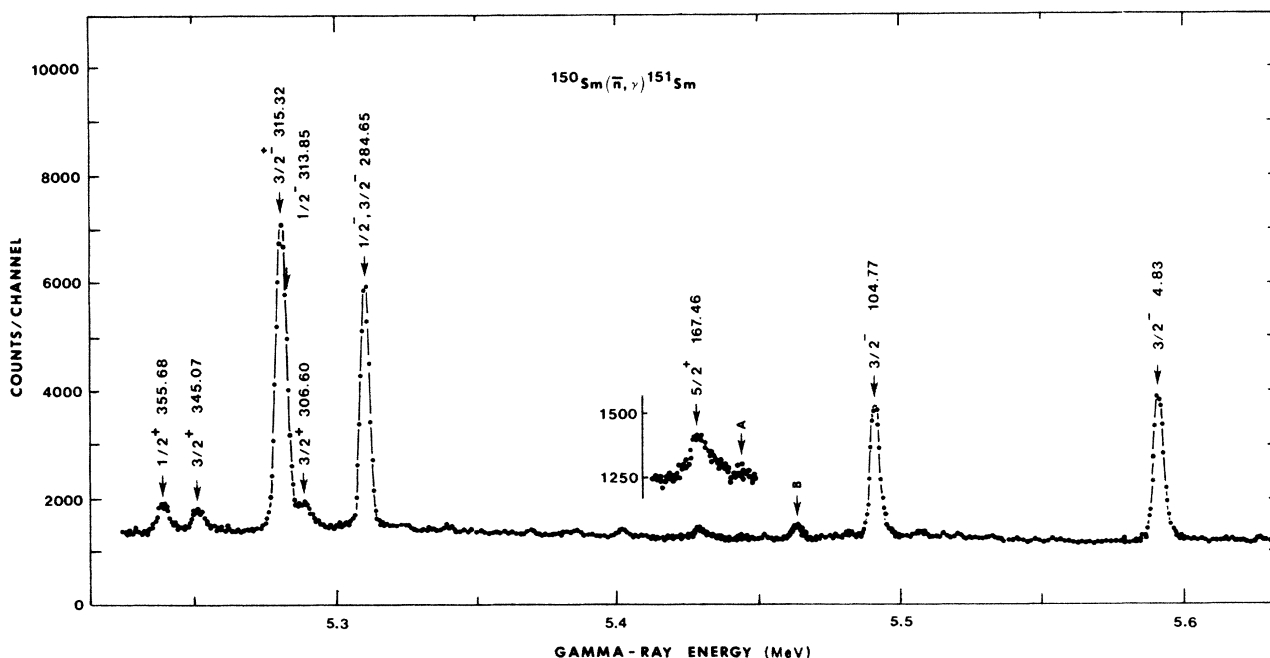


FIG. 4. Part of the ARC γ -ray spectrum obtained from the $^{150}\text{Sm}(\bar{n}, \gamma)^{151}\text{Sm}$ reaction. The labels on the peaks give the spin, parity, and energy of the level to which the associated γ rays decay. These values are taken from Table V. The arrows labeled "A" and "B" indicate typical ARC lines from other isotopes of Sm.

TABLE V. Summary of the ARC data for the $^{150}\text{Sm}(\bar{n}, \gamma)^{151}\text{Sm}$ reaction. E_0 equals E_γ for the ground state (5596.46 keV). The notation $S-E1$, $S-M1$, and $P-E1$ in the sixth column translates as s -wave neutron capture followed by $E1$ transitions, s -wave capture followed by $M1$ transitions, and p -wave capture followed by $E1$ transitions, respectively. The asterisk denotes energy values deduced from the level energies in the final level scheme.

E_γ (keV)	ΔE_γ (keV)	I_γ (rel)	$\frac{\Delta I_\gamma}{I_\gamma}$ (%)	$\frac{I_\gamma(E_0)^5}{(E_\gamma)^5}$ (rel)	Group $L_n-M\lambda$	$E_L(\text{ARC})$ (keV)	$J^\pi(\text{ARC})$	J^π		Remarks
								(Level)	scheme	
5591.63	0.2	2894	5	2907	$S-E1$	4.83	$\frac{1}{2}^-, \frac{3}{2}^-$	$\frac{3}{2}^-$		
5530.62*		<20		<21		65.84*	$\geq \frac{5}{2}^-, \frac{7}{2}^+$	$\frac{7}{2}^-$		
5526.75*		<20		<21		69.71*	$\geq \frac{5}{2}^-, \frac{7}{2}^+$	$\frac{5}{2}^-$		
5504.91*		<30		<33		91.55*	$\geq \frac{5}{2}^-, \frac{7}{2}^+$	$\frac{9}{2}^+$		
5491.70	0.2	2506	5	2755	$S-E1$	104.77	$\frac{1}{2}^-, \frac{3}{2}^-$	$\frac{3}{2}^-$		
5429.00	0.4	130	30	151	$P-E1$	167.46	$\frac{5}{2}^+$	$\frac{5}{2}^+$		
5428.04*		<40		<44		168.42*	$\geq \frac{5}{2}^-, \frac{7}{2}^+$	$\frac{5}{2}^-$		
5421.05*		<30		<34		175.41*	$\geq \frac{5}{2}^-, \frac{7}{2}^+$	$\frac{9}{2}^-$		
5387.43		<40		<48		209.03*	$\geq \frac{5}{2}^-, \frac{7}{2}^+$	$\frac{7}{2}^-$		
5310.81	0.2	4678	5	6079	$S-E1$	284.65	$\frac{1}{2}^-, \frac{3}{2}^-$	$\frac{1}{2}^-, \frac{3}{2}^-$		
5301.60*		<30		<39		294.86*	$\geq \frac{5}{2}^-, \frac{7}{2}^+$	$\frac{9}{2}^-$		Composite with $^{149}\text{Sm}(\bar{n}, \gamma)^{150}\text{Sm}$
5293.81*		<53		<70		302.65*	$\geq \frac{5}{2}^-, \frac{7}{2}^+$	$\frac{5}{2}^-, \frac{7}{2}^-$		
5289.86	0.2	440	10	584	$S-M1$	306.60	$\frac{1}{2}^+, \frac{3}{2}^+$	$\frac{3}{2}^+$		
5282.61*		593	20	791	$S-E1$	313.85*	$\frac{1}{2}^-, \frac{3}{2}^-$	$\frac{1}{2}^-$		E_γ 's fixed by level scheme energies
5281.14*		5483	10	7328	$S-E1$	315.32*	$\frac{1}{2}^-, \frac{3}{2}^-$	$\frac{3}{2}^\pm$		during analysis, only I_γ 's were varied
5272.47*		<30		<40		323.99*	$\geq \frac{5}{2}^-, \frac{7}{2}^+$	$\frac{7}{2}^+$		
5251.40	0.2	375	10	516	$S-M1$	345.07	$\frac{1}{2}^+, \frac{3}{2}^+$	$\frac{3}{2}^+$		
5240.78*		331	20	460	$S-M1$	355.68*	$\frac{1}{2}^+, \frac{3}{2}^+$	$\frac{1}{2}^+$		Composite with $^{149}\text{Sm}(\bar{n}, \gamma)$ and $^{152}\text{Sm}(\bar{n}, \gamma)$
5200.57	0.4	89	20	128	$P-E1$	395.90	$\frac{5}{2}^+$	$\frac{5}{2}^+$		
5180.77*		<30		<43		415.69*	$\geq \frac{5}{2}^-, \frac{7}{2}^+$	$\frac{5}{2}^-, \frac{7}{2}^-$		
5159.00	0.3	118	20	178	$P-E1$	437.46	$\frac{5}{2}^+$	$\frac{5}{2}^+$		
5150.71*		180	25	268	$P-E1$	445.75*	$\frac{5}{2}^+$	$\frac{5}{2}^+$		
5147.33	0.2	2168	5	3325	$S-E1$	449.16	$\frac{1}{2}^-, \frac{3}{2}^-$	$\frac{3}{2}^-$		Poor energy fit
5126.02*		<30		<46		470.44*	$\geq \frac{5}{2}^-, \frac{7}{2}^+$	$\frac{5}{2}^-$		
5106.04*		<30		<46		490.42*	$\geq \frac{5}{2}^-, \frac{7}{2}^+$	$\frac{7}{2}^-$		
5093.99	0.2	286	20	458	$S-M1$	502.49	$\frac{1}{2}^+, \frac{3}{2}^+$	$\frac{1}{2}^+$		

TABLE V. (Continued).

E_γ (keV)	ΔE_γ (keV)	I_γ (rel)	$\frac{\Delta I_\gamma}{I_\gamma}$ (%)	$\frac{I_\gamma(E_0)^5}{(E_\gamma)^5}$ (rel)	Group $L_n M \lambda$	$E_L(\text{ARC})$ (keV)	$J^\pi(\text{ARC})$	J^π (Level scheme)	Remarks
5091.66	0.4	99	30	158	P-E1	504.81	$\frac{5}{2}^+$	$\frac{3}{2}^+$	Questionable isotopic assignment
5075.32	0.2	296	10	483	S-M1	521.15	$\frac{1}{2}^+, \frac{3}{2}^+$	$\frac{3}{2}^+$	
4975.90*		<30		<54		620.56	$\geq \frac{5}{2}^-, \frac{7}{2}^+$	$\frac{5}{2}^-$	
4963.38	0.4	119	20	217	P-E1	632.58	$\frac{5}{2}^+$	$\frac{5}{2}^+$	
4933.27	0.4	239	10	448	S-M1	663.20	$\frac{1}{2}^+, \frac{3}{2}^+$	$\frac{3}{2}^+$	
4932.27*						663.59*	$\frac{5}{2}^-, \frac{7}{2}^-$	$\frac{5}{2}^-, \frac{7}{2}^-$	
4923.35	0.2	1144	10	2171	S-E1	693.12	$\frac{1}{2}^-, \frac{3}{2}^-$	$\frac{1}{2}^-, \frac{3}{2}^-$	
4893.00	0.2	847	10	1659	S-E1	703.46	$\frac{1}{2}^-, \frac{3}{2}^-$	$\frac{3}{2}^-$	
4878.59*		<40		<80		717.87*	$\geq \frac{5}{2}$		
4874.44	0.2	629	10	1263	S-E1	722.02	$\frac{1}{2}^-, \frac{3}{2}^-$	$\frac{1}{2}^-, \frac{3}{2}^-$	E1 shape
4855.28*						741.18*	$\frac{1}{2}^-, \frac{3}{2}^-$	$\frac{1}{2}^-, \frac{3}{2}^-$	Unresolved from 4854.48 keV line
4854.48	0.2	620	10	1263	S-E1	741.98	$\frac{1}{2}^-, \frac{3}{2}^-$	$\frac{5}{2}^-, \frac{7}{2}^-$	E1 shape
4841.66*		<40		<83		754.80*	$\geq \frac{5}{2}$		
4826.00	0.2	873	10	1831	S-E1	770.46	$\frac{1}{2}^-, \frac{3}{2}^-$	$\frac{5}{2}^-, \frac{7}{2}^-$	
4822.47*		<40		<84		773.99*	$\geq \frac{5}{2}$	$\frac{5}{2}^-$	
4804.53	0.4	91	20	194	P-E1	791.93	$\frac{5}{2}^+$	$\frac{5}{2}^-$	Questionable isotopic assignment
4791.71*		<30		<66		804.75*	$\geq \frac{5}{2}$	$\frac{5}{2}^-$	
4779.46*		<60		<132		822.00*	$\geq \frac{5}{2}$	$\frac{3}{2}^-, \frac{5}{2}^-$	
4773.37	0.2	656	10	1453	S-E1	823.10	$\frac{1}{2}^-, \frac{3}{2}^-$	$\frac{3}{2}^-, \frac{5}{2}^-$	E1 shape
4760.30	0.4	91	20	204	P-E1	836.17	$\frac{5}{2}^+$	$\frac{3}{2}^+, \frac{5}{2}^+$	Questionable isotopic assignment
4752.01	0.2	1475	10	3348	S-E1	844.45	$\frac{1}{2}^-, \frac{3}{2}^-$	$\frac{1}{2}^-, \frac{3}{2}^-$	
4737.71	0.4	71	20	165	P-E1	869.84	$\frac{5}{2}^+$	$\frac{5}{2}^+$	

the background lines appear with about the same intensity in all of the ARC spectra. *S*-wave capture in the 0^+ ground state of ^{150}Sm will always result in a $\frac{1}{2}^+$ capture state. Thus primary *E*1 transitions will be transitions to $\frac{1}{2}^-$ and $\frac{3}{2}^-$ states and appear as the strongest lines in Fig. 4 while *M*1 transitions from the $\frac{1}{2}^+$ capture state will be associated with transitions to $\frac{1}{2}^+$ and $\frac{3}{2}^+$ states and appear as the second strongest group of lines. The energies and relative intensities of these primary γ -ray transitions are calibrated with the $^{14}\text{N}(\bar{n},\gamma)^{15}\text{N}$ spectrum. This spectrum was obtained by adding a small amount of nitrogen gas to the He atmosphere that surrounds the in-pile sample.

The results are summarized in Table V. The first column is the energy of the primary γ ray, E_γ , obtained from the ARC data. These energies are corrected for the average energy of the captured neutron (see later discussion). The second column gives the error in this ARC gamma energy. The third column is the relative intensity of the γ ray and is followed (fourth column) by its error in percent. The fifth column is the normalized intensity, defined as the relative intensity multiplied by the ratio of $(E_0/E_\gamma)^5$ where E_0 is the neutron binding energy (5596.46 keV). This normalization is necessary to remove the energy dependence from the relative gamma strengths. After this normalization all of the *E*1 transitions to the $\frac{1}{2}^-$ and $\frac{3}{2}^-$ states should have about the same normalized intensity and the *M*1 transitions to the $\frac{1}{2}^+$ and $\frac{3}{2}^+$ states should have a consistently lower normalized intensity.

A plot of these normalized γ -ray intensities versus γ -ray energy appears in Fig. 5. Note how well the *E*1

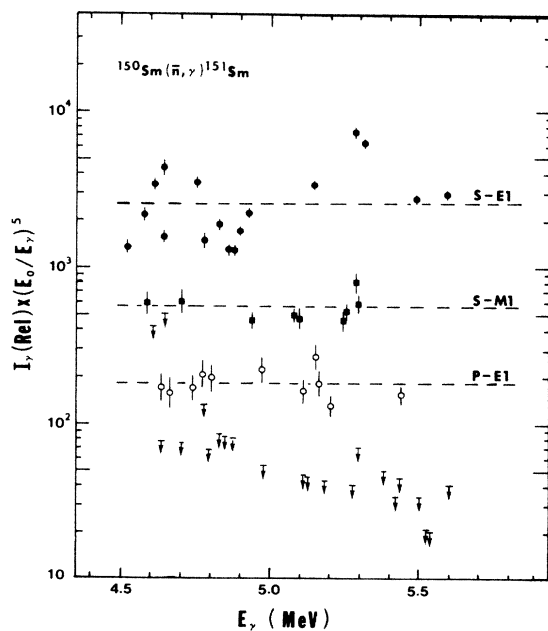


FIG. 5. Plot of the normalized ARC γ -ray intensities versus γ -ray energy. The filled circles, filled squares, and open circles are associated with the following intensity groups: *s*-wave capture followed by *E*1 radiation, *s*-wave capture followed by *M*1 radiation, and *p*-wave capture followed by *E*1 radiation, respectively. The horizontal bars with downward pointing arrows are upper limits on transitions to the other known levels.

transitions to $\frac{1}{2}^-$ and $\frac{3}{2}^-$ states separate from the *M*1 transitions to the $\frac{1}{2}^+$ and $\frac{3}{2}^+$ states. The lowest intensity group in Fig. 5 corresponds to either *s*-wave capture followed by *E*2 transitions to $\frac{5}{2}^+$ states or *p*-wave capture followed by *E*1 transitions to $\frac{5}{2}^+$ states. Most of the intensity in these transitions is believed to result from *p*-wave capture rather than *s*-wave capture. This fact is deduced from analysis of the line shapes of the three different intensity groups. The line shape of the *p*-wave group is much wider and its centroid is shifted farther up in energy than it is for the line shapes of the lines in the other two groups. This occurs because the *p*-wave capture process has a neutron energy distribution that is wider and extends higher in neutron energy than the *s*-wave capture distribution. This quite different line shape is shown in the insert in Fig. 4 where the region near the line associated with transitions to the $\frac{5}{2}^+$ level at 167.46 keV is shown in an expanded view. This shape is typical of the lines associated with *p*-wave neutron capture (see later discussion). The line shape of the “*S*-*M*1” group is slightly wider than the “*S*-*E*1” group. This suggests that the *S*-*M*1 transitions contain a *p*-wave component. This is expected, and, based on the population systematics of the capture states,³⁶ this component should be approximately equal to the intensity of the “*P*-*E*1” group. The multipole assignments obtained from these normalized relative intensities are given in the sixth column. The level energies deduced from the ARC gamma energies appear in the seventh column. In some cases only upper limits are given for gamma intensities where no primary transition was observed. In these cases the gamma energy is calculated using the energy level spacings in the final level scheme. The upper limits are plotted in Fig. 5 as horizontal bars with downward pointing arrows. These upper limits help confirm the higher spin assignment made for the associated levels based on other information. At the lower gamma energies the *E*1 and *M*1 intensity groups tend to merge so that it is sometimes harder to tell in which group to place a particular transition. In some cases it is possible to use the line shape to help make the assignment. When this was done it is noted in the “Remarks” column.

The small energy shifts associated with the average energy of the captured neutrons were removed from the ARC γ -ray energies given in the first column of Table V. This was done by first fitting the lines in each group with a standard line shape appropriate for each group and then subtracting the average energy shift for each group from the centroid energy. The average shifts (relative to thermal capture) for the groups *S*-*E*1, *S*-*M*1, and *P*-*E*1 were 0.22, 0.53, and 1.84 keV, respectively. The relative intensities quoted in Table V (third column) also come from this fit with standard line shapes and reflect the peak height of the fitted shape for each line. To obtain relative areas under each peak one should multiply the relative intensities of the *S*-*M*1 and *P*-*E*1 groups by 1.18 and 1.67, respectively.

C. Measurement of the $^{150}\text{Sm}(n_{\text{th}}, e^-)^{151}\text{Sm}$ reaction

The conversion electron spectrum of the reaction $^{150}\text{Sm}(n_{\text{th}}, e^-)^{151}\text{Sm}$ has been measured with the double-

TABLE VI. Conversion-electron data from thermal neutron capture in ^{150}Sm , measured with the Munich magnetic spectrometer.

E_γ (ΔE_γ) (keV)	I_γ (relative units)	Shell	E_e (ΔE_e) (keV)	I_e ($\Delta I_e/I_e$) (relative units)	α (expt)	$\Delta\alpha/\alpha$ (%)	α (theor) (Ref. 40)		Multipolarity	Remarks
							$\alpha(E1)$	$\alpha(E2)$		
35.15(6)	10.4±3.5	L1	27.33(15)	39(40)			0.32	0.62	4.04	$M1 + (20 \pm 10)\% E2$ E_γ, I_γ deduced from E_e, I_e
		L2	27.85(10)	117(20)			0.14	58.7	0.35	
		L3	28.29(10)	194(20)			0.21	76.6	0.07	
		M	33.44(15)	97(20)			0.21	49.0	1.3	
46.545(3)	3.6	L1	39.00(10)	51	7.1	35	0.16	0.49	1.69	Unresolved + KMN Auger
		L2	39.85(4)	54	7.5	35	0.056	14.1	0.15	
		L3	39.85(4)	54	7.5	35	0.077	17.4	0.027	
46.819(1)	3.5	L2	39.38(15)	58	17	35	0.056	14.1	0.15	$E2(+M1)$
		L3	40.20(7)	47	13	35	0.077	17.4	0.027	
		K	18.05(4)	78	3.7	25	0.74	3.29	5.12	
64.887(1)	21.3	L1	56.81(10)	20	0.94	40	0.075	0.30	0.70	$M1 + (50 \pm 30)\% E2$
		L2	57.36(10)	34	1.6	35	0.021	3.46	0.059	
		L3	58.05(3)	21	0.99	40	0.028	4.06	0.011	
		K	19.00(2)	76	3.5	25	0.71	3.21	4.87	
65.839(2)	21.9	L1	58.06(3)	13.2	0.60	35	0.072	0.29	0.68	$M1 + (15 \pm 5)\% E2$ $-K(104.851), -L3(64.887)$
		L2	58.42(13)	13.6	0.62	35	0.020	3.28	0.057	
		L3	59.08(23)	7.8	0.36	40	0.027	3.85	0.011	
		K	53.19(3)	42.3	1.46	15	0.23	1.20	1.46	
100.019(2)	29.0	L1	92.11(11)	11.3	0.39	40	0.024	0.11	0.20	Calibration line for I_e relative to I_γ
		L3		<5.8	<0.20		0.006	0.45	0.003	
		K	55.14(5)	<21	<0.96		0.22	1.15	1.35	
101.933(2)	21.9	K	55.14(5)	<21	<0.96		0.22	1.15	1.35	$M1 + E2$ $-L3(64.887), -L1(65.839)$
		L1	58.06(3)	42.73	1.0	30	0.20	1.05	1.25	
		L3		<5.8	<0.14		0.021	0.09	0.16	
104.851(5)	42.6	L3		<5.8	<0.14		0.0051	0.32	0.0024	$E2$ ^{152}Sm
		K	74.96(2)	260(10)			0.14	0.69	0.84	
		L1, L2		109(10)			0.017	0.24	0.12	
121.791(2)	(163.6)	L3		117(10)			0.0032	0.17	0.0016	$-K(167.772), -K(168.418)$
		M	120.38(4)	43(15)			0.0049	0.12	0.029	
		N	121.28(20)	12(30)						

TABLE VI. (Continued).

E_γ (ΔE_γ) (keV)	I_γ (relative units)	Shell	E_e (ΔE_e) (keV)	I_e ($\Delta I_e/I_e$) (relative units) (%)	α (expt)	$\Delta\alpha/\alpha$ (%)	$\alpha(E1)$	α (theor) (Ref. 40) $\alpha(E2)$	$\alpha(M1)$	Multipolarity	Remarks
147.546(2)	64.3	K	100.57(7)	23	0.36	25	0.082	0.39	0.49	$E2(+M1)$	
		L	140.40(10)	12.4	0.19	25	0.012	0.18	0.07		
167.772(3)	100.0	K	121.28(20)	4.7	0.05	60	0.056	0.25	0.33	E1	$-N(121.791), -K(168.418)$
168.418(3)	16.9	K	121.28(20)	4.7	0.28	60	0.056	0.25	0.33	$M1+(60\pm35)\% E2$	$-N(121.791), -K(168.418)$
244.725(3)	(54.3)	K	197.88(10)	23(30)	0.023		0.023	0.064	0.13	E2	^{152}Sm
		L	237.79(30)	5.8(50)	0.0032		0.0032	0.025	0.019		
280.151(3)	53.4	K	237.90(20)	17.5	0.33	30	0.015	0.053	0.087		^{152}Sm

focusing magnetic electron spectrometer at the FRM reactor in Munich.³⁷⁻³⁹ The target material was the same used before for the bent-crystal spectrometer measurements at Risø. Therefore, the ^{149}Sm contamination had been burnt up because of the high neutron capture cross section. The target was fabricated by electrospraying of $0.2 \text{ mg/cm}^2 \text{ Sm}_2\text{O}_3$ on an $80 \times 10 \text{ mm}^2$ Al foil. The spectrum was scanned repeatedly from 1 to 400 keV. Electrons up to 50 keV were preaccelerated by a -12 kV bias at the target. The momentum resolution was 0.4% at 200 keV. The results are shown in Table VI together with the theoretical conversion coefficients of Ref. 40.

The energies were calibrated with the precise bent-crystal spectrometer values. The L -subshell ratio of the 100.02 keV transition was used to determine the multipolarity of this line to be $M1$. The theoretical K -conversion coefficient of this line served to relate the conversion electron intensities to the γ intensities. Experimental conversion coefficients and deduced multipolarities are given also in Table VI.

III. LEVEL SCHEME OF ^{151}Sm

A. Generalities

Based on the (n, γ) results reported in the previous section, a level scheme for ^{151}Sm has been established. This level scheme, and the details of the γ transitions connecting individual levels, are presented partially in Fig. 6 and completely in Table VII. In Fig. 6 each level is characterized by its excitation energy (in keV) and its assignment for spin and parity. The shaded and unshaded width of a line representing a transition is related, respectively, to its measured γ intensity and its conversion electron intensity. Primary transitions feeding the low-energy levels are classified according to their $E1$, $M1$, or $E2$ character. A dashed line indicates an uncertain placement in the level scheme. Each transition in the scheme is furthermore identified by its energy (in keV). The arrangement of the data in Table VII is self-explanatory.

The approximate locations of many of the levels presented in this paper have been suggested by the primary transitions observed in the average resonance neutron capture experiment of Sec. II B, or by previously published measurements.^{2,6-10} These levels have been confirmed independently by using the crystal diffraction data of Sec. II A. This is done by the application of the Ritz combination principle. After an extensive search procedure, several new levels have been proposed. Up to a certain point, this can be done with sufficient confidence, owing to the superior precision of the transition energies measured by crystal diffraction. However, the Ritz combination principle clearly loses its usefulness above $\sim 900 \text{ keV}$. It breaks down because of an excessive number of accidental combinations. A number of possible additional levels are listed in Table VIII. These have been suggested by primary (\bar{n}, γ) transitions, and, in a few cases, by β decay¹⁰ or (d, p) measurements.⁶ However, the diffraction data cannot provide conclusive evidence for their existence due to interference from accidental combinations.

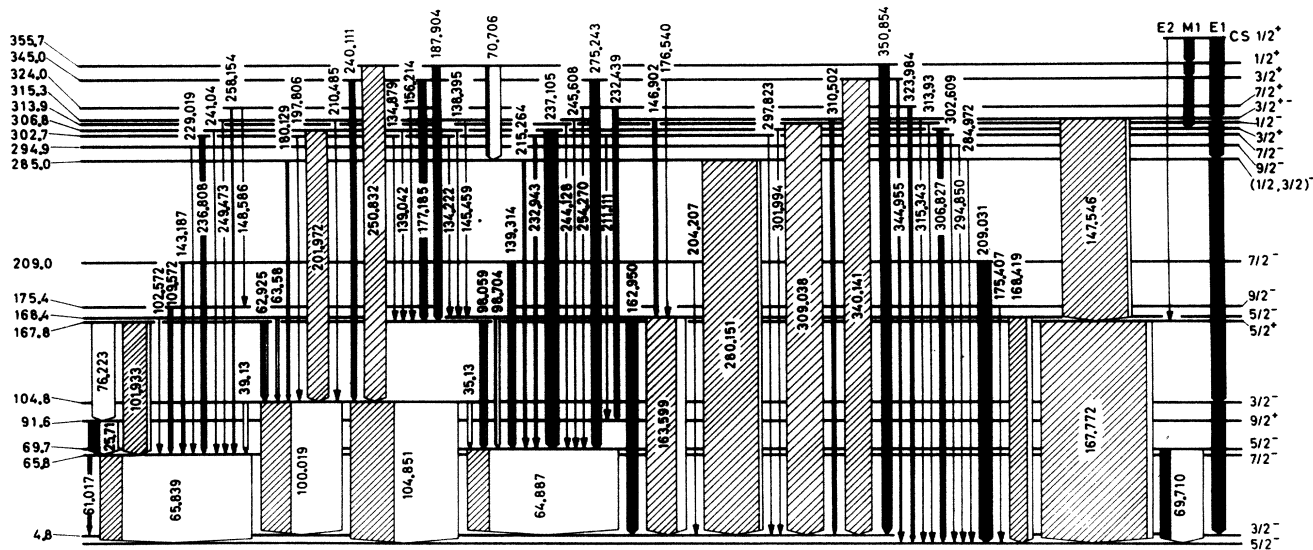


FIG. 6. Level scheme of ^{151}Sm up to 360 keV as deduced from (n,γ) measurements reported in this paper. Level energies (keV) and J^π assignments are given on the left and the right, respectively. Shaded and unshaded width of transitions indicate γ intensity and e^- intensity, respectively. A dashed line for a transition means that its placement in the scheme is uncertain. Primary transitions from average resonance neutron capture are drawn with different widths according to their multipole character.

Precise level energies are obtained from a least-squares calculation, minimizing the sum of squares of deviations between γ -transition energies and corresponding level energy differences. The resulting level energies and their errors are listed in Table IX. In the same sense as discussed in Sec. IIA, the consistency of the level energies can be checked by evaluating the Birge ratio for each level. One verifies that the values of the Birge ratio for the levels contained in Table IX are distributed around an average of 0.96 with a standard deviation of 0.18, which indeed testifies to an overall consistency. The consistency for individual levels can be checked by application of the F test to the variance ratio.

Concerning the assignment of J^π values to the levels, we have most heavily relied on multipolarities of primary transitions from (\bar{n},γ) reactions (Sec. IIB) and low-energy cascade transitions (Table VII), and on l -transfer values in (d,p) reactions.⁸ In addition, weaker arguments such as $\log ft$ values from β decay,¹⁰ selection rules involving asymptotic quantum numbers, and the decay pattern of a level are invoked as corroborative evidence or used to limit possible J^π values.

There are no serious discrepancies in the level structure below 600 keV based on (n,γ) data in comparison with that resulting from β decay proposed in Ref. 10. However, many complex lines occurring in the singles spectra of the latter work could only be unravelled by $\text{Ge}(\text{Li})$ - $\text{Ge}(\text{Li})$ coincidences, whereas these structures are clearly resolved in the crystal diffraction spectra. This is incisively illustrated by considering the line around 237 keV in the singles spectra. To explain the presence of all coincident lines one has to assume the existence of four transitions contained in the 237 keV structure. These correspond to the following four diffraction lines which are uniquely fitted in the level scheme at those locations consistent with

the coincidences: 236.711 keV (445.75 \rightarrow 209.03); 236.197 keV (521.18 \rightarrow 284.98); 236.808 keV (302.65 \rightarrow 65.84); and 237.105 keV (306.82 \rightarrow 69.71). Moreover, a fifth and previously unobserved transition of 236.421 keV (632.06 \rightarrow 395.62) has been found to belong to this multiplet as well (Table VII). It has been instructive to make a detailed comparison between the branching ratios of transitions deexciting from a particular level in both the (n,γ) and the β -decay work. Discrepancies often result from the difficulty in the $\text{Ge}(\text{Li})$ spectra to accurately divide the intensity between composing lines in a multiplet. Sometimes, transitions in one experiment or the other fall below the limit of sensitivity. An estimate of their intensity can then be made from the branching ratio of the corresponding transitions in the other measurement. This has helped to explain why some transitions are unobserved. It should be noted that above 600 keV the level schemes derived from (n,γ) and β decay diverge considerably.

B. Discussion of individual levels

In this subsection the characteristics of the most important levels of ^{151}Sm will be discussed for each level individually. First, it will be indicated how a particular level has been located in the level scheme. Then, the arguments for its spin-parity assignment will be presented. In order to avoid duplication of arguments, we refer the reader to previous work on the β decay to levels of ^{151}Sm (Ref. 10) and single-particle transfer reactions⁸ for well-established levels and their spin-parity assignments, especially those at low energy.

The ground state ($J^\pi = \frac{5}{2}^-$) and the 4.82 keV ($J^\pi = \frac{3}{2}^-$) level

The ground state spin of ^{151}Sm has been measured by electron paramagnetic resonance¹¹ and was found to be

TABLE VII. Summary of proposed levels in ^{151}Sm and their deexciting γ transitions. See also footnotes to Table II. Birge ratios and multiplicity are not given in this table.

E_i (keV)	I_i^π	E_f (keV)	I_f^π	E_γ (σE_γ) (keV)	I_γ ($\gamma/1000$ n)	σI_γ (%)	Comment
65.839	$\frac{7}{2}^-$	0.000	$\frac{5}{2}^-$	65.839(2)	18	22	$M1+E2$
69.712	$\frac{5}{2}^-$	0.000	$\frac{5}{2}^-$	69.710(2)	5.4	24	$M1+E2$
		4.824	$\frac{3}{2}^-$	64.887(1)	17	22	$M1+E2$
104.845	$\frac{3}{2}^-$	0.000	$\frac{5}{2}^-$	104.851(5)	34	20	$M1+E2$
		4.824	$\frac{3}{2}^-$	100.019(2)	23	20	$M1(+E2)$
167.773	$\frac{5}{2}^+$	0.000	$\frac{5}{2}^-$	167.772(3)	81	13	$E1$
		4.824	$\frac{3}{2}^-$	162.950(3)	8.6	13	($E1$)
		65.839	$\frac{7}{2}^-$	101.933(2)	18	20	$E1(+M2)$
		69.712	$\frac{5}{2}^-$	98.059(4)	4.3	21	($E1$)
		91.550	$\frac{9}{2}^+$	76.223(3)	2.5	25	($E2$)
		104.845	$\frac{3}{2}^-$	62.925(3)	2.8	33	
168.419	$\frac{5}{2}^-$	0.000	$\frac{5}{2}^-$	168.419(3)	13.8	13	$M1+E2$
		4.824	$\frac{3}{2}^-$	163.599(3)	21.7	14	$M1+E2$
		65.839	$\frac{7}{2}^-$	102.572(5)	0.39	41	
		69.712	$\frac{5}{2}^-$	98.704(2)	0.93	23	($M1,E2$)
175.411	$\frac{9}{2}^-$	0.000	$\frac{5}{2}^-$	175.407(15)	0.19	29	
		65.839	$\frac{7}{2}^-$	109.572(3)	1.5	21	
209.028	$\frac{7}{2}^-$	0.000	$\frac{5}{2}^-$	209.031(5)	8.8	9	$M1(+E2)$
		4.824	$\frac{3}{2}^-$	204.207(3)	0.65	10	($E2$)
		65.839	$\frac{7}{2}^-$	143.187(3)	1.19	17	$M1+E2$
		69.712	$\frac{5}{2}^-$	139.314(3)	2.9	17	$M1+E2$
284.976	$(\frac{1}{2}, \frac{3}{2})^-$	0.000	$\frac{5}{2}^-$	284.972(11)	0.32	10	
		4.824	$\frac{3}{2}^-$	280.151(3)	43	7	
		69.712	$\frac{5}{2}^-$	215.264(4)	1.74	11	
		104.845	$\frac{3}{2}^-$	180.129(3)	1.62	12	
294.857	$\frac{9}{2}^-$	0.000	$\frac{5}{2}^-$	294.850(7)	0.46	9	
		65.839	$\frac{7}{2}^-$	229.019(4)	0.84	9	
302.650	$\frac{7}{2}^-$	0.000	$\frac{5}{2}^-$	302.609(23)	0.8	56	
		4.824	$\frac{3}{2}^-$	297.823(5)	0.99	7	
		65.839	$\frac{7}{2}^-$	236.808(3)	4.1	9	
		69.712	$\frac{5}{2}^-$	232.943(3)	1.64	9	
		91.550	$\frac{9}{2}^+$	211.111(10)	0.19	18	
		104.845	$\frac{3}{2}^-$	197.806(8)	0.19	17	
		167.773	$\frac{5}{2}^+$	134.879(7)	0.28	29	
		168.419	$\frac{5}{2}^-$	134.222(8)	0.70	32	

TABLE VII. (Continued).

E_i (keV)	I_i^π	E_f (keV)	I_f^π	E_γ (σE_γ) (keV)	I_γ ($\gamma/1000$ n)	σI_γ (%)	Comment
306.818	$\frac{3}{2}^+$	0.000	$\frac{5}{2}^-$	306.827(5)	4.03	7	
		4.824	$\frac{3}{2}^-$	301.994(8)	0.73	10	
		65.839	$\frac{7}{2}^-$	241.04(7)	0.15	48	(M2)?
		69.712	$\frac{5}{2}^-$	237.105(3)	10.2	8	
		104.845	$\frac{3}{2}^-$	201.972(3)	16.6	10	E1(+M2)
		167.773	$\frac{5}{2}^+$	139.042(3)	0.62	19	
		168.419	$\frac{5}{2}^-$	138.395(4)	0.93	18	
313.854	$\frac{1}{2}^-$	0.000	$\frac{5}{2}^-$	313.93(3)	0.21	20	
		4.824	$\frac{3}{2}^-$	309.038(5)	26.2	5	
		69.712	$\frac{5}{2}^-$	244.128(8)	0.39	12	
315.320	$\frac{3}{2}^\pm$	0.000	$\frac{5}{2}^-$	315.343(8)	1.01	6	
		4.824	$\frac{3}{3}^-$	310.502(6)	3.48	8	
		65.839	$\frac{7}{2}^-$	249.473(6)	0.36	13	
		69.712	$\frac{5}{2}^-$	245.608(4)	1.01	8	
		104.845	$\frac{3}{2}^-$	210.485(9)	0.31	12	
		167.773	$\frac{5}{2}^+$	147.546(2)	50	16	E2(+M1)
		168.419	$\frac{5}{2}^-$	146.902(2)	1.60	15	
323.988	$\frac{7}{2}^+$	0.000	$\frac{5}{2}^-$	323.984(5)	3.18	6	E1(+M2)
		65.839	$\frac{7}{2}^-$	258.154(4)	1.60	7	E1(+M2)
		69.712	$\frac{5}{2}^-$	254.270(6)	0.43	9	
		91.550	$\frac{9}{2}^+$	232.439(3)	3.04	9	M1+E2
		167.773	$\frac{5}{2}^+$	156.214(4)	0.47	15	
		175.411	$\frac{9}{2}^-$	148.586(16)	0.23	35	
344.958	$\frac{3}{2}^+$	0.000	$\frac{5}{2}^-$	344.955(7)	1.72	7	E1(+M2)
		4.824	$\frac{3}{2}^-$	340.141(5)	20.2	6	
		69.712	$\frac{5}{2}^-$	275.243(5)	7.0	6	E1(+M2)
		104.845	$\frac{3}{2}^-$	240.111(3)	3.98	7	E1(+M2)
		167.773	$\frac{5}{2}^+$	177.185(2)	4.4	12	M1+E2
		168.419	$\frac{5}{2}^-$	176.540(3)	1.02	12	(E1)
355.678	$\frac{1}{2}^+$	4.824	$\frac{3}{2}^-$	350.854(5)	6.4	6	
		104.845	$\frac{3}{2}^-$	250.832(3)	15.3	8	
		167.773	$\frac{5}{2}^+$	187.904(2)	4.3	11	
		284.976	$(\frac{1}{2}, \frac{3}{2})^-$	70.706(3)	2.1	32	
395.625	$\frac{5}{2}^+$	0.000	$\frac{5}{2}^-$	395.75(7)	0.27	34	
		4.824	$\frac{3}{2}^-$	390.79(4)	0.23	20	
		65.839	$\frac{7}{2}^-$	329.785(6)	1.24	6	E1(+M2)
		69.712	$\frac{5}{2}^-$	325.906(8)	0.82	7	
		104.845	$\frac{3}{2}^-$	290.775(4)	5.2	6	E1(+M2)

TABLE VII. (*Continued*).

E_i (keV)	I_i^π	E_f (keV)	I_f^π	E_γ (σE_γ) (keV)	I_γ ($\gamma/1000$ n)	σI_γ (%)	Comment
395.625		167.773	$\frac{5}{2}^+$	227.850(6)	0.39	12	(M1, E2)
		168.419	$\frac{5}{2}^-$	227.206(4)	2.27	9	(E1)
		209.028	$\frac{7}{2}^-$	186.595(2)	1.19	11	(E1)
		302.650	$\frac{7}{2}^-$	92.978(5)	0.49	36	
415.689	$(\frac{5}{2}, \frac{7}{2})^-$	0.000	$\frac{5}{2}^-$	415.715(29)	0.79	14	
		4.824	$\frac{3}{2}^-$	410.865(12)	2.20	5	
		65.839	$\frac{7}{2}^-$	349.856(6)	4.6	7	M1+E2
		69.712	$\frac{5}{2}^-$	345.976(10)	0.83	8	
		104.845	$\frac{3}{2}^-$	310.853(7)	1.59	12	
		167.773	$\frac{5}{2}^+$	247.911(4)	0.87	8	
		168.419	$\frac{5}{2}^-$	247.263(4)	1.10	11	
		209.028	$\frac{7}{2}^-$	206.669(5)	1.17	10	M1+E2
		302.650	$\frac{7}{2}^-$	113.040(3)	0.56	23	
		445.747	$\frac{5}{2}^+$	0.000	$\frac{5}{2}^-$	445.758(9)	11.4
4.824	$\frac{3}{2}^-$			440.942(11)	3.2	22	E1(+M2)
65.839	$\frac{7}{2}^-$			379.917(8)	2.09	6	E1(+M2)
91.550	$\frac{9}{2}^+$			354.14(5)	0.27	16	
104.845	$\frac{3}{2}^-$			340.86(4)	0.51	22	
167.773	$\frac{5}{2}^+$			277.99(4)	0.22	37	(E2)
168.419	$\frac{5}{2}^-$			277.29(5)	0.17	22	
209.028	$\frac{7}{2}^-$			236.711(10)	0.40	21	(E1)
315.320	$\frac{3}{2}^\pm$			130.426(5)	0.32	28	
448.624	$\frac{3}{2}^-$			0.000	$\frac{5}{2}^-$	448.613(9)	10.4
		4.824	$\frac{3}{2}^-$	443.809(13)	8.7	6	
		69.712	$\frac{5}{2}^-$	378.912(6)	3.14	7	
		104.845	$\frac{3}{2}^-$	343.788(16)	0.32	10	
		167.773	$\frac{5}{2}^+$	280.851(8)	0.55	10	
		168.419	$\frac{5}{2}^-$	280.210(11)	2.1	34	
470.442	$\frac{5}{2}^-$	0.000	$\frac{5}{2}^-$	470.471(14)	2.40	7	
		65.839	$\frac{7}{2}^-$	404.617(9)	5.62	5	
		69.712	$\frac{5}{2}^-$	400.738(15)	0.93	8	
		167.773	$\frac{5}{2}^+$	302.666(6)	1.76	6	
		209.028	$\frac{7}{2}^-$	261.416(5)	1.03	7	
		323.988	$\frac{7}{2}^+$	146.453(3)	0.71	16	
		344.958	$\frac{3}{2}^+$	125.485(8)	0.31	48	
490.426	$\frac{7}{2}^-$	0.000	$\frac{5}{2}^-$	490.36(4)	0.64	14	
		65.839	$\frac{7}{2}^-$	424.637(30)	0.89	7	
		69.712	$\frac{5}{2}^-$	420.73(6)	0.46	26	

TABLE VII. (Continued).

E_i (keV)	I_i^π	E_f (keV)	I_f^π	E_γ (σE_γ) (keV)	I_γ ($\gamma/1000$ n)	σI_γ (%)	Comment
490.426		91.550	$\frac{9}{2}^+$	398.87(6)	0.29	29	
		104.845	$\frac{3}{2}^-$	385.59(5)	0.26	27	
		168.419	$\frac{5}{2}^-$	322.016(10)	0.66	6	
		175.411	$\frac{9}{2}^-$	315.004(17)	0.24	13	
		294.857	$\frac{9}{2}^-$	195.559(17)	0.17	53	
502.324	$\frac{1}{2}^+$	4.824	$\frac{3}{2}^-$	497.488(13)	6.53	4	
		104.845	$\frac{3}{2}^-$	397.45(8)	0.19	39	
		167.773	$\frac{5}{2}^+$	334.554(7)	1.10	6	
		306.818	$\frac{3}{2}^+$	195.500(4)	0.60	11	
		313.854	$\frac{1}{2}^-$	188.471(2)	3.6	11	
		315.320	$\frac{3}{2}^\pm$	187.006(2)	4.2	11	
		344.958	$\frac{3}{2}^+$	157.371(5)	1.99	15	
521.177	$\frac{3}{2}^+$	0.000	$\frac{5}{2}^-$	521.21(6)	0.85	12	
		4.824	$\frac{3}{2}^-$	516.364(17)	5.22	6	
		69.712	$\frac{5}{2}^-$	451.467(9)	7.6	4	$E1(+M2)$
		167.773	$\frac{5}{2}^+$	353.396(6)	2.47	6	$M1+E2$
		168.419	$\frac{5}{2}^-$	352.74(4)	0.17	22	
		284.976	$(\frac{1}{2}, \frac{3}{2})^-$	236.197(3)	2.53	8	
		313.854	$\frac{1}{2}^-$	207.342(10)	0.18	18	
		315.320	$\frac{3}{2}^\pm$	205.868(5)	0.25	13	
		344.958	$\frac{3}{2}^+$	176.225(8)	0.20	21	
		355.678	$\frac{1}{2}^+$	165.501(11)	0.14	33	
		395.625	$\frac{5}{2}^+$	125.548(4)	0.47	23	
		415.689	$(\frac{5}{2}, \frac{7}{2})^-$	105.492(6)	0.32	46	
		620.568	$\frac{5}{2}^-$	0.000	$\frac{5}{2}^-$	620.562(24)	5.66
65.839	$\frac{7}{2}^-$			554.76(6)	1.10	12	
69.712	$\frac{5}{2}^-$			550.86(3)	1.22	8	
168.419	$\frac{5}{2}^-$			452.161(18)	1.53	8	
209.028	$\frac{7}{2}^-$			411.50(5)	0.24	21	
344.958	$\frac{3}{2}^+$			275.601(21)	0.27	25	
632.061	$\frac{5}{2}^+$			0.000	$\frac{5}{2}^-$	632.07(5)	2.13
		69.712	$\frac{5}{2}^-$	562.30(20)	0.41	46	
		167.773	$\frac{5}{2}^+$	464.29(3)	0.91	17	
		209.028	$\frac{7}{2}^-$	423.038(18)	0.84	8	
		306.818	$\frac{3}{2}^+$	325.242(8)	0.88	6	
		323.988	$\frac{7}{2}^+$	308.083(9)	0.48	9	
		355.678	$\frac{1}{2}^+$	276.347(24)	0.19	35	
		395.625	$\frac{5}{2}^+$	236.421(17)	0.23	20	
		415.689	$(\frac{5}{2}, \frac{7}{2})^-$	216.31(9)	0.20	74	
		448.624	$\frac{3}{2}^-$	183.437(4)	0.34	12	
		521.177	$\frac{3}{2}^+$	110.885(3)	1.00	22	

TABLE VII. (*Continued*).

E_i (keV)	I_i^π	E_f (keV)	I_f^π	E_γ (σE_γ) (keV)	I_γ ($\gamma/1000$ n)	σI_γ (%)	Comment
663.052	$\frac{3}{2}^+$	4.824	$\frac{3}{2}^-$	658.16(9)	1.39	15	$^{151}\text{Sm} (+ \ ^{114}\text{Cd})$
		69.712	$\frac{5}{2}^-$	593.47(9)	0.67	20	
		104.845	$\frac{3}{2}^-$	558.15(6)	1.33	10	
		167.773	$\frac{5}{2}^+$	495.246(17)	3.26	5	
		168.419	$\frac{5}{2}^-$	494.59(14)	0.47	48	
		284.976	$(\frac{1}{2}, \frac{3}{2})^-$	378.066(9)	1.50	7	
		306.818	$\frac{3}{2}^+$	356.20(4)	0.17	19	
		313.854	$\frac{1}{2}^-$	349.198(6)	3.23	7	
		315.320	$\frac{3}{2}^\pm$	347.734(10)	0.88	14	
		355.678	$\frac{1}{2}^+$	307.378(6)	0.73	8	
		395.625	$\frac{5}{2}^+$	267.407(11)	0.21	16	
		415.689	$(\frac{5}{2}, \frac{7}{2})^-$	247.365(14)	0.22	20	
		445.747	$\frac{5}{2}^+$	217.309(4)	1.07	10	
		470.442	$\frac{5}{2}^-$	192.611(4)	1.92	10	
		663.587	$(\frac{5}{2}, \frac{7}{2})^-$	0.000	$\frac{5}{2}^-$	663.64(13)	
65.839	$\frac{7}{2}^-$			597.81(12)	1.7	39	
294.857	$\frac{9}{2}^-$			368.67(6)	0.15	25	
302.650	$\frac{7}{2}^-$			360.95(4)	0.24	20	
703.272	$\frac{3}{2}^-$	0.000	$\frac{5}{2}^-$	703.34(17)	1.3	27	
		4.824	$\frac{3}{2}^-$	698.51(9)	1.89	12	
		65.839	$\frac{7}{2}^-$	637.39(21)	0.64	39	
		167.773	$\frac{5}{2}^+$	535.513(28)	2.50	7	
		168.419	$\frac{5}{2}^-$	534.85(7)	0.79	18	
		306.818	$\frac{3}{2}^+$	396.47(4)	0.30	17	
		315.320	$\frac{3}{2}^\pm$	387.89(3)	0.28	22	
		355.678	$\frac{1}{2}^+$	347.598(8)	1.59	5	
		395.625	$\frac{5}{2}^+$	307.66(4)	0.31	45	
		445.747	$\frac{5}{2}^+$	257.523(6)	0.44	11	
		448.624	$\frac{3}{2}^-$	254.645(14)	0.19	15	
		721.955	$(\frac{1}{2}, \frac{3}{2})^-$	4.824	$\frac{3}{2}^-$	717.11(4)	5.7
306.818	$\frac{3}{2}^+$			414.93(21)	0.25	47	
313.854	$\frac{1}{2}^-$			408.07(17)	0.24	38	
315.320	$\frac{3}{2}^\pm$			406.644(14)	1.32	5	
355.678	$\frac{1}{2}^+$			366.275(8)	1.72	5	
448.624	$\frac{3}{2}^-$			273.333(8)	0.31	11	
521.177	$\frac{3}{2}^+$			200.776(7)	0.19	15	
741.181	$\frac{3}{2}^-$			4.824	$\frac{3}{2}^-$	736.24(12)	2.7
		69.712	$\frac{5}{2}^-$	671.43(4)	7.0	13	
		104.845	$\frac{3}{2}^-$	636.317(25)	7.3	4	

TABLE VII. (Continued).

E_i (keV)	I_i^π	E_f (keV)	I_f^π	E_γ (σE_γ) (keV)	I_γ ($\gamma/1000$ n)	σI_γ (%)	Comment
741.181		313.854	$\frac{1}{2}^-$	427.25(4)	0.40	16	
		344.958	$\frac{3}{2}^+$	396.06(13)	0.36	26	
		445.747	$\frac{5}{2}^+$	295.53(10)	0.14	45	
		470.442	$\frac{5}{2}^-$	270.748(11)	0.28	12	
754.793	$(\frac{5}{2}, \frac{7}{2})^-$	209.028	$\frac{7}{2}^-$	545.93(11)	0.41	30	
		294.857	$\frac{9}{2}^-$	459.80(12)	0.89	18	
		315.320	$\frac{3}{2}^\pm$	439.466(12)	1.6	74	$^{150}\text{Sm} (+ ^{151}\text{Sm})$
		323.988	$\frac{7}{2}^+$	430.89(12)	0.20	49	
		395.625	$\frac{5}{2}^+$	359.21(6)	0.18	37	
		490.426	$\frac{7}{2}^-$	264.41(4)	0.15	44	
774.009	$\frac{5}{2}^-$	69.712	$\frac{5}{2}^-$	704.29(6)	3.4	9	
		104.845	$\frac{3}{2}^-$	669.23(5)	2.81	8	
		175.411	$\frac{9}{2}^-$	598.73(9)	1.6	19	
		294.857	$\frac{9}{2}^-$	479.52(21)	0.47	37	
		302.650	$\frac{7}{2}^-$	471.33(9)	0.41	26	
		306.818	$\frac{3}{2}^+$	466.88(25)	0.32	46	
		415.689	$(\frac{5}{2}, \frac{7}{2})^-$	358.317(10)	0.78	6	
804.721	$\frac{5}{2}^-$	65.839	$\frac{7}{2}^-$	739.02(21)	1.5	27	
		104.845	$\frac{3}{2}^-$	699.77(10)	1.54	15	
		167.773	$\frac{5}{2}^+$	636.71(17)	1.8	55	
		209.028	$\frac{7}{2}^-$	595.71(11)	0.74	21	
		284.976	$(\frac{1}{2}, \frac{3}{2})^-$	519.65(5)	0.55	21	
		313.854	$\frac{1}{2}^-$	490.77(19)	0.30	62	
		344.958	$\frac{3}{2}^+$	459.80(12)	0.89	18	
		445.747	$\frac{5}{2}^+$	358.995(23)	0.21	22	
821.986	$(\frac{3}{2}, \frac{5}{2})^-$	0.000	$\frac{5}{2}^-$	822.0(6)	2.6	36	
		4.824	$\frac{3}{2}^-$	817.1(3)	1.5	44	
		69.712	$\frac{5}{2}^-$	752.42(12)	2.9	46	
		104.845	$\frac{3}{2}^-$	717.11(4)	5.7	9	
		209.028	$\frac{7}{2}^-$	612.93(15)	1.3	31	
		284.976	$(\frac{1}{2}, \frac{3}{2})^-$	536.82(12)	0.50	25	
		313.854	$\frac{1}{2}^-$	508.25(25)	1.0	40	
		344.958	$\frac{3}{2}^+$	477.18(22)	0.46	38	(^{114}Cd)
		445.747	$\frac{5}{2}^+$	376.27(4)	0.29	35	
822.752	$(\frac{3}{2}, \frac{5}{2})^\pm$	69.712	$\frac{5}{2}^-$	752.96(14)	2.0	18	
		104.845	$\frac{3}{2}^-$	717.90(4)	7.3	7	
		344.958	$\frac{3}{2}^+$	477.94(13)	0.34	47	
		415.689	$(\frac{5}{2}, \frac{7}{2})^-$	407.08(5)	0.30	22	
		445.747	$\frac{5}{2}^+$	376.998(10)	0.79	7	

TABLE VII. (*Continued*).

E_i (keV)	I_i^π	E_f (keV)	I_f^π	E_γ (σE_γ) (keV)	I_γ ($\gamma/1000$ n)	σI_γ (%)	Comment
822.752		703.272	$\frac{3}{2}^-$	119.480(5)	0.55	33	
920.772	$(\frac{1}{2}, \frac{3}{2})^\pm$	284.976	$(\frac{1}{2}, \frac{3}{2})^-$	635.83(10)	3.3	51	
		355.678	$\frac{1}{2}^+$	565.121(28)	2.36	6	
		448.624	$\frac{3}{2}^-$	472.29(8)	0.63	26	
		502.324	$\frac{1}{2}^+$	418.48(5)	0.47	21	
		822.752	$(\frac{3}{2}, \frac{5}{2})^\pm$	98.008(13)	0.64	46	
951.404	$\frac{3}{2}^-$	0.000	$\frac{5}{2}^-$	951.28(15)	7.0	14	$E1(+M2)$
		65.839	$\frac{7}{2}^-$	885.97(23)	3.0	28	
		167.773	$\frac{5}{2}^+$	783.57(8)	4.0	10	
		302.650	$\frac{7}{2}^-$	648.78(6)	0.92	19	
		313.854	$\frac{1}{2}^-$	637.39(21)	0.64	39	
		344.958	$\frac{3}{2}^+$	606.56(6)	1.51	9	
		355.678	$\frac{1}{2}^+$	595.71(11)	0.74	21	
		395.625	$\frac{5}{2}^+$	555.84(11)	0.72	27	
		445.747	$\frac{5}{2}^+$	505.70(6)	2.3	47	
		521.177	$\frac{3}{2}^+$	430.22(11)	0.24	43	
953.575	$\frac{3}{2}^+$	4.824	$\frac{3}{2}^-$	948.73(22)	5.1	19	$E1(+M2)$
		104.845	$\frac{3}{2}^-$	848.81(14)	3.4	17	$E1(+M2)$
		168.419	$\frac{5}{2}^-$	785.23(14)	1.9	23	$E1(+M2)$
		804.721	$\frac{5}{2}^-$	148.853(13)	0.17	49	
960.484	$\frac{7}{2}^\pm$	168.419	$\frac{5}{2}^-$	792.08(13)	2.0	21	
		445.747	$\frac{5}{2}^+$	514.786(29)	2.47	10	
		632.061	$\frac{5}{2}^+$	328.383(26)	0.6	53	
1017.296	$\frac{3}{2}^+$	344.958	$\frac{3}{2}^+$	672.52(12)	2.22	12	
		355.678	$\frac{1}{2}^+$	661.75(14)	0.91	25	
		415.689	$(\frac{5}{2}, \frac{7}{2})^-$	601.46(15)	0.90	32	
		448.624	$\frac{3}{2}^-$	568.55(8)	0.64	19	
		620.568	$\frac{5}{2}^-$	396.75(13)	0.32	29	
		741.181	$\frac{3}{2}^-$	276.104(17)	0.50	46	
		951.404	$\frac{3}{2}^-$	65.894(6)	1.5	49	

$J = \frac{5}{2}$. We have reevaluated the multipolarity of the ground state transition from the first excited state at 4.82 keV to be $M1 + (0.5 \pm 0.2)\% E2$. This is derived from a measurement of internal conversion M -subshell ratios by Geiger *et al.*¹² The $E2$ admixture is enhanced by a factor of 10 compared to Geiger's original derivation because of the present availability of improved tables of conversion coefficients.⁴⁰ In any case, the ground state must have the

same parity as the 4.82 keV state. The latter state is fed by an $E1$ transition in average resonance capture (Table V). One therefore concludes that $J^\pi(4.82 \text{ keV}) = \frac{3}{2}^-$ and $J^\pi(\text{g.s.}) = \frac{5}{2}^-$. This also explains why no ground state transition is observed in (\bar{n}, γ) . The same conclusions can be drawn from angular distribution measurements in (d, t) , $(^3\text{He}, \alpha)$, (t, p) , and (p, t) reactions to levels of ^{151}Sm (Refs. 8 and 13).

TABLE VIII. Additional levels of ^{151}Sm suggested by (\bar{n}, γ) , β decay, and (d,p) measurements. The evidence from (n_{th}, γ) measurements is not conclusive because of interference from accidental combinations. Level energies derived from Ritz combinations are listed with an appropriate qualification describing their likelihood of not being spurious.

(\bar{n}, γ)	β^{-a}	E_x (keV)		(n_{th}, γ) , bent crystal
		(d,p) ^b		
357.98(M 1)			357.923(26)	Not conclusive
505.28(E 2)			505.030(10)	Not conclusive
673.12(E 1)		672	672.815(6)	Probable
		713	712.773(7)	Possible
770.46(E 1)		767	769.662(15)	Doubtful
	777.4		777.603(5)	Not conclusive
791.93(E 2)			792.458(9)	Not conclusive
836.17(E 2)		832	836.919(41)	Possible
844.45(E 1)		846	842.719(17)	Doubtful
	851.6		850.637(17)	Not conclusive
869.82(E 2)			869.856(10)	Contradictory to E 2
877.13(E 2)	877.54	875	877.016(13)	Probable
	887.35			
	888.9			
898.38(M 1)			898.835(14)	Possible
937.00(E 2)			936.275(23)	Probable
955.50(E 1)	953.41	954	955.719(8)	Probable
964.90(E 2)	964.15		964.039(13)	Doubtful
1020.74(E 1)		1020	1020.420(10)	Probable
1077.57(E 1)		1080	1077.131(24)	Probable
1087.78(E 1)				
1115.79(M 1)				
1139.89(M 1)				
1193.86(E 1)		1190		
1205.65(M 1)				
1211.60(E 1)		1210		
1220.00(E 1)				

^aFrom Cook *et al.* (Ref. 10).

^bFrom Kenefick and Sheline (Ref. 6).

The 65.84 keV ($J^\pi = \frac{7}{2}^-$) level

This level decays to the ground state by a strong transition (22%) of multipolarity $M1 + (15 \pm 5)\% E2$ (Table VI), suggesting $J^\pi = (\frac{3}{2}, \frac{5}{2}, \frac{7}{2})^-$. The $J = \frac{3}{2}$ possibility contradicts the $l=3$ angular distribution in (d,t) (Ref. 8), as well as the $l=0$ transfer from the $J^\pi = \frac{7}{2}^-$ ground state of ^{149}Sm in $^{149}\text{Sm}(t, p)^{151}\text{Sm}$ (Ref. 13). Since this level is directly populated in the decay of the $J^\pi = \frac{11}{2}^-$ isomeric state at 261.1 keV (Ref. 14), $J^\pi = \frac{7}{2}^-$ is the logical choice. No primary transition to this level has been observed in (\bar{n}, γ) . There is evidence from coincidence measurements¹⁰ for a very weak transition of 61.02 keV to the 4.82 keV level (Fig. 6). The intensity corresponds to only 0.18% in the Risø experiment, which is far below the sensitivity at this energy (Fig. 2). It has been observed, though, in the special run with high sensitivity at the Argonne crystal spectrometer (Table III).

The 69.71 keV ($J^\pi = \frac{5}{2}^-$) level

This level decays by $M1 + (1.8 \pm 1.8)\% E2$ to the ground state³⁻⁵ and by $M1 + (50 \pm 30)\% E2$ to the 4.82

keV state (Table VI). Angular distributions in (d,t), and (d,t) to $(^3\text{He}, \alpha)$ cross section ratios are consistent with $l=3$ transfer.⁸ Therefore, $J^\pi = \frac{5}{2}^-$ is suggested. The primary transition from the capture state in (\bar{n}, γ) accordingly would be $M2$ and, not surprisingly, has not been detected.

The 91.55 keV ($J^\pi = \frac{9}{2}^+$) level

No direct population of this state from the $J^\pi = \frac{1}{2}^+$ compound state in (\bar{n}, γ) or from the β decay of the $J^\pi = \frac{5}{2}^+$ ground state of ^{151}Pm is evident.¹⁰ This may point to a relatively high spin for the 91.55 keV level. Indeed, this level is directly populated in the decay of the 261.1 keV isomeric state ($J^\pi = \frac{11}{2}^-$) as well as through a level at 147.9 keV (Ref. 14). Evidence from single-particle transfer reactions⁸ indicates that the latter has $J^\pi = \frac{13}{2}^+$. Furthermore, the Argonne data (Tables III and IV) reveal a 25.71 keV transition (Fig. 6) from 91.55 keV to 65.84 keV ($J^\pi = \frac{7}{2}^-$). This is the only observable decay channel of this level and, most likely, it proceeds by $E1$.² Therefore, we believe that $J^\pi(91.55 \text{ keV}) = \frac{9}{2}^+$.

TABLE IX. Least-squares adjusted level energies in ^{151}Sm derived from bent-crystal γ data.

E_x (keV)	σ (keV)	J^π	$E_{(n,\gamma)}$ (keV)	$E(M)\lambda$	E_x (keV)	σ (keV)	J^π	$E_{(n,\gamma)}$ (keV)	$E(M)\lambda$
0.0		$\frac{5}{2}^-$			448.624	0.003	$\frac{3}{2}^-$	449.13	$E1$
4.8236	0.0014	$\frac{3}{2}^-$	4.83	$E1$	470.4422	0.0023	$\frac{5}{2}^-$		
65.8395	0.0013	$\frac{7}{2}^-$			490.426	0.007	$\frac{7}{2}^-$		
69.7117	0.0013	$\frac{5}{2}^-$			502.3245	0.0020	$\frac{1}{2}^+$	502.95	$M1$
91.5498	0.0025	$\frac{9}{2}^+$			521.1767	0.0021	$\frac{3}{2}^+$	521.48	$M1$
104.8454	0.0015	$\frac{3}{2}^-$	104.77	$E1$	620.568	0.011	$\frac{5}{2}^-$		
167.7735	0.0013	$\frac{5}{2}^+$	167.46	$E2$	632.0614	0.0027	$\frac{5}{2}^+$	633.08	$E2$
168.4188	0.0014	$\frac{5}{2}^-$			663.0524	0.0026	$\frac{3}{2}^+$	663.20	$M1$
175.4114	0.0029	$\frac{9}{2}^-$			663.587	0.032	$(\frac{5}{2}, \frac{7}{2})^-$		
209.0276	0.0017	$\frac{7}{2}^-$			703.272	0.005	$\frac{3}{2}^-$	703.46	$E1$
284.9758	0.0019	$(\frac{1}{2}, \frac{3}{2})^-$	285.65	$E1$	721.955	0.005	$(\frac{1}{2}, \frac{3}{2})^-$	722.02	$E1$
294.8575	0.0035	$\frac{9}{2}^-$			741.181	0.009	$\frac{3}{2}^-$	741.98	$E1$
302.6496	0.0018	$(\frac{5}{2}, \frac{7}{2})^-$			754.793	0.011	$(\frac{5}{2}, \frac{7}{2})^-$		
306.8180	0.0017	$\frac{3}{2}^+$	307.30	$M1$	774.009	0.010	$\frac{5}{2}^-$		
313.8535	0.0025	$\frac{1}{2}^-$	314.37	$E1$	804.721	0.020	$\frac{5}{2}^-$		
315.3197	0.0016	$\frac{3}{2}^\pm$	315.99	$E1$	821.986	0.029	$(\frac{3}{2}, \frac{5}{2})^-$		
323.9879	0.0020	$\frac{7}{2}^+$			822.752	0.006	$(\frac{3}{2}, \frac{5}{2})^\pm$	823.10	$E1$
344.9575	0.0017	$\frac{3}{2}^+$	345.07	$M1$	920.772	0.012	$(\frac{1}{2}, \frac{3}{2})^\pm$		
355.6783	0.0019	$\frac{1}{2}^+$	355.73	$M1$	951.404	0.016	$\frac{3}{2}^-$	951.59	$E1$
395.6247	0.0019	$\frac{5}{2}^+$	395.90	$E2$	953.575	0.023	$\frac{3}{2}^+$		
415.6888	0.0020	$(\frac{5}{2}, \frac{7}{2})^-$			960.484	0.020	$\frac{7}{2}^\pm$		
445.7472	0.0027	$\frac{5}{2}^+$	446.06	$E2$	1017.296	0.015	$\frac{3}{2}^+$	1015.90	$M1$

The 104.85 keV ($J^\pi = \frac{3}{2}^-$) level

The principal decay of this level is to the ground state by an $M1 + (1.0 \pm 0.5)\%$ $E2$ transition³⁻⁵ (Table VI) and to the 4.82 keV state by an $M1 + (\leq 1.0 \pm 0.4)\%$ $E2$ transition.^{3,4} Hence, $J^\pi = (\frac{3}{2}, \frac{5}{2})^-$. The $\frac{5}{2}^-$ possibility is excluded on the basis of an $E1$ transition feeding this level in (\bar{n}, γ) . Therefore, $J^\pi = \frac{3}{2}^-$. This is confirmed by the existence of a strong 250.83 keV transition into this level from a state at 355.68 keV, the spin and parity of which can independently be determined to be $J^\pi = \frac{1}{2}^+$ (see below). The decay of the 104.85 keV state by a 35.13 keV transition to the level at 69.71 keV, hinted at by the 291 keV gated coincidences,¹⁰ is supported by the crystal data from Argonne (Fig. 6 and Table III). From subshell ratios of conversion electron intensities in (n_{th}, e^-) , one obtains for the multipolarity of this transition $M1 + (20 \pm 10)\%$ $E2$ (Table VI). Finally, a hitherto unobserved transition of 39.01 keV has been found which fits the decay 104.85 keV \rightarrow 65.84 keV (Fig. 6 and Table III).

The 167.77 keV ($J^\pi = \frac{5}{2}^+$) and 168.42 keV ($J^\pi = \frac{5}{2}^-$) levels

The 167.77 keV level is strongly populated both in (n, γ) and from the β decay of ^{151}Pm . It is firmly established by γ transitions to all lower-lying levels discussed above (Fig. 6). The primary transition into this level after average resonance neutron capture is $E2$, thus indicating $J^\pi = \frac{5}{2}^+$. This assignment is in agreement with $E1$ decay to the ground state (Table VI and Ref. 5) and the 65.84 keV state,³ and $E2$ decay to the $\frac{9}{2}^+$ state at 91.55 keV (Ref. 2). The remaining transitions of 162.95 and 98.06 keV are most likely $E1$ (Ref. 2), thus supporting the given assignment.

The diffraction data clearly demonstrate the existence of a 102.57 keV transition from the 168.42 keV to the 65.84 keV level (Fig. 6). This transition was only weakly observed in the 654 keV gated coincidence spectrum.¹⁰ No contradiction was found in the present data with the assignment $J^\pi(168.42 \text{ keV}) = \frac{5}{2}^-$ in Refs. 8 and 10.

The 175.41 keV ($J^\pi = \frac{9}{2}^-$) and 209.03 keV ($J^\pi = \frac{7}{2}^-$) levels

The position of the 175.41 keV level and its $J^\pi = \frac{9}{2}^-$ assignment are based on single-particle transfer reactions and isomeric decay.¹⁰ In the present data, the previously unobserved ground state transition of 175.41 keV has been identified.

Multipolarities of the deexciting transitions from the 209.03 keV level^{2,4} and (d,t) angular distributions⁸ restrict the choices for the spin to $J^\pi = (\frac{5}{2}, \frac{7}{2})^-$. But the angular correlation measurement of Singh and Johns¹⁵ is consistent only with $J^\pi = \frac{7}{2}^-$.

The 284.98 keV ($J^\pi = \frac{1}{2}^-, \frac{3}{2}^-$) level

Strong direct population from the compound state after thermal neutron capture is characteristic for this level.¹⁶ This has allowed us to identify two new transitions from the present data: a weak ground state transition of 284.97 keV and a 180.13 keV transition to the 104.85 keV level. The $E1$ multipolarity feeding the 284.98 keV level in average resonance capture indicates $J^\pi = (\frac{1}{2}, \frac{3}{2})^-$. However, the former possibility is favored considering the $\log f_0 t > 9.8$ in β decay.¹⁰

*The 294.86 keV ($J^\pi = \frac{9}{2}^-$)
and 302.65 keV ($J^\pi = \frac{5}{2}^-, \frac{7}{2}^-$) levels*

The first of these levels provides important clues as to the model interpretation of the ^{151}Sm structure (Sec. IV). Its spin has been determined from angular distributions of γ rays following Coulomb excitation by Straume *et al.*¹⁷ Based on the decay pattern of the 302.65 keV level and the $\log f_0 t$ value, Cook *et al.*¹⁰ proposed $J^\pi = (\frac{3}{2}, \frac{5}{2}, \frac{7}{2})^-$. Two more deexciting transitions are added from the present data: 197.81 keV to the 104.85 keV ($\frac{9}{2}^+$) level and 211.11 keV to the 91.55 keV ($\frac{7}{2}^-$) level. This would seem to be consistent only with $J^\pi = \frac{7}{2}^-$. However, since this argument hinges on the assumption that the latter weak transition is not $M2$, the possibility of $J^\pi = \frac{5}{2}^-$ cannot be excluded.

The 306.82 keV ($J^\pi = \frac{3}{2}^+$) level

Among all the levels observed in (n_{th}, γ) , this is the one that probably receives the highest fraction of direct population.¹⁶ Results from (\bar{n}, γ) (Table V) indicate $J^\pi = (\frac{1}{2}, \frac{3}{2})^+$. Since this level is strongly excited by $l=2$ transfer in (d,t),⁸ the lower spin is to be rejected. This is confirmed by γ - γ angular correlation measurements.^{3,15} Previously unresolved transitions to the 4.82 and 65.84 keV levels have been found. Though the latter would represent a very weak $M2$, there is little doubt about its placement.

The 313.85 keV ($J^\pi = \frac{1}{2}^-$) and 315.32 keV ($J^\pi = \frac{3}{2}^\pm$) levels

From the serious imbalance between incoming and outgoing intensities, it is deduced that both of these levels are strongly fed by primary (n_{th}, γ) transitions. This is not surprising since average resonance capture indicates $E1$

multipolarity, and hence, $J^\pi = (\frac{1}{2}, \frac{3}{2})^-$. Several γ rays which fall below the sensitivity of previous measurements have been added: 244.13 and 145.46 keV (from the 313.85 keV level), and 249.47, 245.61, and 210.49 keV (from the 315.32 keV level). The 146.90 keV line (315.32 \rightarrow 168.42) was formerly unresolved from a 30 times stronger 147.55 keV line. The 145.46 keV line was observed with the Argonne bent-crystal spectrometer. Only $J^\pi = \frac{3}{2}^-$ seems to be consistent with the decay pattern of the 315.32 keV level, given the strong 315.32 \rightarrow 167.77 keV ($\frac{5}{2}^+$) and the 315.32 \rightarrow 65.84 keV ($\frac{7}{2}^-$) transitions. The lack of any direct β decay to the 313.85 keV level favors $J^\pi = \frac{1}{2}^-$. The $l=1$ transfer in (d,t) could result from contributions of both the 313.85 and 315.32 keV levels. However, a severe problem arises in connection with the multipolarity of the very intense 147.55 keV transition. Our (n, e^-) data unambiguously contradict $E1$ for this transition, and therefore the negative parity assignment of the 315.32 keV level. However, the $\log f_0 t \geq 9.6$ makes an allowed β transition very unlikely, in support of the arguments given above.

The 323.99 keV ($J^\pi = \frac{7}{2}^+$) level

This level is well known from β -decay studies,¹⁰ and the only J^π value consistent with the data is $\frac{7}{2}^+$. More evidence has come from recent γ - γ angular correlation measurements^{3,4,15} and the determination of $M1 + (0.8 \pm 0.2)\%$ $E2$ multipolarity for the transition to the 91.55 keV ($\frac{9}{2}^+$) state.¹⁸

*The 344.96 keV ($J^\pi = \frac{3}{2}^+$), 395.62 keV ($J^\pi = \frac{5}{2}^+$),
and 445.75 keV ($J^\pi = \frac{5}{2}^+$) levels*

Fully 42% of all β intensity feeds into the 344.96 keV level,¹⁰ and it was easily determined from the multipolarity of deexciting transitions⁵ that $J^\pi = (\frac{3}{2}, \frac{5}{2})^+$. This was confirmed by $l=2$ transfer in (d,t).⁸ From the $M1$ primary transition observed in our (\bar{n}, γ) work, one concludes $J^\pi = \frac{3}{2}^+$. Nuclear orientation measurements³ lead to the same conclusion. The levels at 395.62 and 445.75 keV are both unequivocally assigned $J^\pi = \frac{5}{2}^+$ since they are populated by $E2$ transitions (Table V). This result has been confirmed by orientation and correlation studies by Warner *et al.*³ Transitions of 354.14 keV (445.75 \rightarrow 91.55) and 376.04 keV (445.75 \rightarrow 69.71) have been added. The rather weak 121.76 keV γ line (445.75 \rightarrow 323.99) was masked in (n_{th}, γ) by a very strong ^{152}Sm peak (Table II).

The 355.68 keV ($J^\pi = \frac{1}{2}^+$) and 502.32 keV ($J^\pi = \frac{1}{2}^+$) levels

The γ decay of these levels is presented here for the first time. They are populated by $M1$ transitions in (\bar{n}, γ) , and (d,t) angular distributions have the characteristic shape of $l=0$ transfer,⁸ thus indicating $J^\pi = \frac{1}{2}^+$. This explains the lack of any observable β population as well as the γ -decay pattern.

The 415.69 keV ($J^\pi = \frac{5}{2}^-, \frac{7}{2}^-$), 470.44 keV ($J^\pi = \frac{5}{2}^-$),
490.43 keV ($J^\pi = \frac{7}{2}^-$), and 620.56 keV ($J^\pi = \frac{5}{2}^-$) levels

None of these levels has been observed in our average resonance neutron capture work. So, we assume $J^\pi = \frac{5}{2}^-$ or else $J > \frac{5}{2}$. However, all are directly populated by β decay from ^{151}Pm ($J_0^\pi = \frac{5}{2}^+$), which sets an upper limit of $J \leq \frac{7}{2}$ on their possible spin. Cook *et al.*¹⁰ claim that measured $\log f_0 t$ values are such that allowed β transitions are unlikely to any of these levels. Consequently, we propose $J^\pi = (\frac{5}{2}, \frac{7}{2})^-$. The fact that roughly 30% of the γ intensity from the 415.69 keV level branches to the $\frac{3}{2}^-$ states (4.82 and 104.85 keV) strongly favors $J^\pi = \frac{5}{2}^-$. The deexcitation of the 470.44 keV level has been complemented by two additional lines, 146.45 and 125.49 keV. Both formerly remained unresolved as they are part of multiplet structures (Tables II and VII). The latter transition connects this level to a $\frac{3}{2}^+$ state at 344.96 keV, virtually excluding $J^\pi = \frac{7}{2}^-$. To the decay of the 490.43 keV level, a γ ray of 385.59 keV has been added. Appreciable branching (8%) from this level to the $\frac{9}{2}^+$ state at 91.55 keV rules out the $J^\pi = \frac{5}{2}^-$ choice. With regard to the γ decay of the 620.56 keV level, new transitions of 411.50 and 275.60 keV could be placed. Since the latter (620.56 \rightarrow 344.96) represents a branching ratio of as much as 3%, one would not expect it to be $M2$. Therefore, we conclude that J^π (620.56 keV) has $\frac{5}{2}^-$.

The 448.62 keV ($J^\pi = \frac{3}{2}^-$) level

Further evidence is provided by the present data for the existence of a 448.62 keV level, which apparently does not receive any β feeding. Spin $J^\pi = (\frac{1}{2}, \frac{3}{2})^-$ is deduced from (\bar{n}, γ) . This concurs with $l=1$ transfer in (d,t). Only $J^\pi = \frac{3}{2}^-$ is consistent with the γ -decay pattern, which includes a 448.62 \rightarrow 167.77 keV ($\frac{5}{2}^+$) transition. The weak 382.78 keV (448.62 \rightarrow 65.84) transition has only been observed during a measurement with high sensitivity at Argonne.

The 521.18 keV ($J^\pi = \frac{3}{2}^+$) level

The following transitions remained unobserved during previous measurements of the γ decay of this level: 352.74, 176.23, 165.50, and 105.49 keV. Observation of an $M1$ primary γ transition, combined with $l=2$ transfer in (d,t), results in $J^\pi = \frac{3}{2}^+$ assignment. This turns out to be compatible with orientation and correlation data.^{3,15}

The 663.05 keV ($J^\pi = \frac{3}{2}^+$)
and 663.59 keV ($J^\pi = \frac{5}{2}^-, \frac{7}{2}^-$) levels

The diffraction data give convincing evidence for the existence of two closely spaced levels around 663 keV. Apparently, transitions from each of them are revealed by coincidences¹⁰ which, nevertheless, fail to recognize separate states. Our assumption is supported by the fact that branching ratios derived from β decay and (n, γ) , respectively, are in reasonable agreement only if two levels do indeed exist. The level at 663.05 keV is determined by

nine additional γ transitions. A unique assignment, $J^\pi = \frac{3}{2}^+$, can be made on the basis of $M1$ feeding in (\bar{n}, γ) , together with the decay pattern. For the second level, 663.59 keV, choices can be confined to $J^\pi = \frac{5}{2}^-, \frac{7}{2}^-$. Of course, no primary transition to this level has been observed.

The 822.00 keV ($J^\pi = \frac{3}{2}^-, \frac{5}{2}^-$)
and 822.75 keV ($J^\pi = \frac{3}{2}^+, \frac{5}{2}^+$) levels

Similarly, we propose narrowly spaced levels at 822.00 and 822.75 keV. This is substantiated by the occurrence of four doublet lines around 752.43(96), 717.11(90), 477.18(94), and 376.27(99) keV, respectively. At least one of these levels is populated by an $E1$ primary transition. Moreover, the lower-lying level is characterized by a γ -decay pattern that only allows $J^\pi = (\frac{3}{2}, \frac{5}{2})^-$. If one assumes $J^\pi = \frac{5}{2}^-$, the upper level has $J^\pi = \frac{3}{2}^-$. However, allowed β decay has been observed to a level that may correspond to the one at 822.75 keV. This would then have positive parity. Results from correlation studies^{3,15} cannot be relied on, because measured γ rays probably contain contributions from both components of the doublets listed above.

The 741.18 keV ($J^\pi = \frac{3}{2}^-$) and 774.01 keV ($J^\pi = \frac{5}{2}^-$) levels

Levels at roughly these energies are populated by β transitions with relatively low $\log f_0 t$ values ($\log f_0 t = 7.0$ and 7.3, respectively). Therefore, the obvious conclusion is $\frac{3}{2} \leq J \leq \frac{7}{2}$. We can identify these levels with the ones we propose at 741.18 and 774.01 keV because their respective branching ratios agree reasonably well. The first level is connected with the compound state in (\bar{n}, γ) by $E1$, which implies $J^\pi = \frac{3}{2}^-$.

No direct (\bar{n}, γ) feeding to the second level occurs, and this indicates $J \geq \frac{5}{2}$. Its decay to a $J^\pi = \frac{3}{2}^+$ state and to states with $\frac{3}{2}^- \leq J^\pi \leq \frac{5}{2}^-$ further limits the spin to $J^\pi = \frac{5}{2}^-$. The parity of both states contradicts the previous assignment by Cook *et al.*,¹⁰ which, however, solely relies on rather weak $\log f_0 t$ arguments.

The 951.40 keV ($J^\pi = \frac{3}{2}^-$), 953.58 keV ($J^\pi = \frac{3}{2}^+$),
and 1017.30 keV ($J^\pi = \frac{3}{2}^+$) levels

Comparison of respective γ -ray branching ratios leads us to conclude that the 953.58 keV level corresponds to a level which was observed to be populated by allowed β decay. Cook *et al.*¹⁰ erroneously considered this level to be strongly seen in (n, γ) . Indeed, our (\bar{n}, γ) results show that the primary intensity is weak at best. The level populated by a primary $E1$ transition is found at 951.40 keV. These observations, combined with the γ -decay pattern, suffice to establish that J^π (951.40 keV) = $\frac{3}{2}^-$ and J^π (953.58 keV) = $(\frac{3}{2}, \frac{5}{2})^+$. Angular correlation measurements^{3,15} seem to reject the $\frac{5}{2}^+$ possibility for the latter level. Consequently, referring to the (\bar{n}, γ) results, we have to assume that some $M1$ intensity is contained in the tail of the γ line to the 951.40 keV level. It is most unlikely that the level we propose at 1017.30 keV coincides with the

one observed in β decay. However, we suggest that it does relate to the one fed by $M1$ in (\bar{n}, γ) at 1015.90 keV. We tentatively assign $J^\pi = \frac{3}{2}^+$.

Additional levels

The present data provide insufficient evidence to confirm a number of levels that were proposed on the basis of coincidence measurements.¹⁰ These are levels at 777.4, 851.6, 877.54, 887.35, 888.9, 925.9, and 964.15 keV. On the other hand, several new levels are suggested by our (n, γ) data. For instance, the existence of a 632.06 keV level is derived from (d, t) and $(^3\text{He}, \alpha)$ reactions, (\bar{n}, γ) and 12 decay lines from (n_{th}, γ) . Primary $E2$ multipolarity points to $J^\pi = \frac{5}{2}^+$. Two further levels, at 703.27 and 721.96 keV, respectively, are populated by primary $E1$ transitions and therefore $J^\pi = (\frac{1}{2}, \frac{3}{2})^-$. Spin $J = \frac{1}{2}$ is ruled out by the γ decay of the 703.27 keV state. Some levels are proposed almost exclusively on the basis of the combination of energies. Since these are not found in (\bar{n}, γ) , we postulate that they are of spin $J \geq \frac{5}{2}$. Further restrictions on the spin result from the γ -decay pattern. In this way, we deduce J^π (754.79 keV) $= (\frac{5}{2}, \frac{7}{2})^-$, J^π (804.72 keV) $= \frac{5}{2}^-$, and J^π (960.48 keV) $= \frac{7}{2}^\pm$. The γ decay of the 920.77 keV level, however, seems to allow only $J = (\frac{1}{2}, \frac{3}{2})$ and it remains unexplained why no (\bar{n}, γ) transition to this level was detected. In conclusion, we notice that the level scheme above 600 keV inferred from (n, γ) results differs appreciably from that emanating from other measurements.

IV. INTERPRETATION OF LEVEL SCHEME AND MODEL DESCRIPTION OF ^{151}Sm

A. The model

In this section, we shall try to describe the low-energy level structure of ^{151}Sm in terms of the particle-rotor model with inclusion of pair correlations, Coriolis coupling, and, where applicable, $\Delta N = 2$ coupling. The model is fairly standard and several attempts at a partial description of ^{151}Sm along similar lines have already been made, though with varying degrees of success (Ref. 21 and references quoted therein). Consequently, we can limit ourselves to a short outline of the theoretical procedure.

Assuming axial symmetry, the nuclear Hamiltonian is given by

$$H = H_I + H_R, \quad (10a)$$

where the first term describes the intrinsic motion of the many-particle system and the second results from the collective rotational degrees of freedom. First of all, the intrinsic Hamiltonian is supposed to be given by the independent motion of the particles in a deformed harmonic oscillator potential of modified Nilsson-type.^{41,42} It has, however, been extended to include ϵ_6 deformation and is written as

$$H_I = \sum_i H(\rho_i, l_i, s_i), \quad (10b)$$

where

$$\begin{aligned} H = & (\hbar\omega_0/2)(-\Delta + \rho^2) + \epsilon_2(\hbar\omega_0/3)[P_2(\nabla_\rho) - \rho^2 P_2(\hat{\rho})] \\ & + \hbar\omega_0 \rho^2 [\epsilon_4 P_4(\hat{\rho}) + \epsilon_6 P_6(\hat{\rho})] \\ & - \kappa \hbar\omega_0 [2l \cdot s + \mu(l^2 - \langle l^2 \rangle)] \end{aligned} \quad (10c)$$

in so-called stretched coordinates $\rho = (\xi, \eta, \zeta)$.⁴¹

The potential parameters $\kappa = 0.0637$ and $\mu = 0.4377$ are taken from the systematics in the rare-earth region deduced by Nilsson *et al.*⁴³ The harmonic oscillator quantum is taken to be $\hbar\omega_0 = 8.1583$ MeV in accordance with the usual isospin dependent expression.⁴³ Single-particle energies $\epsilon_{\Omega\alpha}$ and wave functions are obtained by diagonalizing the Nilsson Hamiltonian in the coupled representation of spherical oscillator basis states

$$|\Omega\alpha\rangle = \sum_{lj} C_{lj}^\alpha |lj\Omega\rangle, \quad (11)$$

with the usual notation.

The deformation parameters ϵ_2 , ϵ_4 , and ϵ_6 of the potential well are determined in the following way. Assuming that the state at 65.8 keV is the first excited member of a rotational band based on the ground state and that this band contains nearly equal amounts of $\Omega = \frac{3}{2}$ and $\Omega = \frac{5}{2}$ (Ref. 44), then the measured $B(E2) = (0.80 \pm 0.08) e^2 b^2$ from Coulomb excitation⁷ yields an intrinsic quadrupole moment $Q_0 = 4.6$ b. This corresponds to a quadrupole deformation $\epsilon_2 \approx 0.21$. It is well known from calculations of potential energy surfaces⁴³ that nuclei at the border of the deformed region have pronounced hexadecapole deformation. Also, the higher order P_6 deformation seems to show up. From the equilibrium values of Götz *et al.*⁴⁴ and the experimental deformation parameters of Hendrie *et al.*⁴⁵ for neighboring even-even Sm isotopes, we have estimated $\epsilon_4 \approx -0.024$ and $\epsilon_6 \approx 0.018$ for ^{151}Sm . We note that the calculations by Nilsson *et al.*⁴³ indicate somewhat more hexadecapole deformation and β_6 values of different sign in this region.

Subsequently, the effects of pairing correlations are taken into account. The intrinsic Hamiltonian including pairing interactions can be written as

$$H_I = \sum_k \epsilon_k c_k^\dagger c_k - G \sum_{k, k' > 0} c_k^\dagger c_{-k}^\dagger c_{-k'} c_{k'}, \quad (12)$$

where G represents the pairing strength parameter. We have followed the procedure described by Soloviev,⁴⁶ which amounts to solving the Bardeen-Cooper-Schrieffer (BCS) equations for odd particle number N with consideration of the so-called blocking effect (Pauli principle)

$$2/G = \sum_{\substack{k > 0 \\ \neq \nu}} [(\epsilon_k - \lambda_\nu)^2 + \Delta_\nu^2]^{-1/2}, \quad (13)$$

$$N - 1 = \sum_{\substack{k > 0 \\ \neq \nu}} \{1 - (\epsilon_k - \lambda_\nu) / [(\epsilon_k - \lambda_\nu)^2 + \Delta_\nu^2]^{1/2}\}. \quad (14)$$

This yields the Fermi surface λ_ν and the pairing gap parameter Δ_ν . The subscript ν refers to the single-particle state blocked by the odd particle. The quasiparticle energies E_ν^{qp} are given by

$$E_\nu^{\text{qp}} = E_\nu - E_0, \quad (15)$$

$$E_\nu = \epsilon_\nu + \sum_{\substack{k>0 \\ \neq \nu}} 2V_k^2(\nu)\epsilon_k - \Delta_\nu^2/G, \quad (16)$$

where E_ν is the total energy of the system if the odd particle occupies state ϵ_ν . The occupation probabilities $V_k^2(\nu)$ are given by the well-known expression,⁴⁶ except that they slightly vary with the blocked state because of similar dependence of λ_ν and Δ_ν . From the occupation probability amplitudes $V_k(\nu)$, one calculates the reduction factors for matrix elements of single-particle operators. All 58 single-particle states from the $N=4, 5$, and 6 shells are taken into account in our calculation. The pairing strength is chosen in such a way that the calculated odd-even mass difference matches the experimental pairing energy P_n (^{151}Sm) = 1.264 ± 0.006 MeV.⁴⁷ A proper value turns out to be $G = 149.5$ keV. This results in a pairing gap parameter $\Delta = 1.217$ MeV in the ground state.

The rotational part of the Hamiltonian is

$$H_R = \frac{\hbar^2}{2J_m}(I^2 - I_3^2) + \frac{\hbar^2}{2J_m}(J^2 - J_3^2) - \frac{\hbar^2}{2J_m}(I_+ J_- + I_- J_+), \quad (17)$$

where I and J are the total and intrinsic angular momenta, respectively, and the components refer to the intrinsic axes. The principal moment of inertia is denoted by J_m . The first term is diagonal and contributes the rotational energy following the $I(I+1)$ law. The second term is called the recoil term and has been treated as outlined by Osnes *et al.*⁴⁸ This operator contains one-body and two-body parts. Its main effect is to cause a shift of the band-head energies. This recoil energy is strongly state dependent, as pointed out in Ref. 48, and can be appreciable, particularly for transitional nuclei because of their large $\hbar^2/2J_m$ values. It is of the order of $(\hbar^2/2J_m)j(j+1)$ for relatively pure- j states with low Ω . Furthermore, it may be sensitive to the position of the Fermi surface. We do not consider any nondiagonal contributions of recoil, $\langle \Omega\alpha | J^2 - J_3^2 | \Omega'\alpha' \rangle$, which vanish unless $\Omega = \Omega'$. The remaining term in H_R is responsible for Coriolis or rotation-particle coupling (RPC) and has been treated abundantly in the literature ever since the first calculations by Kerman.⁴⁹ This coupling is causing mixing of rotational bands. It is treated by diagonalization in a basis of states for which $K = \Omega$ are good quantum numbers.

$$|IMK; N\Omega\nu\rangle = [(2I+1)/16\pi^2]^{1/2} \times [D_{MK}^I \alpha_{N\Omega\nu}^\dagger + (-)^{I+K} D_{M, -K}^I \alpha_{N, -\Omega\nu}^\dagger] |\bar{0}\rangle, \quad (18)$$

where M is the projection of I on the space-fixed z axis, α^\dagger is a quasiparticle creation operator, and $|\bar{0}\rangle$ is the quasiparticle vacuum state. The symbols D_{MK}^I represent the common rotation matrices. The unperturbed energy of a rotational state belonging to a band based on the intrinsic configuration $|N\Omega\nu\rangle$ is found from the expression

$$E_I(\Omega\nu) = E_{\Omega\nu}^{\text{sp}} + (\hbar^2/2J_m)\langle \Omega\nu | J^2 - J_3^2 | \Omega\nu \rangle + (\hbar^2/2J_m)[I(I+1) - K^2 + \delta_{K,1/2}(-)^{I+1/2}(I+1/2)a_\nu], \quad (19)$$

with the decoupling parameter given by

$$a_\nu = -\langle \Omega = -\frac{1}{2}, \nu | J_- | \Omega = \frac{1}{2}, \nu \rangle. \quad (20)$$

The Coriolis-mixed states will be denoted by

$$|IM\alpha\rangle = \sum_{\Omega\nu} A_{\Omega\nu}^\alpha |IMK; N\Omega\nu\rangle, \quad (21)$$

the mixing amplitudes $A_{\Omega\nu}^\alpha$ being the result of diagonalization of H_{RPC} .

B. The positive-parity states

It has been established for some time that most of the low-lying positive-parity states in odd- N deformed nuclei of the rare-earth region can be interpreted in terms of rotational bands associated with Nilsson orbitals extending from the $i_{13/2}$ ($N=6$) and $d_{3/2}$ ($N=4$) spherical shell model states.^{50,51}

However, strong perturbations due to Coriolis coupling are to be expected—and have been observed—for rotational bands on Nilsson configurations from the $i_{13/2}$ shell. In general, this is the case for Nilsson states originating from unique-parity high- j orbitals within each major shell, such as $h_{11/2}$, $i_{13/2}$, and $j_{15/2}$. The most obvious reason is that Coriolis matrix elements increase approximately proportional to j for low values of Ω . In addition, unique-parity states are well separated from other orbitals of the same parity and are therefore to a high degree pure- j states with $j = j_{\text{max}}$ (maximum value in the shell). These states experience strong Coriolis coupling among themselves, but interact very little with states from other orbitals. At small deformation, characteristic for the transitional region, the strong Coriolis effects ultimately lead to the rotation-alignment coupling scheme of Stephens,⁵² even at low spin. Another phenomenon with important consequences at the lower-mass end of the deformed region is related to the occurrence of crossing of single-particle levels from the $N=4$ and $N=6$ shells, respectively. At the crossing point, $\Delta N=2$ coupling caused by the $r^2 Y_{\lambda 0}$ terms in the Nilsson model, but not properly reproduced by harmonic oscillator wave functions, may become appreciable.⁵³ It has been shown that in several cases neutron transfer reaction cross sections are not given correctly unless this coupling is explicitly introduced.^{50,53}

Reasonably successful attempts have been made before to describe the properties of positive-parity states in ^{151}Sm .^{8,19,20,22-23} All of these calculations use a Coriolis-coupling approach, but they differ in their respective degree of sophistication. Cross sections for one-particle transfer have long been accepted as reliable data for the identification of Nilsson configurations.⁵³ Two states are strongly excited by $l=0$ transfer in (d,t).⁸ They correspond to the $I^\pi = \frac{1}{2}^+$ levels at 355.7 and 502.3 keV discussed in Sec. III B. Just two $I^\pi = \frac{1}{2}^+$ states are

predicted by the Nilsson model, designated in the usual way as $\frac{1}{2}[660]$ and $\frac{1}{2}[400]$. Experimental spectroscopic factors are compared in Table X to the theoretical values given by

$$S_{ij} = C_{ij}^2 V^2. \quad (22)$$

Since the Nilsson model predicts negligible spectroscopic strength to the $\frac{1}{2}[660]$ state, Nelson *et al.*⁸ have suggested strong $\Delta N=2$ coupling with the $\frac{1}{2}[400]$ state. This leads to a redistribution of the $\frac{1}{2}[400]$ strength over the two $I^\pi = \frac{1}{2}^+$ levels. It is clear from Table X that the major component in the 502.3 keV state is $\frac{1}{2}[400]$, while the 355.7 keV state is predominantly $\frac{1}{2}[660]$. It has recently been pointed out by Guttormsen *et al.*⁵⁴ that the coupling revealed in transfer spectroscopic factors is the combined effect of direct $\Delta N=2$ coupling and coupling through off-diagonal matrix elements of the recoil operator. In our calculation, this coupling is taken into account by introducing constant matrix elements in the coupling matrix. Following the procedure suggested by Andersen⁵⁵ and using the cross-section data of Table X, one deduces a coupling matrix element $|V| = 64$ keV and a ratio of mixing amplitudes $|\alpha/\beta| = 1.7$. Combined with the Nilsson prediction for a pure $\frac{1}{2}[400]$ state, the latter value nicely reproduces the experimental spectroscopic factors for ^{151}Sm . We observe that the mixing in ^{153}Gd is much less complete and the experimental spectroscopic strength does not exhaust the Nilsson prediction. Moreover, the level order is reversed relative to ^{151}Sm , a situation similar to the one discussed by Guttormsen *et al.*⁵⁴ with respect to ^{153}Sm - ^{159}Gd .

We have mentioned in Sec. IV A the possibly appreciable shift in the band-head energies caused by the recoil term. The recoil energy $E_{\text{rec}}(\nu\Omega)$ contains contributions from states $|\rho, \Omega \pm 1\rangle$ of the form

$$\frac{\hbar^2}{2J_m} \frac{1}{2} |\langle \rho, \Omega \pm 1 | j_{\pm} | \nu\Omega \rangle|^2 P_{\nu\rho}, \quad (23)$$

where the pairing factor is given by

$$P_{\nu\rho} = (\eta_\nu \eta_\rho / |\eta_\nu \eta_\rho|) \cos(\eta_\nu - \eta_\rho), \quad (24)$$

$$\tan \eta \equiv \Delta / (\epsilon - \lambda). \quad (25)$$

Each contribution depends on the Fermi energy λ through the pairing factor. As one can easily verify, it is only negative if

$$\begin{aligned} \text{(i)} \quad & \epsilon_\nu < \lambda < \epsilon_\rho, \quad \text{or} \quad \epsilon_\rho < \lambda < \epsilon_\nu, \\ \text{(ii)} \quad & |(\epsilon_\nu - \lambda)(\epsilon_\rho - \lambda)| > \Delta^2. \end{aligned} \quad (26)$$

It can be seen from the matrix element in Eq. (23) that the main contributions come from states that also contribute strongly to Coriolis coupling. For the $\frac{1}{2}[660]$ band these are the $\frac{1}{2}[660]$ and $\frac{3}{2}[651]$ configurations. The former contribution is diagonal, and hence $P_{\nu\nu} = 1$. The latter contribution is also positive since $|\epsilon_\nu - \epsilon_\rho| < \Delta$ and therefore conditions (i) and (ii) are never simultaneously fulfilled. For any value of λ the $\frac{1}{2}[660]$ band is therefore shifted up by including the effect of recoil. It turns out that the recoil energy for this band amounts to 600–650 keV for values of λ consistent with the number of particles. On the other hand, the recoil energy does not exceed 50 keV for the $\frac{1}{2}[400]$ band. The Nilsson model predicts $\frac{1}{2}[400]$ as a rather deep-lying hole state, whereas $\frac{1}{2}[660]$ comes close to the Fermi surface. In that case, no appreciable $\Delta N=2$ coupling would be possible. Apparently, the $N=4-6$ gap is not properly represented by the oscillator quantum $2\hbar\omega_0$. In order to correct for this deficiency, we have introduced a common shift $\Delta\epsilon$ to all single-particle energies from the $N=4$ shell. Although the single-particle energy of the $\frac{1}{2}[660]$ band is close to λ , we notice that the band head is pushed up far too much by recoil, if compared to the experimental value of 355.7 keV. This leads us to introduce an empirical attenuation factor for recoil in the same way as this is usually done for the Coriolis interaction. Because of the intimate relationship of the dominant contributions in both cases, it would seem plausible to assume $\alpha_{\text{rec}} \approx \alpha_{\text{Cor}}$, as already suggested by Katajanheimo and Hammarén.²³ Indeed, the experimental band-head energies are adequately reproduced with $\alpha_{\text{rec}} = 0.43$, whereas an overall Coriolis coupling attenuation factor $\alpha_{\text{Cor}} = 0.67$ is found to be necessary to obtain the calculated level structure of Table XI.

The characteristic structure of a highly decoupled $j = \frac{13}{2}$ band in ^{151}Sm has been revealed through $^{150}\text{Nd}(\alpha, 3n\gamma)^{151}\text{Sm}$ work by several authors.^{19,20} The sequence of levels with $I = j, j+2, j+4, \dots$ has been continued up to $I = \frac{33}{2}$. The lowest two members of this sequence have, moreover, been identified as the 147.9 keV ($\frac{13}{2}^+$) and 383.2 keV ($\frac{17}{2}^+$) levels in (d,t) and ($^3\text{He}, \alpha$).⁸ Linked to the low-spin levels observed in the present (n, γ) work at 355.7 keV ($\frac{1}{2}^+$), 167.8 keV ($\frac{5}{2}^+$), and 91.5 keV

TABLE X. Experimental spectroscopic factors from neutron pickup reactions to $I^\pi = \frac{1}{2}^+$ states in ^{151}Sm and ^{153}Gd compared to Nilsson predictions.

Isotope	E_x (keV)	θ	$d\sigma/d\Omega$ ($\mu\text{b}/\text{sr}$)	$S_{0,1/2}$ Expt.	$S_{0,1/2}$ Nilsson model	
					$\frac{1}{2}^+[400]$	$\frac{1}{2}^+[660]$
^{151}Sm	356	$\pi/2$	172	0.14	0.54	0.36×10^{-3}
	502		451	0.42		
^{153}Gd	328	$\pi/4$	1063	0.44		
	483		23	0.01		

TABLE XI. Results of Coriolis coupling calculations among positive-parity states in ^{151}Sm .

E_x (keV)		Amplitudes in the wave function							
Expt.	Theor.	I	$\frac{1}{2}[660]$	$\frac{1}{2}[400]$	$\frac{3}{2}[651]$	$\frac{3}{2}[402]$	$\frac{5}{2}[642]$	$\frac{7}{2}[633]$	
355.7	355.7	$\frac{1}{2}$	0.862	-0.507					
(663.1)	763.8	$\frac{3}{2}$	0.940	0.263	-0.217	-0.028			
167.8	166.5	$\frac{5}{2}$	0.796	-0.125	0.566	-0.065	0.161		
91.5	93.0	$\frac{9}{2}$	0.827	-0.067	0.509	-0.023	0.217	0.068	
147.9	146.9	$\frac{13}{2}$	0.861	-0.043	0.454	-0.012	0.210	0.080	
383.2	383.7	$\frac{17}{2}$	0.897	-0.030	0.398	-0.007	0.177	0.072	
502.3	502.2	$\frac{1}{2}$	0.507	0.862					
521.2	521.2	$\frac{3}{2}$	-0.242	0.949	0.124	-0.158			
(632.1)	631.8	$\frac{5}{2}$	0.187	0.935	-0.034	-0.243	-0.177		
	790.2	$\frac{7}{2}$	-0.075	0.920	0.169	-0.276	-0.164	-0.132	
345.0	345.8	$\frac{3}{2}$	0.203	0.024	0.844	0.496			
445.7	448.5	$\frac{5}{2}$	-0.543	0.207	0.677	-0.44	0.450		
324.0	324.1	$\frac{7}{2}$	0.220	-0.044	0.819	-0.074	0.500	0.151	
306.8	306.6	$\frac{3}{2}$	-0.132	0.171	-0.475	0.853			
395.6	395.6	$\frac{5}{2}$	0.082	0.241	0.041	0.966	0.022		
	514.0	$\frac{7}{2}$	-0.014	0.293	0.052	0.951	0.079	0.032	

($\frac{9}{2}^+$), they represent the chain of favored ($I+1/2$)-odd members of the strongly Coriolis perturbed $\frac{1}{2}(660)$ band. The elegant parabolic presentation of this sequence by Scheck and Vandenput⁵⁶ has later been described in a semiclassical approximation by Løvholden and Reksstad.⁵⁷ A comparison of these and other positive-parity states with the corresponding ones in the neighboring $N=89$ isotones can be found in Ref. 58.

Following Nelson *et al.*,⁸ we assume that the appreciable spectroscopic strength predicted for the $\frac{3}{2}^+[402]$ Nilsson state is fragmented over the levels at 306.8 and 345.0 keV, which feature prominently in (d,t). Given a cross-section ratio of 4.5 at 60° , the former state is mainly composed of $\frac{3}{2}^+[402]$, while the latter is dominated by $\frac{3}{2}^+[651]$ character. The last assumption is supported by the occurrence of a strongly enhanced $E2$ component (14%) in the γ decay to the 167.8 keV level. Indeed, the $\frac{1}{2}[660]$ and $\frac{3}{2}[651]$ orbitals are coupled by large Coriolis matrix elements, and, as the results in Table XI show, the 167.8 keV state has a 32% $\frac{3}{2}[651]$ component. The $\Delta N=2$ coupling between $\frac{3}{2}[402]$ and $\frac{3}{2}[651]$ orbitals can be treated in analogous fashion as for the crossing $K^\pi=\frac{1}{2}^+$ levels discussed above. A $\Delta N=2$ interaction matrix element $|V|=15$ keV then results, with some uncertainty due to interfering Coriolis coupling. The effect of the recoil energy on the $\frac{3}{2}[651]$ band head is comparable to that on the $\frac{1}{2}[660]$ band. It is mainly due to con-

tributions from the $\frac{1}{2}[660]$ and $\frac{5}{2}[642]$ quasiparticle states. Of course, it is attenuated by the common factor α_{rec} in our calculations. The $\frac{3}{2}[402]$ recoil energy is small, as expected.

The $I=\frac{5}{2}$ members of both $K^\pi=\frac{3}{2}^+$ bands can be identified as follows. Negligible (d,t) spectroscopic factors are predicted for the $I=\frac{5}{2}$ rotational states in the $\frac{3}{2}[651]$ and $\frac{5}{2}[642]$ bands. So, we propose $\frac{5}{2}\frac{3}{2}^+[402]$ for the 395.6 keV level, which is populated in (d,t) and ($^3\text{He},\alpha$). Although our Coriolis coupling calculations (Table XI) predict the $I=\frac{7}{2}$ state of this band around 514 keV, we disagree with Katajanheimo and Hammarén²³ who suggested this assignment for the level found at 490.4 keV. Recall that we adopted negative parity for this level in Sec. III B. Based on energy considerations, we furthermore identify the 445.7 keV level as the $I=\frac{5}{2}$ member of the $\frac{3}{2}[651]$ rotational band. This is in contradiction with the assignment of this level as the $\frac{5}{2}[642]$ band head by Cook *et al.*,¹⁹ but in agreement with the suggestion in Ref. 23 that the $\frac{5}{2}[642]$ band should occur at higher energy. In our Coriolis calculation, a strongly depressed $\frac{7}{2}\frac{3}{2}[651]$ is produced. Accordingly, we suggest that the 324.0 keV ($I=\frac{7}{2}$) level can be interpreted as such.

As in previous work,^{19,23} the 521.2 keV state is interpreted as the $I=\frac{3}{2}$ state in the $\frac{1}{2}[400]$ band. In addition, we propose the 632.1 keV ($I=\frac{5}{2}$) level as its next rota-

tional member. This follows from the observation of a relatively strong transition to this level in (d,t) and from the fact that its position agrees well with that resulting from the calculation. Highly tentative, however, is our assignment of the 663.1 keV ($I = \frac{3}{2}^+$) level as $\frac{3}{2}^+ \frac{1}{2} [660]$. This state is predicted about 100 keV higher in excitation. Finally, the experimental positive-parity level scheme below 700 keV, with an indication of the major state components, is shown in Fig. 7. Above that energy, any model interpretation on the basis of present experimental information reduces to mere speculation.

The Coriolis coupling calculation alluded to in previous paragraphs follows the procedure outlined in Sec. IV A and includes six rotational bands. Initial values for the moment of inertia parameter, $A \equiv \hbar^2/2J_m$, and the customary B parameter were derived from a fit to the unperturbed $\frac{11}{2}^- [505]$ band:¹⁹ $A = 14.1$ keV, $B = -11.6$ eV. The $\frac{1}{2}^+ [400]$ band head was used to determine $\Delta\epsilon = 1517$ keV for $N=4$ single-particle states, with λ fixed from the BCS calculation. Decoupling parameters were taken as calculated from the Nilsson model. The resulting perturbed excitation energies and mixed wave functions are given in Table XI, together with the experimental level energies. In order to obtain the excellent agreement between theoretical and experimental energies, a multiparameter least-squares fit was performed. The parameter values found from the fit depend somewhat on whether or not the high-spin states from the $\frac{1}{2}^+ [660]$ band ($I = \frac{21}{2}^+, \frac{25}{2}^+, \frac{29}{2}^+$) are included. If they are, a remarkable agreement is also obtained for the unfavored states at 672 keV ($\frac{15}{2}^+$), 1054 keV ($\frac{19}{2}^+$), and 1531 keV ($\frac{23}{2}^+$),¹⁹ which are predicted at

648 keV, 1081 keV, and 1540 keV, respectively, the parameter values having been determined exclusively from the favored states. We observe that the quality of the fit has been handsomely improved compared to previous calculations.¹⁹

Concerning the composition of the wave functions, we notice that the $\frac{3}{2}^+ [651]$ and $\frac{5}{2}^+ [642]$ amplitudes in the $\frac{1}{2}^+ [660]$ band have been reduced. On the other hand, the mixing of the $N=4$ states among themselves has been increased. Moreover, the character of the 445.7 keV state has been shifted from $\frac{5}{2}^+ [642]$ to $\frac{3}{2}^+ [651]$.

In an attempt to lend support to the level interpretations given above, the wave functions of Table XI have been used to calculate γ -ray branching ratios. In Table XII experimental branching ratios are given for comparison. Severe discrepancies arise for transitions decaying from the 663.1 and 632.1 keV levels. The tentative interpretation given to these states therefore remains inconclusive. The agreement for all other states, however, is gratifying. This also applies to the $E2/M1$ multipole mixing ratio obtained for the 324.0–91.5 keV transition, $\delta^2 = 0.030$ ($\delta_{\text{expt}}^2 \leq 0.031$), and to the virtually pure $E2$ multipolarity predicted for the 445.7–167.8 keV transition.

C. The negative-parity states

The interpretation of the low-lying odd-parity excitations of ^{151}Sm has been severely complicated by the apparent lack of any rotational band structure among the low-spin states. If the particle-rotor model were applic-

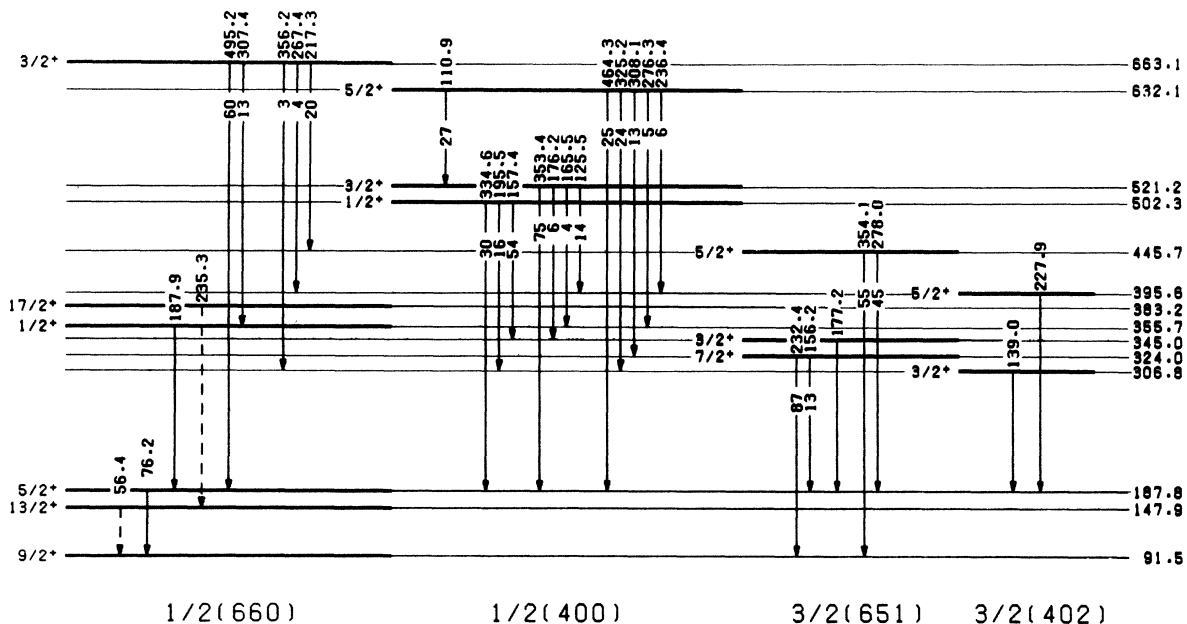


FIG. 7. Low-energy positive-parity level structure of ^{151}Sm based on the present study. Dashed lines indicate transitions taken from Ref. 19. Given are the excitation energy (in keV) and the spin for each level as well as the transition energy (in keV) and the branching ratio, where applicable, for each transition. At the bottom, the major components in the mixed wave function of the levels above are given.

TABLE XII. Branching ratios and $E2/M1$ multipole mixing ratios for γ -ray transitions between positive-parity states in ^{151}Sm .

Initial		Final		Branching ratio		$\delta^2(E2/M1)$
E_x	I	E_x	I	Expt. (error)	Theor.	Theor.
663.1	$\frac{3}{2}$	167.8	$\frac{5}{2}$	59.9(1.9)	8.04	4.6
		355.7	$\frac{1}{2}$	13.4(1.1)	11.4	0.44
		306.8	$\frac{3}{2}$	3.1(0.7)	14.1	0.025
		395.6	$\frac{5}{2}$	3.9(0.7)	0.94	0.011
		445.7	$\frac{5}{2}$	19.8(1.7)	65.6	0.005
502.3	$\frac{1}{2}$	167.8	$\frac{5}{2}$	29.8(2.9)	13.8	
		306.8	$\frac{3}{2}$	16.4(2.0)	29.8	0.001
		345.0	$\frac{3}{2}$	53.8(4.0)	56.4	<0.001
521.2	$\frac{3}{2}$	167.8	$\frac{5}{2}$	75.2(3.2)	67.7	0.053
		345.0	$\frac{3}{2}$	6.1(1.3)	2.87	0.003
		355.7	$\frac{1}{2}$	4.4(1.4)	6.19	30
		395.6	$\frac{5}{2}$	14.3(3.0)	23.3	<0.001
632.1	$\frac{5}{2}$	521.2	$\frac{3}{2}$	27.1(4.6)	19.6	0.003
		167.8	$\frac{5}{2}$	24.5(3.7)	15.2	0.009
		306.8	$\frac{3}{2}$	23.8(2.2)	3.70	0.48
		324.0	$\frac{7}{2}$	13.1(1.5)	37.5	0.022
		355.7	$\frac{1}{2}$	5.2(1.8)	2.17	
		395.6	$\frac{5}{2}$	6.3(1.4)	21.8	0.011
324.0	$\frac{7}{2}$	91.6	$\frac{9}{2}$	86.6(2.0)	91.3	0.031
		167.8	$\frac{5}{2}$	13.4(2.0)	8.7	0.007
445.7	$\frac{5}{2}$	91.6	$\frac{9}{2}$	55.0(10.0)	30.8	
		167.8	$\frac{5}{2}$	45.0(10.0)	69.2	82

able at all, it would be obscured by strong mixing phenomena. Consequently, early attempts at such a description completely failed to explain the observed level structure and the experimental cross sections for Coulomb excitation⁷ and neutron-transfer reactions.⁸ Nevertheless, the rotational degree of freedom has proved to be very significant in determining the properties of ^{151}Sm . This was demonstrated by the partial success in the description of positive-parity states associated with the $i_{13/2}$ single-particle configuration (Sec. IV B). Other evidence has been provided by the identification in $^{150}\text{Nd}(\alpha, 3n\gamma)^{151}\text{Sm}$ reactions^{19,20} of a very regular rotational band ($I \leq \frac{29}{2}$) based on the $\frac{11}{2}[505]$ configuration. In addition, the same experiments support the possibility of two more bands. The first of these, the ground state band, has a fairly regular structure at high spin ($I \geq \frac{11}{2}$), while the second displays features of a partly decoupled band based

on the 175.4 keV ($\frac{9}{2}^-$) level.

A thorough investigation of the various couplings among the configurations in the neighborhood of the Fermi level has recently been reported by Guttormsen *et al.*²¹ These authors argue that the single-particle level scheme in the spherical limit for any deformed mass number can be consistently determined by linear interpolation between experimental single-particle levels in the spherical regions at the lower ($N=82$) and upper ($N=126$) mass end. Subsequently, one can deduce l -dependent potential parameters κ_l and μ_l which allow one to reproduce the interpolated levels at $\epsilon=0$. Those values are inserted in the Nilsson Hamiltonian of Eq. (10c) to generate deformed single-particle energies and wave functions. Upon comparison with the Nilsson scheme obtained in the conventional way, as used for the positive-parity states under Sec. IV B, one observes some important rearrangements of

spherical orbits. Most notably, the distance between the $f_{7/2}$ and $h_{9/2}$ orbitals is more than tripled, and the $p_{3/2}$, $p_{1/2}$, and $f_{5/2}$ states are lowered to cluster around the $h_{9/2}$ orbital.

This changes the position of the Nilsson states originating from these spherical orbitals relative to the Fermi level. More importantly, it modifies the composition of the Nilsson wave functions. Those originating from $h_{9/2}$ contain smaller $j = \frac{7}{2}$ components and, conversely, the $f_{7/2}$ states have less $j = \frac{9}{2}$ contamination. The $p_{3/2}$ Nilsson states acquire larger $j = \frac{7}{2}$ and $\frac{9}{2}$ components at the expense of the $j = \frac{5}{2}$ component. The latter is due to interaction with $f_{5/2}$, for which the distance from $p_{3/2}$ has been enhanced. All these states belong to the $N=5$ shell.

The Coriolis coupling calculations of Ref. 21 are able to reproduce the experimental level scheme moderately well. A satisfactory agreement is also obtained for neutron stripping and pickup spectroscopic factors, and for the available $B(E2)$ values from (d,d') reactions.⁷ This agreement is in large measure obtained by avoiding too much mixing of $f_{7/2}$ and $h_{9/2}$ in the Nilsson states, as mentioned above, and by virtually limiting the Coriolis coupling to configurations originating from the same spherical shell. This is exactly what is needed to explain the experimental particle-transfer spectroscopic factors, i.e., the large S_{ij} value for the 65.8 keV ($\frac{7}{2}^-$) and 175.4 keV ($\frac{9}{2}^-$) levels. Indeed, these states are interpreted as predominantly $\frac{7}{2} \frac{3}{2}[532]$ and $\frac{9}{2} \frac{3}{2}[521]$, which have large $j = \frac{7}{2}$ and $\frac{9}{2}$ components, respectively. However, the same mechanism causes the only real discrepancy. The 209.0 keV level is calculated to be as much as 75% $\frac{7}{2} \frac{3}{2}[521]$. Since this is an $h_{9/2}$ state with rather less $j = \frac{7}{2}$ strength, a much too low spectroscopic factor is found. The $B(E2)$ results summarized in the fifth column of Table XIII are readily understood from the lack of any appreciable mixing between the $f_{7/2}$ ground state band and the first excit-

ed $h_{9/2}$ band. Again, this very characteristic results in too large a $B(E2)$ to the 294.9 keV ($\frac{9}{2}$) member of the ground state band.

As a further test, we have used the wave functions obtained by Guttormsen *et al.*²¹ to calculate γ -ray branching ratios and $E2/M1$ multipole mixing ratios. The branching ratios are given in Table XIV and are compared to experimental values deduced from our (n, γ) intensities. One observes that there is acceptable agreement for transitions from levels in the ground state band and from the 285.0 keV and the 502.3 keV levels. Serious discrepancies occur for the other levels. The mixing ratios $\delta^2(E2/M1)$ are compared in Table XV to values found in the literature or deduced from the conversion coefficients of Sec. IIC. The comparison is often not conclusive because several of the experimental values are not very meaningful. One can see, though, that the $M1$ components in the transitions 104.8 \rightarrow 69.7 keV and 209.0 \rightarrow 69.7 keV are grossly underestimated.

It appears to us that the severe shortcomings remnant in the model discussed above justify another attempt at improving the wave functions and level energies. In order to retain as much as possible the attractive features of Guttormsen's calculation, we have employed the same single-particle potential. We have restricted the Nilsson basis to the $K = \frac{1}{2}, \frac{3}{2},$ and $\frac{5}{2}$ states emanating from the $f_{7/2}$ and $h_{9/2}$ spherical orbitals. They are depicted schematically in Fig. 8. The model states and energy levels of ^{151}Sm were found by diagonalization of the Coriolis interaction in this limited basis, as described in Sec. IV A. Coriolis matrix elements are largest between K and $K \pm 1$ states within the same shell. The Fermi level was located about halfway between the $\frac{3}{2}[532]$ hole state and the $\frac{3}{2}[521]$ particle state, but was allowed to vary slightly. Small changes ($\Delta E < 60$ keV) to the band-head energies were also introduced. The $\frac{5}{2}[523]$ band head was given somewhat more freedom ($\Delta E < 110$ keV).

Only levels with $I \leq \frac{11}{2}$ in the $\frac{3}{2}[532]$ and $\frac{3}{2}[521]$ bands were included in the fit of free parameters. Other levels were calculated from the parameters found in that way. Because of the uncertainties concerning shape and effective moment of inertia of transitional nuclei, the rotational parameter was given a great margin to vary. From the level spacings in neighboring even ^{150}Sm and ^{152}Sm nuclei, we also inferred the necessity to introduce a negative B parameter. This accounts for a spin-dependent increase in the effective moment of inertia. The best fit was obtained for

$$A = 32.7 \text{ keV} ,$$

$$B = -50.8 \text{ eV} .$$

These values may seem unusually large, but they are intermediate between those appropriate for ^{150}Sm and ^{152}Sm , respectively.²¹ As a matter of fact, the 6^+ level in the ground state band of ^{150}Sm is nicely reproduced by these values. No improvement was obtained in the fit by using individual A and B values for different bands, nor by attenuating the Coriolis interaction. The reduction due to pairing correlations, however, was not neglected. Finally, the decoupling parameters for $K = \frac{1}{2}$ bands were given

TABLE XIII. Reduced $E2$ excitation probabilities from the $\frac{5}{2}^-$ ground state. Experimental values are from Ref. 7. Theoretical values are based on wave functions from Ref. 21 (I) and from this work (II).

E_x	I	$B(E2)$ (e^2b^2)			
		5 MeV	12 MeV	Theory I	Theory II
65.8	$\frac{7}{2}$	0.82 \pm 0.08	0.75	0.59	0.61
294.9	$\frac{9}{2}$	0.45 \pm 0.04	0.48	0.83	0.45
4.8	$\frac{3}{2}$				0.44
168.4	$\frac{5}{2}$	0.14 \pm 0.03	0.16	0.06	0.24
104.8	$\frac{3}{2}$		0.013	0.01	0.02
209.0	$\frac{7}{2}$		0.010		0.11
175.4	$\frac{9}{2}$			0.02	0.15
69.7	$\frac{5}{2}$				0.006
302.7	($\frac{5}{2}$)				0.001

TABLE XIV. Branching ratios for γ -ray transitions between negative-parity states in ^{151}Sm . Experimental values are derived from the (n,γ) data. Theoretical values are based on wave functions by Guttorf *et al.* (Ref. 21) (I) and from this work (II).

Initial		Final		Expt. (error)	Branching ratio	
E_x	I	E_x	I		Theory I	Theory II
65.8	$\frac{7}{2}$	0.0	$\frac{5}{2}$	99.2(0.3)	97.5	99.5
		4.8	$\frac{3}{2}$	0.8(0.3)	2.5	0.5
168.4	$\frac{5}{2}$	0.0	$\frac{5}{2}$	37.2(4.3)	52.6	24.0
		4.8	$\frac{3}{2}$	58.7(4.5)	42.1	72.2
		65.8	$\frac{7}{2}$	1.1(0.5)	0.5	2.3
		69.7	$\frac{5}{2}$	2.5(0.6)	2.5	.2
		104.8	$\frac{3}{2}$	0.6(0.1)	2.3	1.3
294.9	$\frac{9}{2}$	0.0	$\frac{5}{2}$	35.0(3.1)	41.4	36.2
		65.8	$\frac{7}{2}$	65.0(3.1)	58.6	63.8
423.2	$\frac{11}{2}$	65.8	$\frac{7}{2}$	85.0(5.7)	97.4	84.4
		294.9	$\frac{9}{2}$	15.0(5.7)	2.6	15.6
69.7	$\frac{5}{2}$	0.0	$\frac{5}{2}$	24.0(6.1)	75.4	92.6
		4.8	$\frac{3}{2}$	76.0(6.1)	24.6	7.4
104.8	$\frac{3}{2}$	69.7	$\frac{5}{2}$	0.9(0.2)	0.1	0.5
		0.0	$\frac{5}{2}$	58.9(6.8)	9.8	32.9
		4.8	$\frac{3}{2}$	40.1(6.7)	90.1	66.6
		65.8	$\frac{7}{2}$	0.1(0.1)	0.01	0.01
175.4	$\frac{9}{2}$	0.0	$\frac{5}{2}$	11.3(3.7)	0.03	41.0
		65.8	$\frac{7}{2}$	88.7(3.7)	99.97	59.0
209.0	$\frac{7}{2}$	69.7	$\frac{5}{2}$	21.6(3.2)	2.6	2.1
		0.0	$\frac{5}{2}$	64.8(3.3)	85.1	45.4
		4.8	$\frac{3}{2}$	4.9(0.6)	0.3	0.3
		65.8	$\frac{7}{2}$	8.8(1.5)	12.0	52.2
285.0	$\frac{1}{2}$	69.7	$\frac{5}{2}$	3.7(0.5)	3.2	3.0
		104.8	$\frac{3}{2}$	3.5(0.5)	4.5	5.5
		0.0	$\frac{5}{2}$	0.7(0.1)	1.7	0.3
		4.8	$\frac{3}{2}$	92.1(0.7)	90.6	91.2
(302.6)	$\frac{5}{2}$	69.7	$\frac{5}{2}$	19.4(2.1)	6.5	12.8
		104.8	$\frac{3}{2}$	2.3(0.4)	10.2	10.2
		0.0	$\frac{5}{2}$	9.4(4.8)	44.2	1.1
		4.8	$\frac{3}{2}$	11.8(1.2)	37.7	4.4
		65.8	$\frac{7}{2}$	48.9(3.8)	0.4	58.7
		168.4	$\frac{5}{2}$	8.2(2.5)	1.0	12.9

TABLE XIV. (Continued).

Initial E_x	I	Final		Expt. (error)	Branching ratio	
		E_x	I		Theory I	Theory II
502.3	$\frac{11}{2}$	175.4	$\frac{9}{2}$	14.4(3.9)	26.0	36.5
		209.0	$\frac{7}{2}$	53.5(4.8)	39.3	61.4
		295.0	$\frac{9}{2}$	32.1(4.9)	34.7	2.0
(315.3)	$\frac{3}{2}$	0.0	$\frac{5}{2}$	13.0(0.9)		26.9
		4.8	$\frac{3}{2}$	44.7(2.5)		28.1
		65.8	$\frac{7}{2}$	4.7(0.7)		0.2
		168.4	$\frac{5}{2}$	20.5(2.6)		12.1
		69.7	$\frac{5}{2}$	13.0(1.1)		27.5
		104.8	$\frac{3}{2}$	4.0(0.5)		5.3

TABLE XV. Multipole mixing ratios for γ -ray transitions between negative-parity states based on wave functions by Guttormsen *et al.* (Ref. 21) (I) and from this work (II) compared to experimental values.

Initial E_x	I	Final		$\delta^2(E2/M1)$				
		E_x	I	Theory I	Theory II	Expt. (error)		
4.8	$\frac{3}{2}$	0.0	$\frac{5}{2}$	3.0×10^{-4}	6.3×10^{-1}	$5(2) \times 10^{-3}$	b	
					6.6×10^{-3a}			
65.8	$\frac{7}{2}$	0.0	$\frac{5}{2}$	5.8×10^{-2}	1.8×10^{-2}	$18(6) \times 10^{-2}$	c	
						$4.3(0.4) \times 10^{-2}$	d	
						$9(5) \times 10^{-2}$	e,f	
168.4	$\frac{5}{2}$	0.0	$\frac{5}{2}$	2.1×10^{-2}	1.9×10^{-1}	$1.5(0.8)$	c	
			4.8	$\frac{3}{2}$	1.5×10^{-2}	5.1×10^{-2}	$\leq 4.0(0.6) \times 10^{-2}$	f
69.7	$\frac{5}{2}$	0.0	$\frac{5}{2}$	3.6×10^{-4}	1.4×10^{-4}	$1.7(1.7) \times 10^{-2}$	f	
			4.8	$\frac{3}{2}$	5.4×10^{-4}	2.0×10^{-3}	$2.6(0.3) \times 10^{-2}$	d
104.8	$\frac{3}{2}$	0.0	$\frac{5}{2}$	8.6×10^{-3}	5.3×10^{-3}	$1.0(0.5) \times 10^{-2}$	f	
			4.8	$\frac{3}{2}$	1.9×10^{-3}	1.2×10^{-4}	$1.4(0.6) \times 10^{-2}$	d
			69.7	$\frac{5}{2}$	46	3.1×10^{-2}	$\leq 1.0(0.4) \times 10^{-2}$	f
209.0	$\frac{7}{2}$	0.0	$\frac{5}{2}$	3.6×10^{-2}	1.1×10^{-1}	$< 0.1(0.1) \times 10^{-2}$	d	
			65.8	$\frac{7}{2}$	6.5×10^{-3}	1.0×10^{-3}	$0.25(0.13)$	c
			69.7	$\frac{5}{2}$	3.6	3.9	$\leq 5 \times 10^{-2}$	e,f

^aBased on a pure $\frac{3}{2}[532]$ wave function for the 4.8 keV state.

^bFrom Geiger *et al.* (Ref. 12).

^cBased on conversion coefficients of Table VI.

^dFrom Singh *et al.* (Ref. 15).

^eFrom Yamada *et al.* (Ref. 4).

^fFrom Warner *et al.* (Ref. 3).

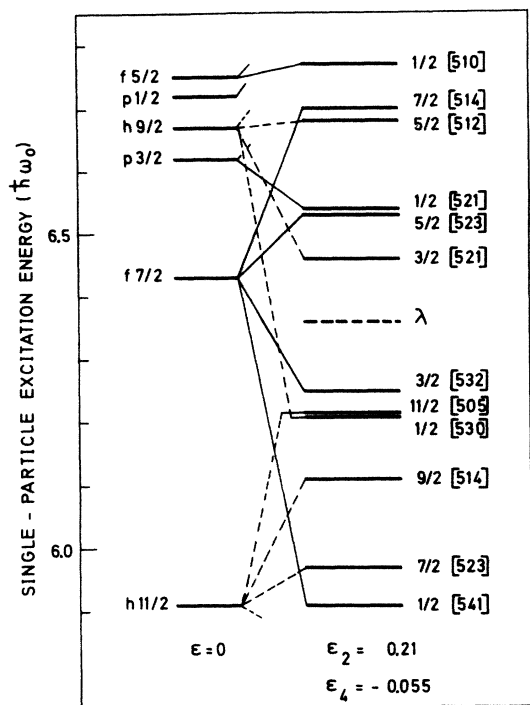


FIG. 8. Theoretical excitation energies of negative-parity single-particle states relevant to the discussion in Sec. IV C. These states were obtained from a Nilsson model calculation using the potential and deformation parameters of Ref. 21. Single-particle energies in the spherical limit are given on the left.

their Nilsson values.

The level energies and the wave functions resulting from our calculation are contained in Table XVI. The $B(E2)$ values, branching ratios, and multipole mixing ratios based on these results are found in Tables XIII, XIV, and XV, respectively, under the heading "Theory II." Figure 9 shows the relevant levels and transitions. The Nilsson interpretation of the observed levels corresponds to the one accepted by Guttormsen *et al.*,²¹ except for the 302.6 keV level. Our data of Sec. III B seem to exclude a spin $\frac{3}{2}$ for this level. A close inspection of Guttormsen's results already provides a hint as to how to overcome some remaining problems, as observed by that author. The $\frac{5}{2}[523]$ band-head energy remains much higher than its experimental position at 168.4 keV and the $\frac{5}{2}\frac{3}{2}[532]$ state is not depressed far enough to become the ground state. Lowering the $\frac{5}{2}[523]$ state would increase its mixing into the $\frac{3}{2}[532]$ band and push down its $\frac{5}{2}$ member without affecting its $\frac{3}{2}$ band head. This is what we have tried to bring about in this new calculation. It is seen from Table XVI that the level order is markedly improved. The 4.8 keV level still is almost a pure $\frac{3}{2}[532]$ state. All the other states are characterized by somewhat increased mixing of $\frac{5}{2}[523]$ into $\frac{3}{2}[532]$ on the one hand, and of $\frac{1}{2}[530]$ into $\frac{3}{2}[521]$ on the other. Also, slightly more mixing between $f_{7/2}$ and $h_{9/2}$ states can be observed for most states. This is what was actually called for by the pickup spectroscopic factors.²¹ Unfortunately, we have not succeeded in bringing the $\frac{5}{2}[523]$ state further down without dramatically destroying the agreement obtained.

The $B(E2)$ results in Table XIII show that agreement

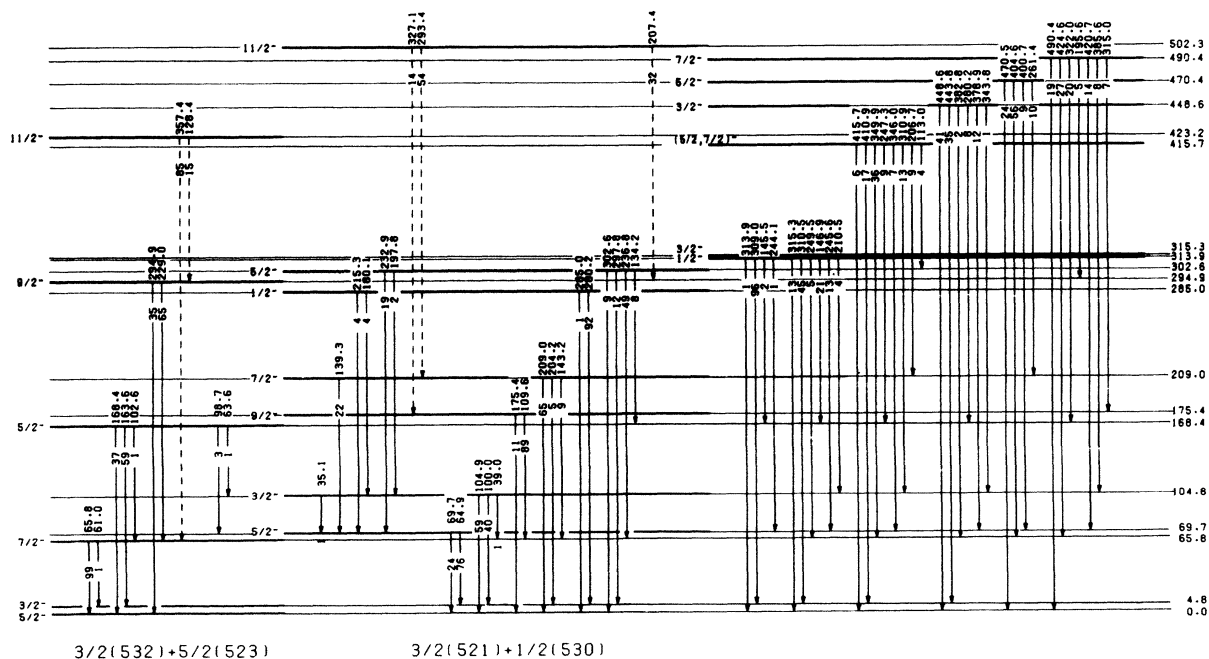


FIG. 9. Similar to Fig. 7 for the low-energy negative-parity level structure of ¹⁵¹Sm.

TABLE XVI. Results of Coriolis coupling calculations among negative-parity states in ^{151}Sm .

E_x (keV)		I	Amplitudes in the wave function					
Expt.	Theor.		$\frac{5}{2}$ [523]	$\frac{3}{2}$ [532]	$\frac{1}{2}$ [541]	$\frac{5}{2}$ [512]	$\frac{3}{2}$ [521]	$\frac{1}{2}$ [530]
4.8	2.9	$\frac{3}{2}$		0.989	0.079		-0.084	-0.096
0.0	0.0	$\frac{5}{2}$	0.595	0.792	0.091	0.034	0.062	0.070
65.8	82.5	$\frac{7}{2}$	0.569	0.733	0.142	-0.048	-0.254	-0.227
294.9	281.2	$\frac{9}{2}$	0.600	0.702	0.078	-0.081	-0.304	-0.206
423.2	397.7	$\frac{11}{2}$	0.419	0.550	0.200	-0.186	-0.524	-0.416
705.8	764.2	$\frac{13}{2}$	0.611	0.726	0.124	-0.074	-0.244	-0.137
974.7	840.7	$\frac{15}{2}$	-0.304	-0.420	-0.228	0.267	0.614	0.482
1321.9	1390.0	$\frac{17}{2}$	0.604	0.727	0.154	-0.089	-0.248	-0.119
168.4	399.4	$\frac{5}{2}$	0.795	-0.599	-0.065	-0.007	0.053	0.052
104.8	106.8	$\frac{3}{2}$		0.121	-0.026		0.885	0.448
69.7	62.9	$\frac{5}{2}$	-0.115	-0.042	0.069	0.170	0.777	0.590
209.0	196.6	$\frac{7}{2}$	0.209	0.270	-0.023	0.261	0.783	0.449
175.4	191.1	$\frac{9}{2}$	0.178	0.319	0.153	0.254	0.676	0.567
502.3	526.2	$\frac{11}{2}$	0.420	0.544	0.062	0.291	0.595	0.292
531.8	515.3	$\frac{13}{2}$	0.111	0.246	0.180	0.304	0.679	0.584
1091.5	1051.9	$\frac{15}{2}$	0.481	0.644	0.139	0.289	0.471	0.171
994.8	972.3	$\frac{17}{2}$	0.098	0.238	0.206	0.329	0.666	0.583
1490.5	1488.8	$\frac{21}{2}$	0.095	0.240	0.229	0.344	0.654	0.579
285.0	286.5	$\frac{1}{2}$			0.047			0.999
(315.3)	545.4	$\frac{3}{2}$		0.054	-0.091		-0.457	0.883
(302.6)	658.9	$\frac{5}{2}$	-0.018	-0.014	0.106	-0.216	-0.565	0.789

is now established in the ground state band. The attenuation of the $\frac{3}{2}$ [532] component in the 294.9 keV state is responsible for this. The 175.4 keV state remains a problem. It is clear from the branching ratios based on Guttormsen's wave functions (Table XIV, Theory I) that the $E2$ transition $175.4 \rightarrow 0$ keV is far too weak because there is almost no $\frac{3}{2}$ [532] component present in the wave function of the 175.4 keV state. However, our calculation obviously transfers too much $\frac{3}{2}$ [532] strength to this state. It is hard to strike a balance here since the $\frac{9}{2}$ $\frac{3}{2}$ [521] level has to be pushed down from an unperturbed position above the $\frac{9}{2}$ $\frac{3}{2}$ [532] level. The rather pure $M1$ branchings from the 69.7 keV level clearly stand at variance with the data in both models. It is not obvious how this can be avoided with the present interpretation of this level. The branching ratios are consistent with our tentative interpretation of $\frac{5}{2}$ $\frac{1}{2}$ [530] for the 302.6 keV level. The Guttormsen interpretation leads to totally erroneous branching ratios for this level. The $\frac{3}{2}$ $\frac{1}{2}$ [530] assignment to the 315.3 keV level is highly speculative. Both of these levels are predicted at much higher energies

than their experimental values. Finally, we remark that the branching ratios within the ground state band are nicely reproduced in our calculation.

A word of caution should be added regarding the multipole mixing ratio for the ground state transition from the 4.8 keV level (Table XV). Due to a cancellation of major terms in the $M1$ transition matrix element, the normally negligibly small components in the wave function of the 4.8 keV state become decisive. A pure $\frac{3}{2}$ [532] wave function would lead to $\delta^2 = 6.6 \times 10^{-3}$, in complete accord with experiment. This means that the basic interpretation appears to be sound, but that δ^2 is in this case inappropriate to gauge the detailed structure of the 4.8 keV state wave function. The most striking discrepancies that are found in the calculated branching ratios and δ^2 values always involve the 69.7 or 209.0 keV states. The data seem to suggest that the important $\frac{1}{2}$ [530] admixtures in these states have an adverse effect on the $M1$ transition rates. The strong coupling with the $\frac{1}{2}$ [530] band is needed, however, to achieve the required level displacements.

We wish to draw attention to the remarkable agreement between predicted and experimental energies of levels with $I \geq \frac{13}{2}$ in the $\frac{3}{2}[532]$ and $\frac{3}{2}[521]$ bands. It should be stressed that these states were not included in the parameter fit and these levels have experienced large shifts from their unperturbed positions ($\Delta E = -1820$ keV for the $\frac{21}{2}$ $\frac{3}{2}[521]$ level). The particular decoupled structure of the $\frac{3}{2}[521]$ band can be understood in the following way. The positive decoupling parameter of the $\frac{1}{2}[530]$ band causes a depression of the $(I + \frac{1}{2})$ -odd states in this band. As a result, these states approach the unperturbed positions of corresponding states in the $\frac{3}{2}[521]$ band. A strong Coriolis interaction takes place and the $I = \frac{5}{2}, \frac{9}{2}, \frac{13}{2}, \dots$ members of the latter band get strongly depressed. On the other hand, the $(I + \frac{1}{2})$ -even states of the $\frac{3}{2}[521]$ band do not suffer this strong downward pressure from the $\frac{1}{2}[530]$ states and ultimately the repulsion from the $f_{7/2}$ states dominates. The effects of this sort of coupling are clearly reflected in the alternating size of the $\frac{1}{2}[530]$ and $\frac{3}{2}[532]$ components in the wave functions of the $I = \frac{9}{2}, \frac{11}{2}, \frac{13}{2}, \dots$ members of the $\frac{3}{2}[521]$ band. Our calculations contradict the interpretations of the $\frac{11}{2}, \frac{13}{2},$ and $\frac{15}{2}$ states of Ref. 23. But we noticed that we would obtain comparable results if the $\frac{5}{2}[523]$ state were forced down significantly. We have also observed that no further improvements were obtained by including the $\frac{1}{2}[521]$ state from the $p_{3/2}$ shell in the calculation.

A convincing interpretation for the low-spin states populated by (n, γ) above 400 keV cannot be offered at this moment because of the scant experimental data available. Presumably, they are to be identified with Nilsson configurations in the $p_{3/2}, p_{1/2},$ and $f_{5/2}$ shells (Fig. 8), though these excitations would be found at somewhat higher energy in the present model. The assignment of $\frac{11}{2}[505]$ to the 261.1 keV level is well founded by virtue of its isomeric character ($T_{1/2} = 1.4 \pm 0.1 \mu\text{sec}$),¹⁴ the fine agreement with theoretical transfer spectroscopic factors,^{8,21} and its

TABLE XVII. Results of Coriolis coupling calculations on the $\frac{11}{2}[505]$ rotational band and comparison to experimental level energies from Ref. 19.

E_x (keV)		Amplitudes in the wave function			
Expt.	Theor.	I	$\frac{11}{2}[505]$	$\frac{9}{2}[514]$	$\frac{7}{2}[523]$
261.1	262.5	$\frac{11}{2}$	0.984	0.174	0.023
445.1	443.0	$\frac{13}{2}$	0.967	0.251	0.042
648.2	646.1	$\frac{15}{2}$	0.948	0.312	0.062
869.4	869.5	$\frac{17}{2}$	0.928	0.363	0.083
1107.5	1110.9	$\frac{19}{2}$	0.908	0.407	0.104
1361.3	1367.3	$\frac{21}{2}$	0.887	0.445	0.124
1630.0	1635.5	$\frac{23}{2}$	0.866	0.478	0.145
1912.2	1912.1	$\frac{25}{2}$	0.846	0.507	0.165
2205.6	2193.3	$\frac{27}{2}$	0.826	0.533	0.185

systematic occurrence in neighboring Sm, Gd, Dy, and Er isotopes.⁵⁹ None of the rotational band members based on this level have been observed in our experiments, given their large spin values. Nor is this configuration of any consequence for the other states discussed in this section. For the sake of completeness, however, we list the results of our Coriolis calculation for the $\frac{11}{2}[505]$ band in Table XVII. There is an excellent agreement with the experiment, although the only free parameter was the effective moment of inertia. Three configurations from the $h_{11/2}$ shell were allowed to interact in this calculation: $\frac{11}{2}[505]$, $\frac{9}{2}[514]$, and $\frac{7}{2}[523]$. The rotational parameters obtained from the fit were

$$A = 17.0 \text{ keV} ,$$

$$B = -13.7 \text{ eV} .$$

The spin dependence of the moment of inertia contained in the B term is essential to obtain this substantial improvement over previously published calculations.²¹

V. CONCLUSION

In this work we have combined a number of complementary experimental techniques and used the available theoretical tools in an attempt to further the understanding of the highly puzzling low-energy structure of transitional ¹⁵¹Sm. In the energy range from x-ray energies up to 500 keV and higher, where the bulk of the γ transitions from the ¹⁵⁰Sm(n, γ) reaction are located, the resolution and precision of curved-crystal spectrometers is unrivaled. This has made it possible to completely resolve many complex structures, most notably those made up of transitions involving the closely spaced levels around 168, 663, and 822 keV. The level scheme has been firmly established and level energies have been obtained with much enhanced precision. Taking into account all previous studies and the results from (\bar{n}, γ) and (n_{th}, e^-) experiments contained in this paper, spin-parity assignments for most levels below 1 MeV have been narrowly defined. Moreover, many new proposals for levels, spin-parity values, and decay patterns have been made.

It has been demonstrated, through improved particle-rotor model calculations, that the positive-parity states are adequately described as moderately mixed configurations originating from the spherical $i_{13/2}$ and $d_{3/2}$ ($N=4$) shells. Considering the remaining discrepancies in the decay of some of the levels higher up in energy, it must be concluded that their interpretation still is uncertain. Concerning the negative-parity states, it is observed that the present calculations provide a satisfactory description for the high-spin levels of the ground state band, the partly decoupled $h_{9/2}$ band, and the $\frac{11}{2}[505]$ band. Moreover, in spite of the tangled structure of low-energy low-spin states, an acceptable picture starts to emerge which is based on a virtually complete mixture of configurations from the spherical $f_{7/2}$ and $h_{9/2}$ shells. Problems are encountered relating to the position of the 168.4 keV level and the γ decay involving the levels at 69.7 and 209.0 keV. Finally, as far as the many excitations at higher energy ($E_x > 600$ keV) are concerned, more experimental

work is called for in order to provide signatures that would relate these states to model interpretations.

ACKNOWLEDGMENTS

Professor O. Schult, Kernforschungsanlage Julich, has been the initiator and great driving force of much of the curved-crystal spectrometry work in Europe over the last two and a half decades. Some of us (G.V., P.V.A., L.J.,

and J.V.dC.) gratefully recognize his inspiration, his guidance, and his generosity. One of the authors (G.V.) acknowledges the kind encouragement of Dr. M. Nève de Mévergnies in the course of his work at Mol. The same author wishes to express his indebtedness for the gracious support of Dr. S. P. Yun of the University of Sao Paulo, Brazil. Part of this work was done in the framework of a Cooperation Agreement, University of Leuven-Nuclear Energy Centre with financial support from the Interuniversity Institute for Nuclear Science, Belgium.

*Present address: Commission of the European Communities, Jean Monnet Building, Kirchberg, Luxembourg.

- ¹K. Kumar, Phys. Scr. **6**, 270 (1972).
- ²U. Bertelsen, G. T. Ewan, and H. L. Nielsen, Nucl. Phys. **50**, 657 (1964).
- ³D. D. Warner, W. D. Hamilton, R. A. Fox, and T. Al-Janabi, J. Phys. G **2**, 230 (1975).
- ⁴S. Yamada, T. Sev, and T. Hayashi, Ann. Rep. Res. React. Inst. Kyoto Univ. **8**, 93 (1975).
- ⁵R. B. Begzhanov, D. G. Gaffarov, I. Ilkhamzhanov, A. I. Muminov, and K. T. Salikhbaev, Dokl. Akad. Nauk Uzb SSR **1**, 18 (1970).
- ⁶R. A. Kenefick and R. K. Sheline, Phys. Rev. **139**, B1479 (1965).
- ⁷D. E. Nelson, D. G. Burke, W. B. Cook, and J. C. Waddington, Can. J. Phys. **49**, 3166 (1971).
- ⁸D. E. Nelson, D. G. Burke, J. C. Waddington, and W. B. Cook, Can. J. Phys. **51**, 2000 (1973).
- ⁹P. Locard, J. Berthier, J. C. Hocquenghem, and R. Henck, Nucl. Phys. **89**, 497 (1966).
- ¹⁰W. B. Cook, J. C. Waddington, D. G. Burke, and D. E. Nelson, Can. J. Phys. **51**, 1978 (1973).
- ¹¹R. G. H. Robertson, S. H. Choh, R. G. Summers-Gill, and C. V. Stager, Can. J. Phys. **49**, 2227 (1971).
- ¹²J. S. Geiger, R. L. Graham, and J. S. Merritt, Nucl. Phys. **48**, 97 (1963).
- ¹³R. D. Gadsby, D. G. Burke, and J. C. Waddington, Can. J. Phys. **51**, 203 (1973).
- ¹⁴W. B. Cook and J. C. Waddington, Can. J. Phys. **51**, 2612 (1973).
- ¹⁵B. Singh and M. W. Johns, Can. J. Phys. **52**, 1160 (1974).
- ¹⁶L. V. Groshev, A. M. Demidov, V. F. Leonov, and L. L. Sokolovskii, Yad. Fiz. **13**, 681 (1971).
- ¹⁷O. Straume, D. G. Burke, and J. C. Waddington, Can. J. Phys. **52**, 1648 (1974).
- ¹⁸H. Drost, H. von Lojewski, K. Palov, R. Wallenstein, and G. Weyer, Nucl. Phys. **A223**, 195 (1974).
- ¹⁹W. B. Cook, M. W. Johns, G. Løvholden, and J. C. Waddington, Nucl. Phys. **A259**, 461 (1976).
- ²⁰W. Gelletly, R. Chapman, G. D. Dracoulis, S. Flanagan, A. J. Hartley, J. N. Mo, W. Scheck, R. M. Lieder, H. Beuscher, W. F. Davidson, A. Neskasis, and H. M. Jager, J. Phys. G **2**, L1 (1976).
- ²¹M. Guttormsen, E. Osnes, J. Rekestad, G. Løvholden, and O. Straume, Nucl. Phys. **A298**, 122 (1978).
- ²²G. Vandenput, Ph.D. thesis, University of Leuven, 1976 (unpublished).
- ²³R. Katajanheimo and E. Hammarén, Phys. Scr. **19**, 497 (1979).
- ²⁴S. F. Mughabghab and D. I. Garber, Brookhaven National Laboratory Report BNL-325, 1973.
- ²⁵H. R. Koch, H. A. Baader, D. Breitig, K. Mühlbauer, U. Gruber, B. P. K. Maier, and O. W. B. Schult, in *Proceedings of the International Symposium on Neutron-Capture Gamma-Ray Spectroscopy, Studsvik, 1969* (IAEA, Vienna, 1969).
- ²⁶J. J. Reidy, in *The Electromagnetic Interaction in Nuclear Spectroscopy*, edited by W. D. Hamilton (North-Holland, Amsterdam, 1975).
- ²⁷D. Breitig, Ph.D. thesis, Technical University Munich, 1970.
- ²⁸H. A. Baader, Ph.D. thesis, Technical University Munich, 1970.
- ²⁹B. N. Taylor, W. H. Parker, and D. N. Langenberg, Rev. Mod. Phys. **41**, 375 (1969).
- ³⁰R. T. Birge, Phys. Rev. **40**, 207 (1932).
- ³¹R. K. Smither, Phys. Rev. **150**, 964 (1966).
- ³²J. Barrette, M. Barrette, A. Boutard, G. Lamoureux, S. Monaro, and S. Markiza, Can. J. Phys. **49**, 2462 (1971).
- ³³R. K. Smither, in *Proceedings of the International Conference on Nuclear Physics with Reactor Neutrons*, edited by F. E. Throw, Argonne National Laboratory Report No. ANL-6797, 1963, p. 89.
- ³⁴R. K. Smither, E. Bieber, T. von Egidy, W. Kaiser, and K. Wien, Phys. Rev. **187**, 1632 (1969).
- ³⁵R. K. Smither and A. I. Namenson, Rev. Sci. Instrum. **38**, 52 (1967).
- ³⁶L. M. Bollinger and G. E. Thomas, Phys. Rev. C **2**, 1951 (1970).
- ³⁷T. von Egidy, Ann. Phys. (Leipzig) **7**, 221 (1962).
- ³⁸T. von Egidy, E. Bieber, and Th. Elze, Z. Phys. **195**, 489 (1966).
- ³⁹K. Schreckenbach, Ph.D. thesis, Technical University Munich, 1973.
- ⁴⁰R. S. Hager and E. C. Seltzer, Nucl. Data **A4**, 1 (1968).
- ⁴¹B. Nilsson, Nucl. Phys. **A129**, 445 (1969).
- ⁴²I. L. Lamm, Nucl. Phys. **A125**, 504 (1969).
- ⁴³S. G. Nilsson, C. F. Tsang, A. Sobiczewski, L. Szymanski, S. Wyceck, C. Gustafson, I. L. Lamm, P. Möller, and B. Nilsson, Nucl. Phys. **A131**, 1 (1969).
- ⁴⁴U. Götz, H. C. Pauli, K. Alder, and K. Junker, Nucl. Phys. **A192**, 1 (1972).
- ⁴⁵D. L. Hendrie, N. K. Glendenning, B. G. Harvey, O. N. Jarvis, H. H. Duhm, J. Saudinos, and J. Mahoney, Phys. Lett. **26B**, 127 (1968).
- ⁴⁶V. G. Soloviev, in *Selected Topics in Nuclear Theory*, edited by F. Janouch (IAEA, Vienna, 1963).
- ⁴⁷J. D. MacDougall, W. McLatchie, S. Whineray, and H. E. Duckworth, Nucl. Phys. **A145**, 223 (1970).

- ⁴⁸E. Osnes, J. Rekstad, and O. K. Gjøtterud, *Nucl. Phys.* **A253**, 45 (1975).
- ⁴⁹A. K. Kerman, *K. Dan. Vidensk. Selsk. Mat.-Fys. Medd.* **30**, No. 15 (1956).
- ⁵⁰G. Løvhøiden and I. Kanestrøm, *Phys. Norv.* **6**, 33 (1972).
- ⁵¹M. E. Bunker and C. W. Reich, *Rev. Mod. Phys.* **43**, 348 (1971).
- ⁵²F. S. Stephens, *Rev. Mod. Phys.* **47**, 43 (1975).
- ⁵³B. Elbek and P. O. Tjøm, *K. Dan. Vidensk. Selsk. Mat.-Fys. Medd.* **36**, No. 8 (1967).
- ⁵⁴M. Guttormsen, J. Rekstad, A. Henriquez, G. Løvhøiden, and O. Straume, *Nucl. Phys.* **A334**, 401 (1980).
- ⁵⁵B. L. Andersen, *Nucl. Phys.* **A112**, 443 (1968).
- ⁵⁶W. Scheck and G. Vandenput, in *Proceedings of the International Symposium on Highly Excited States in Nuclei*, edited by A. Faessler, C. Mayer-Böricke, and P. Turek, Kernforschungsanlage Jülich, Jülich, 1975.
- ⁵⁷G. Løvhøiden and J. Rekstad, *Phys. Lett.* **60B**, 335 (1976).
- ⁵⁸J. A. Pinston, R. Roussille, G. Sadler, W. Tenten, J. P. Bocquet, B. Pfeiffer, and D. D. Warner, *Z. Phys. A* **282**, 303 (1977).
- ⁵⁹J. Borggreen and G. Sletten, *Nucl. Phys.* **A143**, 255 (1970).